U.S.NRC
United States Nuclear Regulatory Commission
Protecting People and the Environment

NUREG/CR-6918
Revision 2

VARSKIN 5: A Computer Code for Skin Contamination Dosimetry

Office of Nuclear Regulatory Research

AVAILABILITY OF REFERENCE MATERIALS IN NRC PUBLICATIONS

NRC Reference Material

As of November 1999, you may electronically access NUREG-series publications and other NRC records at NRC's Public Electronic Reading Room at http://www.nrc.gov/reading-rm.html. Publicly released records include, to name a few, NUREG-series publications; *Federal Register* notices; applicant, licensee, and vendor documents and correspondence; NRC correspondence and internal memoranda; bulletins and information notices; inspection and investigative reports; licensee event reports; and Commission papers and their attachments.

NRC publications in the NUREG series, NRC regulations, and Title 10, "Energy," in the *Code of Federal Regulations* may also be purchased from one of these two sources.

1. The Superintendent of Documents
   U.S. Government Printing Office
   Mail Stop SSOP
   Washington, DC 20402–0001
   Internet: bookstore.gpo.gov
   Telephone: 202-512-1800
   Fax: 202-512-2250
2. The National Technical Information Service
   Springfield, VA 22161–0002
   www.ntis.gov
   1–800–553–6847 or, locally, 703–605–6000

A single copy of each NRC draft report for comment is available free, to the extent of supply, upon written request as follows:

Address: U.S. Nuclear Regulatory Commission
Office of Administration
Publications Branch
Washington, DC 20555-0001
E-mail: DISTRIBUTION.RESOURCE@NRC.GOV
Facsimile: 301–415–2289

Some publications in the NUREG series that are posted at NRC's Web site address http://www.nrc.gov/reading-rm/doc-collections/nuregs are updated periodically and may differ from the last printed version. Although references to material found on a Web site bear the date the material was accessed, the material available on the date cited may subsequently be removed from the site.

Non-NRC Reference Material

Documents available from public and special technical libraries include all open literature items, such as books, journal articles, transactions, *Federal Register* notices, Federal and State legislation, and congressional reports. Such documents as theses, dissertations, foreign reports and translations, and non-NRC conference proceedings may be purchased from their sponsoring organization.

Copies of industry codes and standards used in a substantive manner in the NRC regulatory process are maintained at—

The NRC Technical Library
Two White Flint North
11545 Rockville Pike
Rockville, MD 20852–2738

These standards are available in the library for reference use by the public. Codes and standards are usually copyrighted and may be purchased from the originating organization or, if they are American National Standards, from—

American National Standards Institute
11 West 42nd Street
New York, NY 10036–8002
www.ansi.org
212–642–4900

Legally binding regulatory requirements are stated only in laws; NRC regulations; licenses, including technical specifications; or orders, not in NUREG-series publications. The views expressed in contractor-prepared publications in this series are not necessarily those of the NRC.

The NUREG series comprises (1) technical and administrative reports and books prepared by the staff (NUREG–XXXX) or agency contractors (NUREG/CR–XXXX), (2) proceedings of conferences (NUREG/CP–XXXX), (3) reports resulting from international agreements (NUREG/IA–XXXX), (4) brochures (NUREG/BR–XXXX), and (5) compilations of legal decisions and orders of the Commission and Atomic and Safety Licensing Boards and of Directors' decisions under Section 2.206 of NRC's regulations (NUREG–0750).

U.S.NRC
United States Nuclear Regulatory Commission
Protecting People and the Environment

NUREG/CR-6918
Revision 2

VARSKIN 5: A Computer Code for Skin Contamination Dosimetry

Manuscript Completed: October 2013
Date Published: July 2014

Prepared by:
D. M. Hamby, C. D. Mangini, J. A. Caffrey, M. Tang

Department of Nuclear Engineering and Radiation Health Physics
Oregon State University
Corvallis, OR 97331-5902

M. Saba, NRC Project Manager
S. Sherbini, NRC Technical Monitor

Office of Nuclear Regulatory Research

ABSTRACT

The original VARSKIN computer code, an algorithm to calculate skin dose from radioactive skin contamination, has been modified on several occasions. This program is a rewrite of the U.S. NRC computer program VARSKIN 4 which is used by staff members and NRC licensees to calculate occupational dose to the skin resulting from exposure to radiation emitted from hot particles or other contamination on or near the skin. These assessments are required by 10 CFR 20.1201(c) in which the assigned shallow dose equivalent is to the part of the body receiving the highest exposure over a contiguous 10 cm^2 of skin at a tissue depth of 0.007 centimeters (7 mg/cm^2).

As with VARSKIN 4, five different predefined source configurations are available in VARSKIN 5 to allow simulations of point, disk, cylinder, sphere, and slab sources. Improvements to the earlier VARSKIN 3 and 4 included an enhanced photon dosimetry model, as well as models to account for air gap and cover materials for photon dosimetry. The new VARSKIN 5 version has been updated to better predict beta dosimetry in shallow skin targets. Although the user can choose any dose-averaging area, the default area for skin dose calculations in VARSKIN 5 is 10 square centimeters, to conform to regulatory requirements pursuant to Title 10 of the *Code of Federal Regulations*, Section 20.1201(c). Data entry is condensed to a single screen, a variety of unit options are provided (including both British and International System (SI) units), and the source strength can be entered in units of total activity or distributed in units of activity per unit area or activity per unit volume. The output page and the user's ability to add radionuclides to the library are greatly simplified. A library file contains data on gamma rays, x-rays, beta particles, internal conversion electrons, and Auger electrons. VARSKIN 5 allows the user to eliminate radionuclides that are not of interest and thus build a customized library. Finally, an extensive, context-sensitive help file is made available for VARSKIN 5 to provide guidance and to offer new users a tutorial in the use of the skin dosimetry software.

The enhanced photon model, introduced in VARSKIN 4, accounts for photon attenuation, charged particle buildup, and electron scatter at all depths in skin. The model allows for volumetric sources and clothing/air gaps between source and skin. The beta dosimetry model has been upgraded in VARSKIN 5 to better account for beta energy loss and particle scatter. Dose point kernels are now Monte Carlo based and the code agrees very well with the EGSnrc Monte Carlo code.

This document describes the VARSKIN code, provides basic operating instructions, presents detailed descriptions of dosimetry models, and suggests methods for avoiding misuse of the models.

CONTENTS

Page

CONTENTS (continued)

FIGURES

FIGURES (continued)

Page

TABLES

ACKNOWLEDGMENTS

This report was prepared to document work performed by Oregon State University (OSU) for the U.S Nuclear Regulatory Commission (NRC) under Contract Nos. **NRC-HQ-11-C-04-0011** and **NRC-04-08-137**. Staff at the Pacific Northwest National Laboratory wrote initial versions of VARSKIN; later versions were written at Colorado State University and then the Center for Nuclear Waste Regulatory Analyses. The activities reported here were performed on behalf of the NRC Office of Nuclear Regulatory Research, Division of System Analysis. This report is a product of OSU and does not necessarily reflect the views or regulatory position of the NRC.

We are appreciative of the technical assistance received from J. Parson, M. Ryan, and S. Marshall in the production of this and the previous report and their findings. Our beta testers for various versions of VARSKIN included J. Chase, J. Dubeau, K. Sejkora, M. Thornhill, R. Struckmeyer, and J. DeCicco. We are also grateful to S. Bush-Goddard, M. Saba, and S. Sherbini for their support during the development process of the enhanced photon and beta dosimetry models. Authors of earlier versions of the VARSKIN code were indebted to L. Howard for technical review and D. Turner for programmatic review of reports. These authors also thanked L. Selvey for document preparation; E. Hanson for editorial review; and H. Karagiannis, S. Sherbini, A. Roecklein, S. Bush-Goddard, and E. Dickson of the NRC for their support, suggestions, and patience during the development of VARSKIN 3. The following people helped develop models for VARSKIN 3: J. Chase, B. Plain, M. Wierzbicki, M. Lantz, and K. Krobl. The following people provided comments after testing VARSKIN 3: G. Chabot, J. Dwyer, J. Lebda, E. Mercer, R. Nimitz, A. Salame-Alfie, M. Stabin, G. Sturchio, B. Tharakan, T. Vandermey, and M. Charles.

ABREVIATIONS AND ACRONYMS

2D	Two Dimensional
3D	Three Dimensional
BSCF	**Back Scatter Correction Factor**
CFR	Code of Federal Regulations
CPE	Charged Particle Equilibrium
CPU	Central Processing Unit
CSDA	Continuous Slowing Down Approximation
DPK	Dose Point Kernel
DSP	Depth Scaling Parameter
EDK	Energy Deposition Kernel
EGS	Electron-Gamma Shower
ESP	Energy Scaling Parameter
GUI	Graphical User Interface
ICRP	Interactional Commission on Radiation Protection
ICRU	International Committee on Radiation Units and Measures
KERMA	Kinetic Energy Released in Matter
MCNP	Monte Carlo N-Particle
NCRP	National Commission on Radiation Protection
NIST	National Institute of Standards and Technology
NRC	National Research Council (Canada)
NRC	Nuclear Regulatory Commission
OSU	Oregon State University
RSICC	Radiation Safety Information Computational Center
RSO	Radiation Safety Officer
SADD	Specific Absorbed Dose Distribution
STP	Standard Temperature and Pressure
TCPE	Transient Charged Particle Equilibrium
V&V	Verification and Validation

1 INTRODUCTION

The original VARSKIN computer code (Traub, et al., 1987) was intended as a tool for the calculation of tissue dose at various depths as the result of skin contamination. The contamination was assumed to be a point or an infinitely thin disk source located directly on the skin. Soon after the release of VARSKIN, the industry encountered a "new" type of skin contaminant. This contaminant consists of discrete microscopic radioactive particles, called "hot" particles. These particles differ radically from uniform skin contamination in that the particles have a thickness associated with them, and many of the skin exposures result from particles on the outside of protective clothing.

Originally, there were a few drawbacks to using VARSKIN to calculate skin doses from hot particles or other contaminants on the skin or outside of a cover material such as protective clothing. Formerly, VARSKIN modeled the contaminant as having no thickness; thus, the calculation did not account for source self-shielding. For example, for hot particles containing weak beta-emitting radionuclides (e.g., cobalt-60 (Co-60)), VARSKIN greatly overestimated calculated skin doses from particles that were thicker than about 1 micrometer (μm). Second, VARSKIN did not have the capability of modeling a cover material (e.g., protective clothing) that might exist between the source and skin, again leading to an overestimation of skin dose from skin contamination. Finally, it was shown that the gamma component of a mixed beta/gamma-emitting hot particle becomes increasingly important as the skin depth and the thickness of cover material increase (Durham and Lantz, 1991). Because VARSKIN did not model a cover material or allow skin depths other than 7 milligrams per square centimeter (mg/cm^2), the code's original authors concluded that the photon dose would not be significant compared to the beta dose under these exposure conditions, and thus they did not include the photon dose model. Because of these and other shortcomings of the code, an upgrade of VARSKIN was needed to provide skin dose calculations under a variety of exposure conditions.

VARSKIN Mod 2 (Durham, 1992) contained all the features of the original VARSKIN, with many significant additions. Additional features in VARSKIN Mod 2 included the modeling of three-dimensional sources (cylinders, spheres, and slabs) that accounted for self-shielding, modeling of materials placed between the source and skin (including air gaps) that would attenuate beta particles, and, in specific cases, modeling hot particle photon doses. VARSKIN Mod 2 also used a correction for backscatter for one- and two-dimensional beta sources under limited conditions. Finally, the VARSKIN Mod 2 package incorporated a user interface that greatly simplified data entry for calculating skin dose, in addition to providing guidance in the form of help screens.

The upgraded code also contained a volume-averaged dose model and an offset particle model. The volume-averaged model allowed the user to calculate dose averaged over a volume of tissue defined by a cylinder with a diameter equal to that of the dose averaging area and bounded at the top and bottom by two selected skin depths (see Figure 1-1). This model is useful for calculations of dose that can then be compared to the dose measured by a finite-volume instrument (e.g., a thermoluminescent dosimeter). The offset particle model, which allows dose to be calculated for a particle that is not centered over the dose area of interest, is useful for calculating dose to a singular given skin area from multiple hot particles.

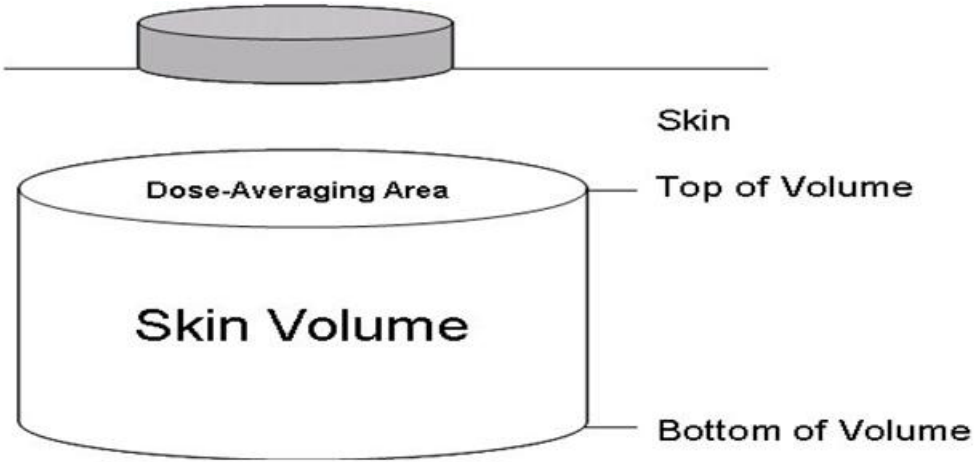

Figure 1-1 Depiction of cylindrical dose averaging volume

Finally, VARSKIN Mod 2 gave the user the ability to select a composite source term, thus allowing the calculation of total dose from a mixture of beta-emitters instead of requiring the code to be run separately for each radionuclide in the mix. This feature was removed in VARSKIN 3 (Durham 2006), and instead, the maximum number of radionuclides included in a single calculation was increased to 20. One drawback of removing this feature in VARSKIN 3 is that the user must explicitly add radioactive progeny. The VARSKIN 3 photon dose model, which has been improved in VARSKIN 4, was an extension of a model published by Lantz and Lambert (1990) that was the basis for the VARSKIN Mod 2 photon dose model. A syringe model was included in VARSKIN 3, but was deactivated in VARSKIN 4. That model employed a major approximation to an actual syringe and, in that respect, had several limitations.

Enhancements that initiated VARSKIN 4 focused on the photon dosimetry model. This model includes charged particle buildup and subsequent transient equilibrium, along with photon attenuation, air and cover materials, and volumetric sources. In VARSKIN 3, only point photon sources could be modeled, charged particle equilibrium (CPE) and attenuation were not considered, and cover materials were not modeled. The VARSKIN 5 package provides an upgraded beta dosimetry model that better accounts for charged-particle energy loss as the particle moves through the source, cover material, air, and tissue.

Section 2 of this report describes the contents of the VARSKIN 5 code package, including instructions for code execution. Section 3 discusses the technical basis for VARSKIN 5 and describes the dosimetry models incorporated in the code, while Section 4 contains the results of validation and verification testing. Section 5 describes the problems and suggestions for improving VARSKIN Mod 2 and VARSKIN 3 that were included in VARSKIN 5, as well as new features of the code and its limitations. Section 6 explains the correct method for modeling "infinite" sources and how to hand-calculate the maximum dose to a single 10-square-centimeter (10 cm^2) area from multiple contamination sources. Additionally, Appendix A provides a graphical display of the results from Section 4, and Appendix B presents three detailed solutions to practical examples using VARSKIN 5.

2 VARSKIN 5 USER'S MANUAL

This section serves as a user's guide for VARSKIN 5. It includes operating instructions and a description of the features of VARSKIN 5.

2.1 Running VARSKIN 5

Users must download and unzip the VARSKIN 5 folder and double-click the V5 icon to execute the VARSKIN code. There is no need to uninstall previous versions of VARSKIN. Upgrades to VARSKIN 5 will be made available, as necessary. Obtaining upgrades is as simple as downloading the new zipped folder and beginning execution.

2.1.1 Hardware and Software Requirements: A personal computer with a Pentium II processor or newer is required. The code requires approximately 10 megabytes of disk space. VARSKIN has been tested under a variety of Windows® operating systems.
Operations within VARSKIN 5 are designed to be intuitive. After double-clicking the V5 icon, the user will see the Main Input screen (Figure 2-1). If necessary, the "About Varskin 5.0" screen provides the user with contact information and basic code information (Figure 2-2).

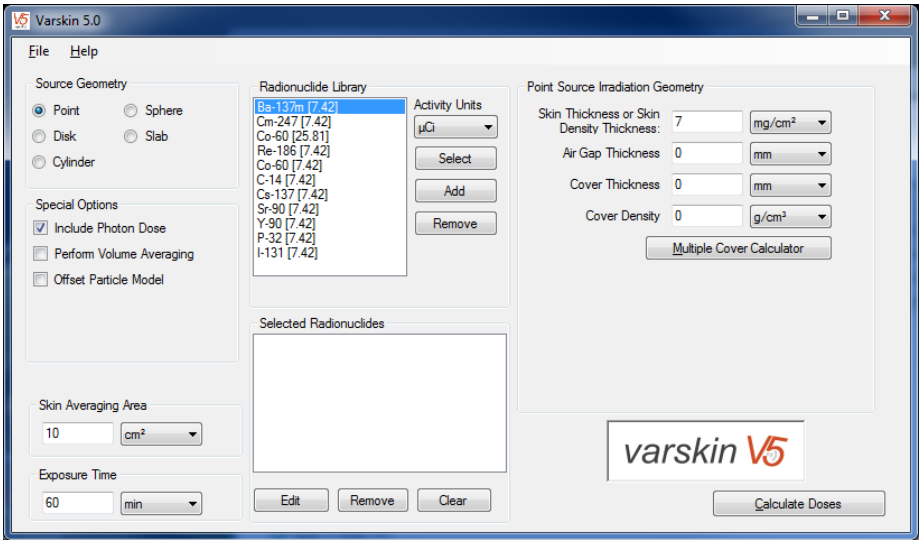

Figure 2-1 Initial view and main input screen (Source Geometry option box in upper left corner)

2.1.2 Source Geometry. The Source Geometry selection box is shown in the initial view "Varskin 5.0" screen in Figure 2-1. This screen contains all of the input information that is needed to perform a dose calculation. Although VARSKIN 5 allows the user to enter data in any order, the **geometry package must be chosen first** because changing the geometry package will cause certain parameters to appear and others to be removed. Five geometry packages are available: point source, disk source (infinitely thin), cylinder source (thick), spherical source, and slab source (rectangular).

Figure 2-2 "About Varskin 5.0" screen

The point source geometry (Figure 2-3(A)) is very simple to use and should be used as an initial screening tool for contamination that is confined to an extremely small area of the skin, or for a quick calculation to determine whether a regulatory limit is being approached or exceeded. The point source geometry does not account for beta self-shielding, so a three-dimensional source geometry should be used for particulate contamination. The point source model does not require any data for the physical description of the source and will generally yield the highest dose rate for a given activity of any of the available source geometries. For beta dosimetry, VARSKIN 5 models a point source as a cylindrical source with a thickness of 1 μm, a radius of 1 μm, and a density of 0.001 grams per cubic centimeter (g/cm^3). The offset particle model is available only when using the point source geometry.

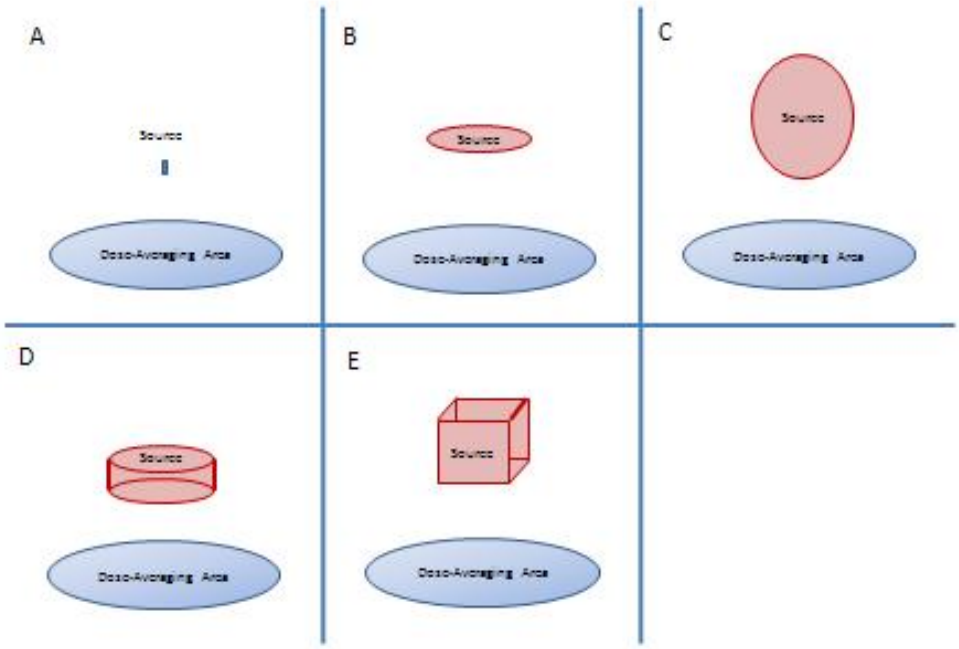

Figure 2-3 Schematic representations of the five geometry options

The infinitely thin disk source geometry model (Figure 2-3(B)) is simple and is recommended for modeling skin contamination events caused by liquid sources. The disk source geometry requires the user to enter either the source diameter or the source area at the bottom of the Disk Source Irradiation Geometry box. Entering the area of the contamination is useful for modeling sources when the area is known. Enter the area of the source in the text box labeled "Source Area." When the user enters the diameter of the source area, VARSKIN 5 calculates the area of the 2D disk with that diameter. Similarly, when the user enters the area of the source, VARSKIN 5 calculates the diameter of the disk with the same area. If the area of contamination is not circular, entering the area of the actual contamination will generally result in a reasonable estimation of skin dose.

The spherical source geometry (Figure 2-3(C)) is perhaps the simplest three-dimensional geometry to use for dose calculations because it requires knowledge of only one source dimension, its diameter. The spherical source geometry assumes that the source is surrounded by air and touches the skin or cover material only at the bottom point of the sphere. For photon dosimetry, it is assumed that the source material is equivalent to air for attenuation calculations.

Choosing a spherical source will generally overestimate dose compared to a similarly sized cylindrical source (same radius and length) with the same total activity.The air surrounding the bottom hemisphere does not shield the source particles as efficiently as the source material (which would be encountered by the particle in the cylinder or slab models), and a larger area of skin will be exposed, resulting in consistently higher doses.

The cylindrical source model (Figure 2-3(D)) requires knowledge of two dimensions, the cylinder diameter and its height. The cylindrical source geometry assumes that the source is surrounded by air and that the entire bottom of the cylinder is in contact with skin or cover material. Of the two cylinder dimensions, the calculated dose is much more sensitive to changes in the cylinder height as opposed to the cylinder diameter.

The slab source geometry (Figure 2-3(E)) requires knowledge of three physical dimensions: the first side length, the second side length, and the slab's thickness. As evidenced by the previous VARSKIN Validation Test Plan and Report, results of beta dose calculations using the slab geometry differ by as much as 35 percent from the results obtained using the other four geometries when modeling the same source. This discrepancy is the result of a fundamental difference between the mathematical approach used for the slab geometry and the other geometry packages when modeling similar sources. The slab geometry should be used only when skin dose from multiple, discrete particles is needed, as described in Section 6 (i.e., when the offset particle model is used).

The following general rules should govern the choice of geometry package, progressing from the most conservative to least conservative dose estimate:

- If nothing is known about the particle size and shape, use the point source geometry option. This option is also recommended for a quick comparison to regulatory limits since the point geometry typically overestimates actual skin dose.

- If the diameter is known, but the thickness cannot be estimated, or if a distributed source is being modeled (i.e., with a known source strength per unit area), use the two-dimensional disk source geometry option.

- If the particle is known to be spherical (few particles are truly spherical) and is not imbedded in another material, use the spherical source geometry option.

- If the thickness and the diameter of the source can be estimated, but the shape is unknown, use the cylindrical source geometry option because this geometry requires only two dimensions (height and radius) to describe the particle.

- If the particle is known to be rectangular, use the cylinder source geometry option. The height of the particle should be preserved, and the area of the contact surface should be selected such that the source volume is preserved.

For all source geometries, doses are calculated to an infinitely thin disk centered below the central axis of the source. When using the offset particle model, dose is calculated to the disk with its center located at the user-supplied offset distance from the center of the source.

2.1.3 Adding Radionuclides to the Library. VARSKIN 5 employs two radionuclide libraries, a master library (supplied with the code) that contains data for all radionuclides available to the user, and a user library that contains only those radionuclides that are selected and added by the user (drawn from the master library). Beta energy emission spectra are obtained from an abridged ICRP–38 (International Commission on Radiological Protection, 1983) dataset using NUCDECAY (RSICC, 1995) data files.

When VARSKIN 5 is first executed, a few preselected radionuclides may appear in the user library. VARSKIN 5 is designed to allow the user to customize the radionuclide library so that only the nuclides of interest can be maintained for ready use. To add a radionuclide to the user library, the user clicks the "Add" button (shown in the upper center of Figure 2-1), and a new screen appears (Figure 2-4) that displays every radionuclide for which data are available (a total of 838 radionuclides). Radionuclides are added to the user library by highlighting the radionuclide and clicking the "Add Radionuclide" button, or simply double-clicking the name of the radionuclide. In building the user library, one can specify a minimum photon energy and minimum photon yield (photons per disintegration) to limit calculation times, if necessary. These defaults are set at 2 kiloelectronvolts (keV) and 1 percent, respectively. In addition to selecting the nuclide from the master library, the user must specify an effective atomic number (Z_{eff}) to characterize the source material in which the source is incorporated. The default value for Z_{eff} is 7.42 (the effective atomic number of water). A total of 838 radionuclides are available in the master library, each of which could be added to the VARSKIN user library, and each with its own effective atomic number (i.e., multiple selections of the same nuclide can be made, but with different values of Z_{eff}). Computational speeds are generally not an issue; therefore, users are advised to use the default settings when building their library.

Once the "Add Radionuclide" button is selected (Figure 2-4), calculations are performed internally to populate the user library for the selected radionuclide; this can take up to a few seconds depending on processing power. In these calculations, data are extracted from the data files *ICRP38.dat*, *ICRP38.idx*, and *ICRP.bet* (all of which are located in the *dat* subdirectory of the application directory). If the radionuclide emits beta radiation or conversion/Auger electrons, an electron energy spectrum is generated for all beta decay routes and other electron emissions. Photon energy and yield data are then collected from the data files.

These data are processed by the FORTRAN executable file *Sadcalc.exe*, and an output file that contains the average beta spectrum energy, the electron and beta yield, the X_{99} distance, the scaled absorbed dose distribution, the photon energies, and the photon yields is generated with the extension ".dat." As discussed in Section 3, the X_{99} distance is used as the range of the beta particles.

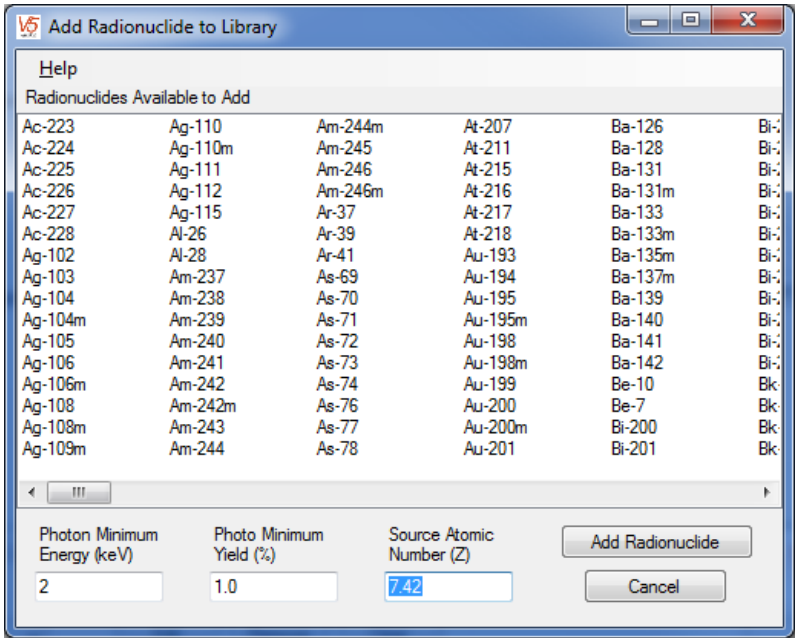

Figure 2-4 Add Radionuclide screen

When the process of adding the radionuclide is completed, the Source Geometry screen will return, and the added radionuclide will be visible in the user list of available radionuclides. The added radionuclide will remain in the user library for subsequent calculations unless the user purposefully removes it using the "Remove" button (Figure 2-1) on the Radionuclide Library frame; the nuclide data will always remain in the master library.

In VARSKIN 5, radioactive progeny do not follow their parent in the dose calculations. To have the code consider progeny, the user must create a user library file for each radioactive decay product. Radioactive decay products are not included, regardless of the half-life of the progeny. If evaluating dose from progeny alone, the user must be cautious and be aware of the half-lives of both parent and progeny and include the correct dose calculation (decay corrected or not) in the dose estimate. For example, in the case of ^{137m}Ba as a stand-alone product of ^{137}Cs decay, the user should report the "Dose (No Decay)" result for ^{137m}Ba dose. If the "Decay-Corrected Dose" is used, the very short decay time of ^{137m}Ba will cause the dose to be significantly underestimated, assuming that ^{137m}Ba is continuously supplied by the decay of ^{137}Cs.

2.1.4 Selecting Radionuclides from the User Library. Radionuclides can be selected for a dose calculation by double-clicking the radionuclide name or by highlighting the desired radionuclide and clicking the "Select" button (Figure 2-1). The default unit of measure for activity is microcuries (μCi). Users may change the activity unit by selecting a different unit from the Activity Units list box. The new unit must be chosen before selecting the radionuclide. When a radionuclide is selected, a message box will appear asking the user to enter the value of the activity in the chosen units. Once the activity is entered, the radionuclide and its activity will be added to the Selected Radionuclide list box. A user may select up to 20 radionuclides for a given calculation.

For geometry packages other than the point source, the “Use Distributed Source” checkbox will appear (Figure 2-1). The distributed source option allows the user to enter the source strength in activity-per-unit-area for the disk sources or activity-per-unit-volume for volumetric sources. The distributed source option applies only to radionuclides that are chosen after the checkbox has been selected. If the distributed source option is unchecked, subsequently selected radionuclides will have activities expressed as total inventory instead of distributed activity. Beta energy emission spectra are obtained from an abridged ICRP–38 (International Commission on Radiological Protection, 1983) dataset using NUCDECAY (RSICC, 1995) data files.

2.1.5 Geometry Parameters and Multiple Cover Calculator. The geometry parameter Source Irradiation Geometry box (Figure 2-5, shown on the right above the VARSKIN logo) changes contingent on the particular geometry chosen for the calculation (slab geometry in this example). The user can choose the units of each parameter from the drop-down lists provided to the right of each input field. The units can be mixed for the different parameters; VARSKIN 5 makes the necessary conversions internally. Table 2-1 shows the default values for the various parameters.

2.1.6 Default State. VARSKIN 5 allows the user to save one default state for easy retrieval at a later time. If the user wishes to change the default settings of Table 2-1, the following actions should be taken. From the File drop-down menu, if the user selects “Save Default State,” a file is written that contains all input parameters for the geometry described at that moment. At a later time, if that geometry is to be run again, the user can select “Load Default State,” and all parameter values will return to their values at the time the default state was last saved.

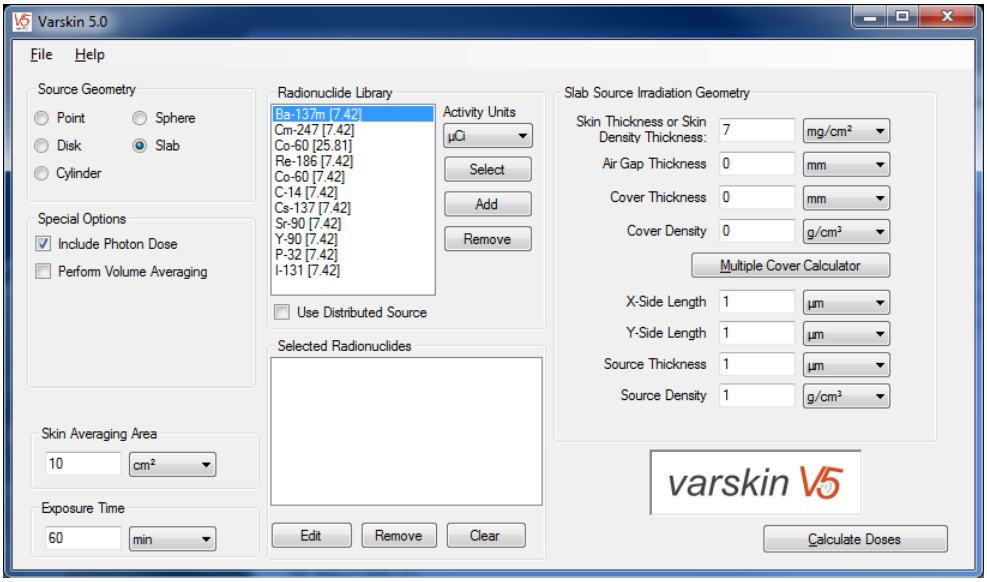

Figure 2-5 Slab source geometry parameters (right)

In the disk geometry package, the user has the option of entering either the source radius or the source area. The units for the radius will be used when the area of the source is displayed. This feature simplifies data entry for two-dimensional sources where the area and the total activity are known.

Source thickness and source density are equally important for calculating skin dose, especially for beta dosimetry. It is essential that these parameters are known accurately; otherwise, their values should be underestimated so that conservative dose calculations will result. If source dimensions are unknown, the following guidelines will help in choosing appropriate values:

- Diameter (disk and cylinder) and side lengths (slab): The dose calculation for most radionuclides is relatively insensitive with respect to these dimensions for sizes below 2 millimeters (mm) with sources of the same activity. Overestimating source dimensions will generally result in an overestimation of dose, unless the source size is larger than the averaging area.

- Thickness (disk and slab) and sphere diameter: The beta dose calculation for all radionuclides is very sensitive to these dimensions, especially for low-energy beta emitters. Minimizing the value of this dimension will provide an overestimate of beta dose. For photons, these dimensions are not as critical for the dose calculation.

- Source density (three-dimensional geometry models): For beta dosimetry, users should choose a source density that is consistent with the material containing the source. For hot particle contaminations, a typical density for stellite (Co-60) is 8.3 g/cm^3, a density of 14 g/cm^3, and an effective Z of 25.81 is typical for fuel. For photon dose estimates, the source is assumed to be air, with negligible consequence, except for large, dense sources and low-energy photons.

Table 2-1 Default Values and Units for Geometry Parameters

Parameter	Default Value
Skin Density Thickness	7 mg/cm^2
Air Gap Thickness	0 mm
Air Density (@ STP)	0.001293 g/cm^3
Cover Thickness	0 mm
Cover Density	0 g/cm^3
Source Area (Disk)	0.785 mm^2
Source Diameter (Disk)	1 mm
Source Diameter (Cylinder)	1 mm
Source Thickness (Cylinder)	1 μm
Source Diameter (Sphere)	1 mm
Source Thickness (Slab)	1 μm
Source X-Side Length (Slab)	1 μm
Source Y-Side Length (Slab)	1 μm
Source Density (Three-Dimensional Geometries)	1 g/cm^3

Users can model the presence of a cover material and/or an air gap. The schematic drawing below (Figure 2-6) depicts the cylindrical source geometry to illustrate the cover/gap model. The required input to describe the cover is material thickness and its corresponding density. Both parameters are needed to account for the $1/r^2$ dependence of the Berger point kernel (geometric attenuation) and for the energy loss due to attenuation (material attenuation). For the air gap model, only the thickness of the air gap is required for input.

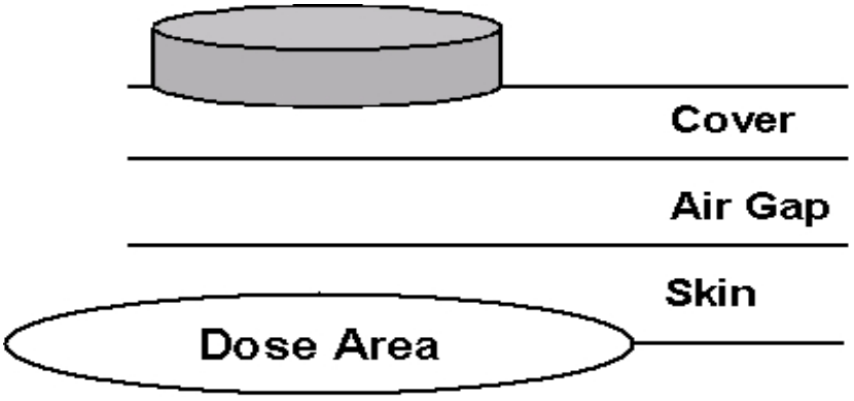

Figure 2-6 Schematic showing the cover material and air gap models

The physical characteristics of the air gap and cover material can significantly affect the calculated skin dose. While the air gap has little consequence for material attenuation, its effect on geometric attenuation can be significant for beta dosimetry. The air gap in photon dosimetry has the effect of disrupting CPE and can appreciably influence dose at very shallow depths in tissue. Cover materials influence both the geometric and material attenuation. Table 2-2 gives some suggested thickness and density values.

VARSKIN 5 allows multiple cover materials to be modeled as a composite cover when the user clicks on the "Multiple Cover Calculator" button (Figure 2-1). The multiple-cover calculator allows the user to combine up to five covers (Figure 2-7). The user must enter a value for two of the following three parameters for each layer (while ensuring that the third parameter is blank): covert, cover density, and cover density thickness. The user can choose the units for density and thickness, but the density thickness must be entered in mg/cm^2. The calculator determines the third parameter, combines the different layers, and calculates an effective thickness and density of the composite cover.The appropriate input boxes in the Source Geometry screen are then populated with the composite cover density (mg/cm^3) and thickness (in cm). If the user enters all the three parameters, VARSKIN 5 will indicate an error and ask the user to enter only two of the three parameters for a given layer. The print out from a dose calculation will include the data for each cover layer, as well as the composite cover data.

Table 2-2 Suggested Values for Cover Thickness and Density

Material	**Thickness (mm)**	**Density (g/cm^3)**
Lab Coat (Plastic)	0.2	0.36
Lab Coat (Cloth)	0.4	0.9
Cotton Glove Liner	0.3	0.3
Surgeon Glove	0.05	0.9
Outer Glove (Thick)	0.45	1.1
Ribbed Outer Glove	0.55	0.9
Plastic Bootie	0.2	0.6
Rubber Shoe Cover	1.2	1
Coveralls	0.7	0.4

To include more than five covers in the composite cover calculation, the user must calculate the composite cover thickness and density for the first five covers. The user must then run the calculator again and enter the first composite cover thickness and density as one of the layers.

Accordingly, if a composite cover is entered as one of the covers, the layers composing the composite cover will not be individually displayed on the printout.

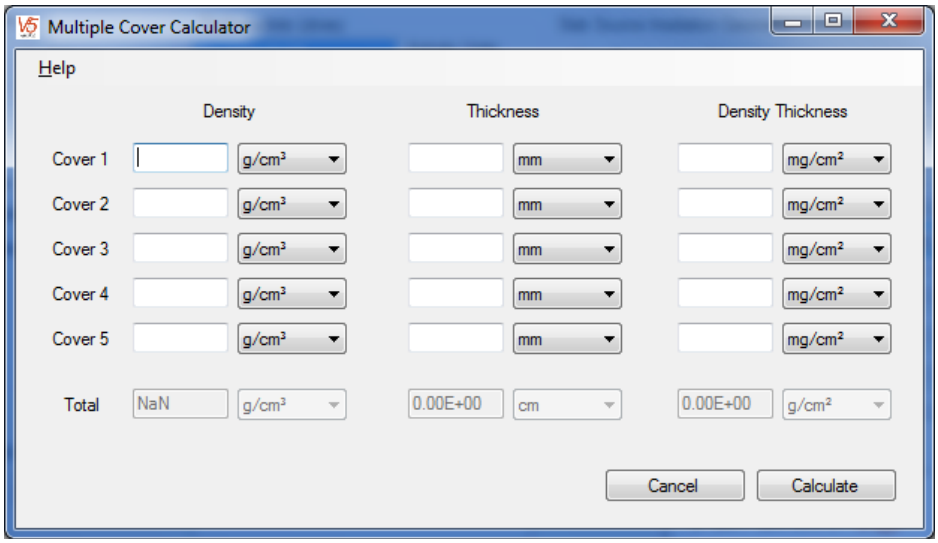

Figure 2-7 Composite cover calculator screen

2.2 Special Options

Depending on the geometry package selected, special options are available that affect the calculation. The first special option, available for all packages, is to include the photon dose in the calculation. The default for this option is to calculate the photon dose, which includes x-rays and gamma rays; the user can, however, de-select this box so the photon dose will not be calculated. If the photon dose option is included when the "Calculate Doses" button is clicked, the photon dose will be calculated for all selected radionuclides. If the radionuclide does not emit photons, a dose of zero will be displayed.

In most cases, the calculated photon skin dose will be negligible relative to the beta skin dose. A noteworthy exception to this is evident when modeling Co-60 or other low-energy beta emitters with significant photons. A cover material can easily shield low-energy beta particles without appreciably affecting photon dose. In this case, the photon dose will account for the majority of the calculated skin dose.

The second special option allows the calculation of dose to be averaged over a volume of tissue defined by a cylinder of specific diameter and thickness. The use of the volume-averaged dose calculation can be important, for example, in evaluating the dose between 10 mg/cm^2 and 15 mg/cm^2, as recommended by the International Commission on Radiological Protection (1991), for evaluating the dermal effects of skin dose.

If volume averaging is chosen, the user is prompted (after selecting the "Calculate Doses" button) to enter the skin density thicknesses associated with the boundaries (shallow and deeper tissue depths defining the cylindrical averaging volume). Skin density thickness must be entered in units of mg/cm^2. A range of suggested values for the shallow and deep tissue depths is provided based on the physical range of beta particles associated with the selected radionuclide(s). Suggested values are from a skin density thickness of 0 mg/cm^2 to the maximum penetration depth of the beta particle(s) being modeled; however, any nonnegative value of density thickness can be entered. The user is cautioned, therefore, to be certain of the depths requested; some depths may result in negative values for beta dose. The VARSKIN 5 model calculates the average dose over the averaging area at 10 discrete depths between the shallow and deep tissue depths (Figure 2-8). Thus, the volume-averaged dose model requires 10 times more execution time than that for a single depth.

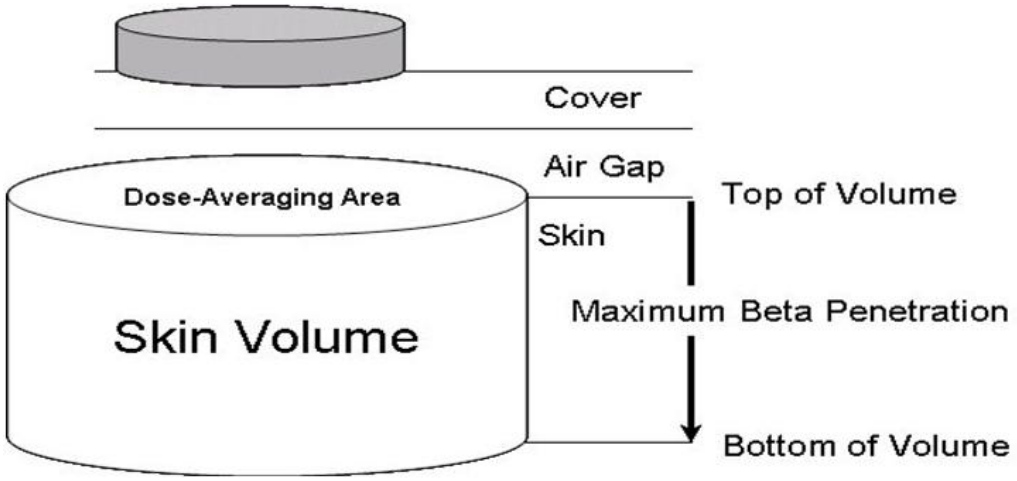

Figure 2-8 Schematic diagram of the volume-averaged dose model geometry

When the point source geometry is selected, the "Offset Particle Model" checkbox appears in the Special Options frame. The offset particle model, which allows dose to be calculated for a particle that is not centered over the dose area of interest, is useful for calculating dose from multiple hot particles. The offset particle model is normally not accessed unless selected by the user. When the "Offset Particle Model" box is checked, the user is prompted to enter the offset distance. The offset distance is the lateral distance between the point source and the center of the dose area. The value of the offset is the only additional input value that is required for the model. The results screen (including the volume-averaged dose results screen) will display the offset value, if this option has been selected. Section 6.2 describes in more detail the use of the offset particle model.

2.2.1 Calculating Doses. Once the desired geometrical parameters and options have been selected, the user initiates the calculation by clicking the "Calculate Doses" button (Figure 2-1). A progress bar will appear below the VARSKIN logo, which will scroll repeatedly depending on the complexity of the calculations. The number of radionuclides to be analyzed and the various options that have been selected will impact the calculation time.

VARSKIN 5 calculates dose using compiled FORTRAN programs entitled *VarCalc.exe* and *GamCalc.exe*. When the user clicks the "Calculate Doses" button, the GUI writes the input data in a file called *output.dat*. *Varcalc.exe* and *GamCalc.exe* read *output.dat*, perform the calculations, and then write results to a file entitled *results.dat*. The GUI reads *results.dat* and displays the results of the calculation. Figure 2-9 depicts the logic flow diagram. Note that *output.dat* and *results.dat* are internal files and are not intended to be accessed or edited by the user.

2.2.2 Output Screen. The Results screen for a non-volume-averaged calculation (Figure 2-10) is displayed immediately after the dose calculation is completed. The screen is separated into three distinct sections: results for individual radionuclides (upper left quadrant), combined results for all radionuclides (upper right quadrant), and source input data (lower half).

In the individual results section of the initial display, only the results for the first radionuclide are shown. The results from other radionuclides are displayed by highlighting the radionuclide of interest in the list box (upper left). This screen will display only the contribution to the dose from the selected radionuclide. The combined results section displays the total dose for all radionuclides. The data in this section cannot be edited and will not change unless a new calculation is made. This section of the output screen also contains unit selection bubbles, which allow the user to select dose results in English or International (SI) units.

The lower half of the results screen contains a mirror of the input data entered in the Source Geometry screen. The format of this section will change depending on the geometry chosen for the calculation. This section of the output screen also contains buttons that allow the user to perform certain functions. Clicking the "Print Results" button will send a hard copy of all results to the default Windows printer. VARSKIN 5 will not allow the user to change the default printer. Additionally, the program will fail if a printer is not installed when the "Print Results" button is selected. The user will be asked to supply a title for the printed output, and then the output file will be sent to the printer. VARSKIN 5 does not allow the user to save the output as a computer file; the only record of the calculation is the printout. However, the user may save the input data to the calculation by closing the output window and selecting "Save" from the "File" dropdown list. Selecting "Exit" from that dropdown list, which also gives the user the option to save the input, allows the user to end VARSKIN 5.

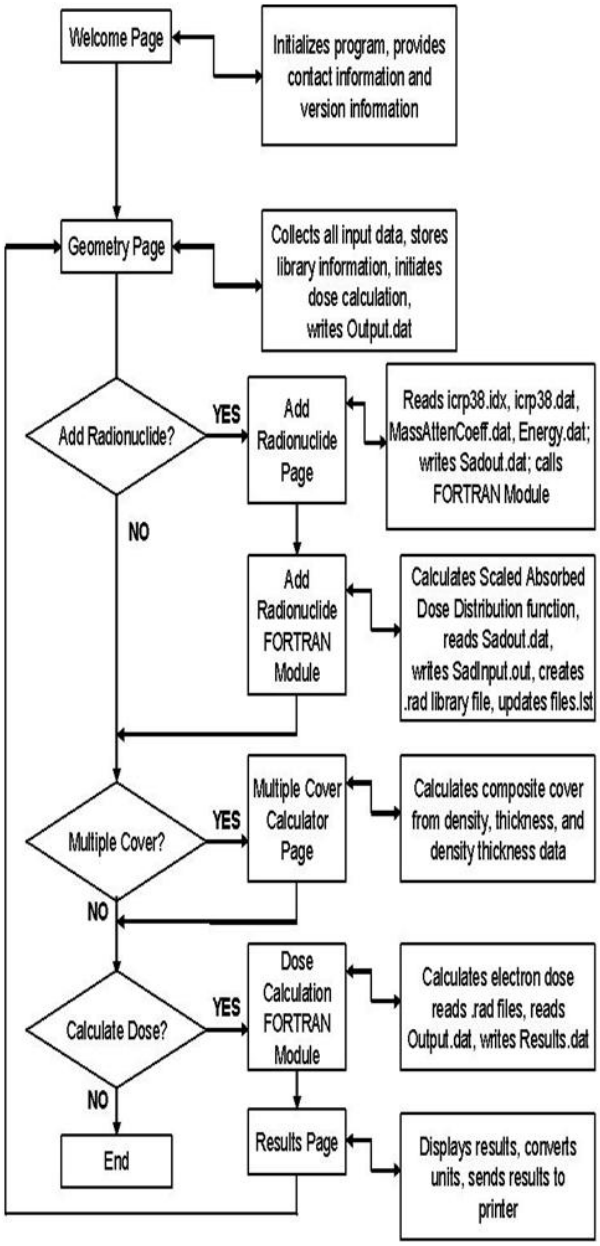

Figure 2-9 General logic flow diagram

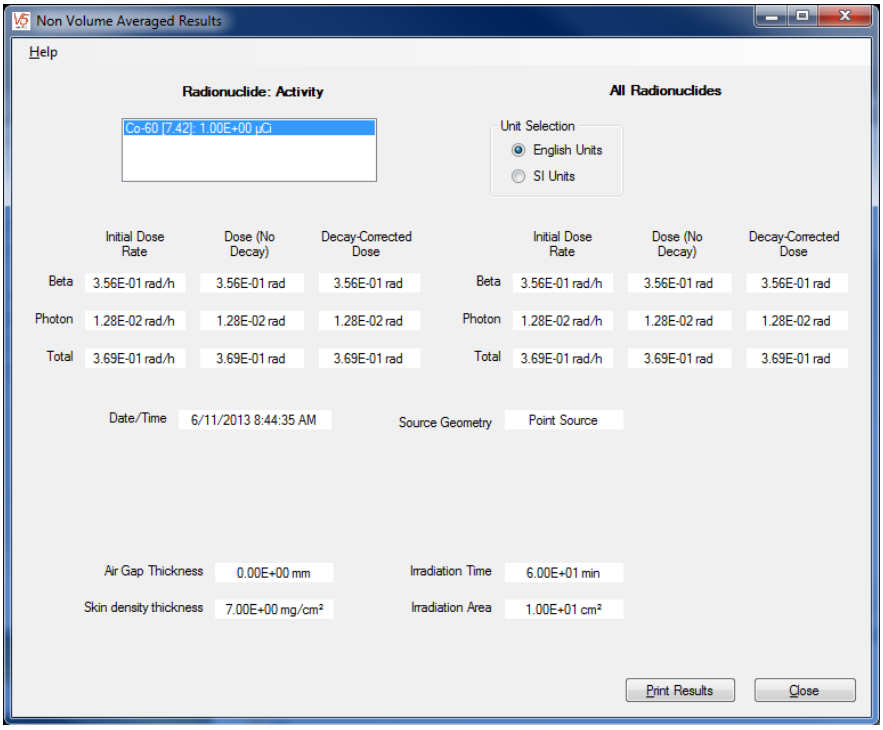

Figure 2-10 Results screen for a typical calculation

A slightly different screen will appear for volume-averaged dose calculations (Figure 2-11). Because the dose can be averaged over different averaging volumes for different radionuclides, VARSKIN 5 does not provide a section for combined results of a volume-averaged dose calculation. Instead, only the results from the highlighted radionuclide are displayed. The upper left section of the volume-averaged results screen displays values of the shallow and deep skin depths, as well as the total volume over which the dose was averaged for the chosen radionuclide. Other radionuclides can be chosen individually by highlighting them in the radionuclide list box. As with the other results screen, this output screen contains unit-selection bubbles allowing the user to select volume-averaged dose results in English or SI units. Again, a summary of the input parameters is displayed on the lower half of the screen.

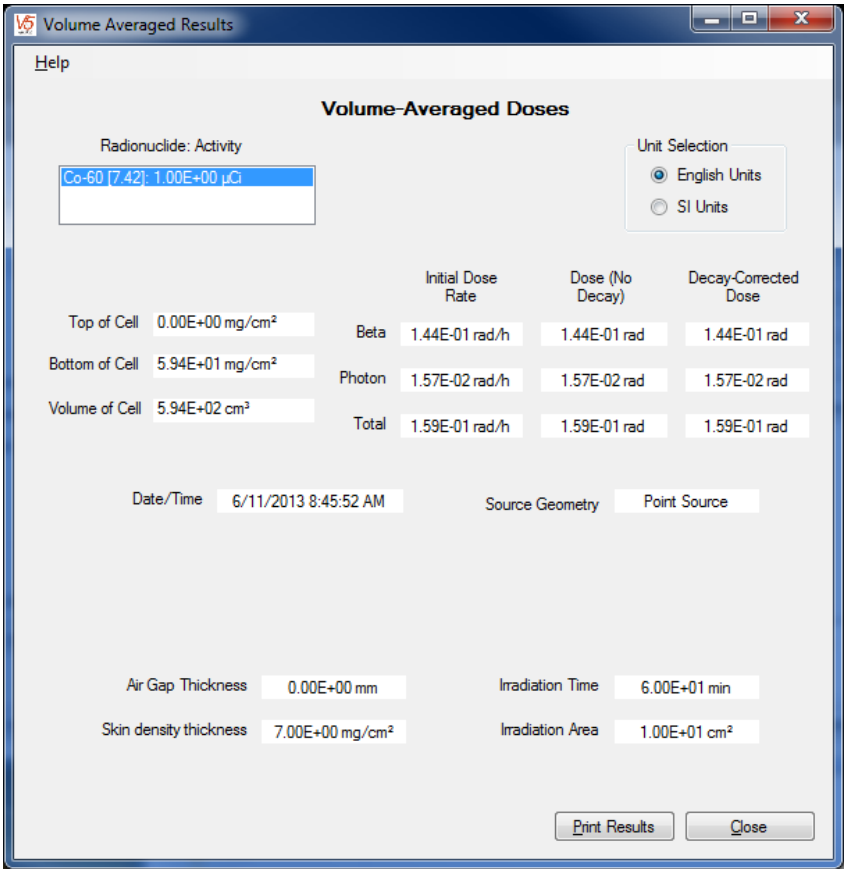

Figure 2-11 Results screen for a volume-averaged calculation

2.3 Exiting VARSKIN 5

The VARSKIN 5 code is exited from the main screen (Figure 2-1), either by clicking the "X" in the upper right corner or by selecting "Exit" from the File drop-down menu. Before exiting, the user is asked if the current input file is to be saved. When the "Yes" button is clicked, the user is asked to create a file name in which the input data will be saved so that the calculation can be recreated. Clicking the "No" button will cause the program to end without saving the current data. Clicking the "Cancel" button will return the user to the main screen.

Data from a saved file are stored with a *.vs3* extension. When a saved file is recalled (by selecting "Open" from the File drop-down menu), VARSKIN 5 reads the *.vs3* to obtain the data for the calculation. These are internal files, not intended to be used or edited by the user.

3 DESCRIPTION OF DOSIMETRY MODELS

VARSKIN 5 includes enhancements to the beta and photon skin dosimetry models which this chapter describes in detail. In addition, improvements to models throughout the VARSKIN series are incorporated in VARSKIN 5 and are also described here.

3.1 Beta Dosimetry

Dosimetry codes based on the dose-point kernel (DPK) method rely on the numerical integration of a point kernel over the source volume and dose region of interest. While this is computationally much faster than Monte Carlo simulation, accuracy is often sacrificed. In one way or another, all DPK's relate the dose at a given point to a radiation source at some other point in the same medium. The medium for which the DPK is defined is typically homogeneous water, as this allows for direct comparison with tissue. If the medium is not water, various scaling techniques (discussed in the sections that follow) can be used to quantify energy loss along the charged-particle track and to simulate the scatter of particle energy.

3.1.1 Dose-Point Kernels. Doses in VARSKIN 5.0 are calculated through numerical integration methods where dose-point kernels are integrated over the entire source volume and dose averaging area. The point kernel is given by

$$\dot{D}_{\beta}(r)\left[\frac{Gy}{\sec}\right] = \frac{1.6x10^{-10}\left[\frac{J\ \mathrm{g}}{MeV\ \mathrm{kg}}\right]\cdot A\left[\frac{dis}{\sec}\right]\cdot Y\left[\frac{\beta}{dis}\right]\cdot \overline{E_{\beta}}\left[\frac{MeV}{\beta}\right]\cdot F_{\beta}(\xi)}{4\pi r^{2}\cdot \rho\left[\frac{\mathrm{g}}{cm^{3}}\right]\cdot X_{90}\left[cm\right]}, \qquad [3.1.1]$$

where $F_{\beta}(\xi)$ is the Berger (1971) scaled absorbed dose distribution. The parameter ξ represents the density scaled distance (includes distances in the source cover, clothing, and air) from the source point to the dose point, written as a ratio with respect to the X_{90} distance. The distance r is the physical distance between the source point and the dose point. Berger's scaled absorbed dose distribution is based on Spencer's (1955, 1959) energy dissipation distribution, as detailed below.

Spencer (1955) used the moments method to numerically solve the electron transport equation in the steady state. His calculations were based on the following assumptions: (1) the electrons are in a homogeneous medium, extending in all directions around the source to a distance greater than the electron range; (2) range straggling due to large single-energy losses occurring in both the radiative and inelastic collisions are neglected; and (3) the electrons lose their energy continuously until their kinetic energy is completely exhausted. The last assumption yields the following expression for the residual range, r_0,

$$r_0 = \int_0^{E_0} \frac{dE}{dE/dr}, \qquad [3.1.2]$$

where E is the kinetic energy of an electron as it slows down, E_0 is the initial electron energy, and dE/dr is the average rate of energy loss, i.e., stopping power. Residual range was later called the 'continuous slowing down approximation' (CSDA) range.

Once the 'residual range moments' for electron flux, $I_0(r/r_0)$, were determined, Spencer (1955) calculated the energy dissipation distribution, $I(r)$, where r is the radial distance from an isotropic point-source at the center of a spherical volume. These two terms can be related using

$$I(r) = \frac{1}{r_0}\int_0^{r_0} dr\left(\frac{dE}{dr}\right) I_0(r/r_0). \qquad [3.1.3]$$

Equation [3.1.3] assumes that each electron contributing to the flux, $I_0(r/r_0)$, at r/r_0 dissipates energy at the average rate dE/dr per unit path length traversed. Spencer (1959) re-wrote the energy dissipation distribution such that it was a scaled, dimensionless function, $J(\mu)$,

$$J(\mu, E_0) = \frac{I(r)}{(dE/dr)_{E_0}}, \qquad [3.1.4]$$

where μ is the scaled distance of r/r_0, $(dE/dr)_{Eo}$ is the stopping power at E_0, and $I(r)dr$ is the average energy per electron dissipated in the spherical shell between r and $r+dr$. Spencer (1959) tabulated $J(\mu,E_0)$ for mono-energetic electron energies ranging from 0.025 to 10 MeV for scaled distance of μ at increments of 0.025μ up to 0.975μ.

Berger (1971) used Spencer's data to tabulate a 'scaled absorbed-dose distribution', F, for a number of radionuclides and monenergtic electrons in water. His tabulated kernels spanned 75 common beta-emitting radionuclide and monenergetic electron energies ranging from 0.025 to 4 MeV. Berger re-wrote Spencer's dimensionless energy dissipation distribution as

$$J(\mu, E_0) = 4\pi r^2 \frac{E_0}{(dE/dr)_{E_0}} \Phi(r, E_0), \qquad [3.1.5]$$

where $\Phi(r,E_0)$ is the 'specific absorbed fraction' and represents the fraction of energy deposited per gram at a distance r from a point-source. The quantity $4\pi\rho r^2\Phi(r,E_0)dr$ is the fraction of emitted energy that is absorbed in a spherical shell of radius r, thickness dr, density ρ, and is normalized such that

$$4\pi\rho\int_0^{\infty} r^2\Phi(r, E_0)dr = 1. \qquad [3.1.6]$$

As with Spencer (1959), Berger (1971) used a scaled distance when tabulating his data. Rather than using the CSDA range, he used the radial distance at which 90% of the emitted electron energy was deposited, X_{90}. His dimensionless scaled distance was written as $\xi = r/X_{90}$.
For mono-energetic electrons, Berger defined the relationship between the scaled absorbed-dose distribution and the specific absorbed fraction as:

$$F(\xi, E_0) = 4\pi\rho r^2 \Phi(r, E_0) \frac{dr}{d\xi} = 4\pi\rho r^2 X_{90} \Phi(r, E_0). \quad [3.1.7]$$

When a distribution of electron energies is considered, the specific absorbed fraction is given by

$$\Phi_\beta = \frac{1}{E_{av}} \int_0^{E_{\max}} E\, N(E) \Phi(x, E) dE, \quad [3.1.8]$$

where

$$E_{av} = \int_0^{E_{\max}} E\, N(E) dE. \quad [3.1.9]$$

The scaled absorbed dose distribution is then

$$F_\beta(\xi) = 4\pi\rho r^2 \Phi_\beta(r) \frac{dr}{d\xi} = 4\pi\rho r^2 X_{90} \Phi_\beta(r), \quad [3.1.10]$$

where X_{90} is determined from the beta-particle energy distribution.

Berger estimated his tabulated $F(\xi,E_0)$ values to have an accuracy of 4% or better at distance $r \leq 0.9X_{90}$ from the source. For $r > 0.9X_{90}$, the results are expected to be less accurate and to underestimate the absorbed dose. Similar results were expected for $F_\beta(\xi)$ with an accuracy of 4% or better at a distance $r \leq X_{90}$ from the source.

In VARSKIN 4, Spencer's energy dissipation distributions were coded into the SPENS function of SADCALC.f for a range of electron energies and radii. When called upon by the SADD subroutine, the SPENS function calculated the mono-energetic electron scaled absorbed dose distribution ($F(\xi,E_0)$) using Spencer's data with Eqs. [3.1.4] and [3.1.5]. The subroutine then used Eqs. [3.1.8] – [3.1.10] to calculate $F_\beta(\xi)$ for the beta-particle.

The development of Monte Carlo electron transport codes over the years has brought with it the tabulation of increasingly accurate electron and beta dose-point kernels. Energy deposition measurements in spherical shells of water centered on an isotropic point-source provide the physical information needed to reproduce the moment-based kernels used in VARSKIN 4. The main advantage of Monte Carlo-based energy deposition kernels over moment-based kernels is the ability to account for energy-loss straggling and provide more accurate results for $r > 0.9X_{90}$. VARSKIN 5 calculates $F_\beta(\xi)$ using the Monte Carlo-based energy deposition kernels ($I(r)$) described below, thereby replacing Spencer's (1955, 1959) moment-based energy dissipation distributions in the SPENS function.

The Monte Carlo transport code, EGSnrc, was used to determine the radial energy distributions (or DPK's) and X_{90} values at electron energies of 0.01 MeV ≤ E ≤ 8 MeV (32 total energies).

An isotropic mono-energetic point-source was positioned at the center of concentric spherical shells of the respective media. For all simulations, the shell thickness was 5% of the CSDA electron range, as taken from ESTAR of the National Institute of Standards and Technology (NIST). The last shell was at a radius 150% of the CSDA range to ensure complete absorption of the electron energy (excluding radiative-losses). The maximum energy of 8 MeV covers all beta-particle endpoint energies published in ICRP Publication 107 (2008). The minimum energy of 0.01 MeV is based on the 0.001 MeV lower limit of electron cross-section data available in EGSnrc. In addition, the ESTAR CSDA range of a 0.01 MeV electron is only 0.252 mg cm^{-2}.

The EGSnrc simulations were performed using the EDKnrc user code. The NRC (National Research Council, Canada) user code EDKnrc can be used to calculate Energy Deposition Kernels (EDK) for photons or electrons (mono-energetic or polyenergtic) forced to interact at the center of a spherical geometry (Rogers 2011). The code can output energy deposition kernels in user defined spherical shells. The number of particle histories was set to one million and transport parameters were set to default settings except that: (1) PEGS data sets used with AE=AP=1 keV; (2) ECUT=PCUT=1 keV; (3) Rayleigh scattering is turned on; and (4) bremsstrahlung cross sections are set to NIST.

PEGSs data sets are the material cross section data used by EGSnrc. The parameters of AE and AP determine the lowest energy for which the cross section values are defined. Generally, when AE and AP are lowered (minimum of 1 keV), the accuracy of the calculation increases; however the computation time (CPU) increases as well (Kawrakow and Rogers 2000). Electrons with energies below AE will not be transported and their energy will be assumed to deposit locally. The same is true for photons (AP). The parameters ECUT and PCUT are related to AE and AP in that when an electron/photon energy falls below ECUT/PCUT, its energy is assumed to deposit locally. It is not possible to set ECUT and PCUT below AE and AP, respectively. These two parameters represent the Δ value in restricted stopping powers.

Turning on the Rayleigh scattering parameter allows for the simulation of coherent scattering. Raleigh scattering for bremsstrahlung photons may become important below ~1 MeV for high-Z materials and below 100-200 keV in low-Z materials. The updated NIST database for nuclear bremsstrahlung is strongly recommended for electron energies below 1-2 MeV with negligible improvements over default Bethe-Heitles cross sections above ~ 50 MeV. Sampling from the NIST database is faster at low energies but slower at high energies (Kawrakow and Rogers 2000).

Once the energy deposition kernels were determined at CSDA range increments, the X_{90} values for each energy, were determined and the kernels were re-tabulated with respect to ξ. These kernels were then read into SADCALC.f for use in the SADD subroutine and SPENS function.

As stated previously, the main advantage of Monte Carlo-based energy deposition kernels over moment-based kernels is the ability to account for energy-loss straggling, thereby improving dose estimations with depth.
This is easily seen by plotting $F(\xi,E_0)$ values determined using both moment-based (VARSKIN 4) and Monte Carlo-based (VARSKIN 5) methods (Figure 3-1 and 3-2).

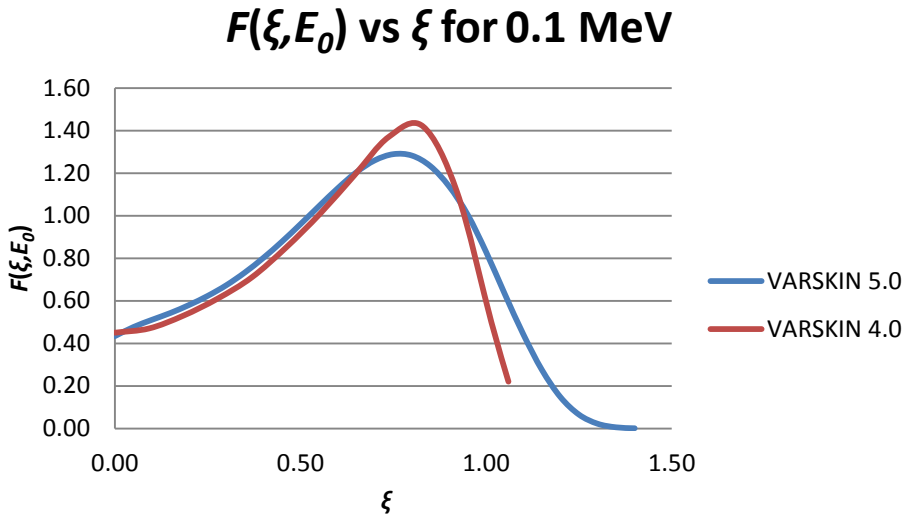

Figure 3-1. Scaled absorbed dose distributions for 0.1 MeV electrons in an infinite homogeneous water medium. VARSKIN 4.0 uses moment-based methods and VARSKIN 5.0 used Monte Carlo-based methods.

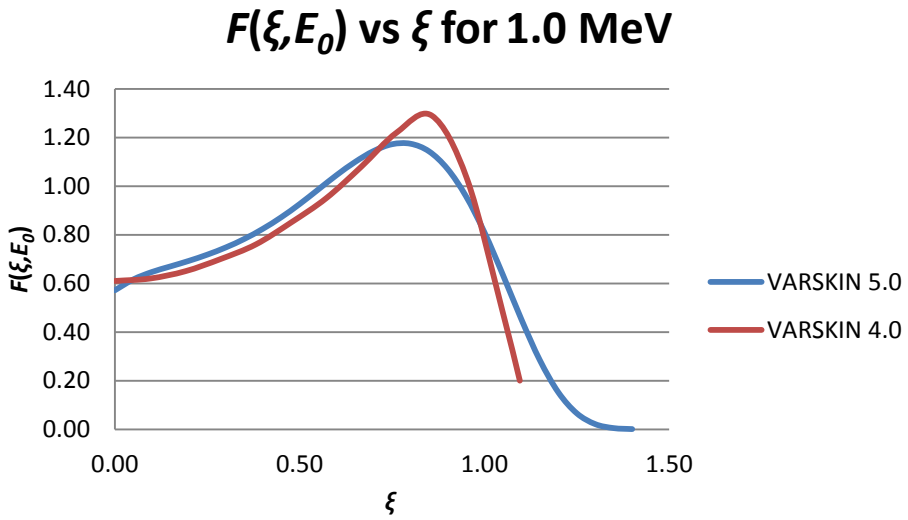

Figure 3-2. Scaled absorbed dose distributions for 1.0 MeV electrons in an infinite homogeneous water medium. VARSKIN 4.0 uses moment-based methods and VARSKIN 5.0 used Monte Carlo-based methods.

3.1.2 Numerical Integration of Dose-Point Kernels. DPK codes rely on an accurate and fast numerical integration method to calculate dose from a volumetric source to a given dose area. A typical integration process divides the source into very small sub-volumes (source points). The dose averaging area is divided into points at which the dose rate is to be calculated (dose points). The dose points (60 are used in VARSKIN 5) are positioned along the

radius of a dose-averaging disk at a specified dose depth (Figure 3-3). Since the source geometry (cylindrical is used for this discussion) is symmetric about the dose-averaging area, dose points represent concentric isodose circles that describe the radial dose profile at a given depth in skin.

For each of the 60 dose points, a numerical integration is performed over the area of the cylindrical source at a given height in the source represented by 8 elevations (*z*), 8 radii (*r'*), and 8 angular locations (θ). The dose rate at a dose point on an isodose circle of radius *d'* is evaluated using

$$\dot{D}(d') = S_v \int_0^{2\pi} \int_0^R \int_0^Z r' \; B(z, r', \theta) \; dz \; dr' \; d\theta, \qquad [3.1.11]$$

where $B(z,r',\theta)$ is the dose per disintegration (rad nt^{-1}) from a source point with source-coordinates (cylindrical) of *z*, *r'*, and θ, *R* and *Z* are the source radius and height, and S_v is the volumetric source strength (nt cm^{-3}). This procedure is repeated for each dose point beginning at the center of the irradiation area and extending to its edge. The dose rate averaged over an area at depth in the tissue is then calculated using

$$\bar{D} = \frac{2\pi \int_0^R \dot{D}(d') \; d' dd'}{\pi R^2}. \qquad [3.1.12]$$

where *R* is the radius of the dose averaging area.

The integration starts by choosing one of the eight elevation points (▲) in the source (Figure 3-3). At one of these elevations, one of eight concentric circles (radial source-points ●) is chosen. One of these circles is then subdivided into eight source-points at 45-degree angles from each other (angular source-points ★). Finally, the dose rate is calculated at each dose point from each of these eight source-points at a given elevation and radius. The contribution to the dose from the first four points is compared to the contribution of the last four points in a given circle. If the relative difference between the two contributions is less than 0.01 percent, then convergence of the integral for the circle is considered to be achieved, and the procedure is repeated at the next radial position. If the relative difference between the two contributions is greater than the relative error, each of the two contributions is further subdivided into eight additional source-points, and the above procedure is repeated for each of the two sets of eight points. This process, known as the Newton-Cotes eight-panel quadrature routine, provides a fast and accurate method of numerically integrating complex functions such as dose-point kernels (Durham 1992, 2006; Hamby 2011).

.

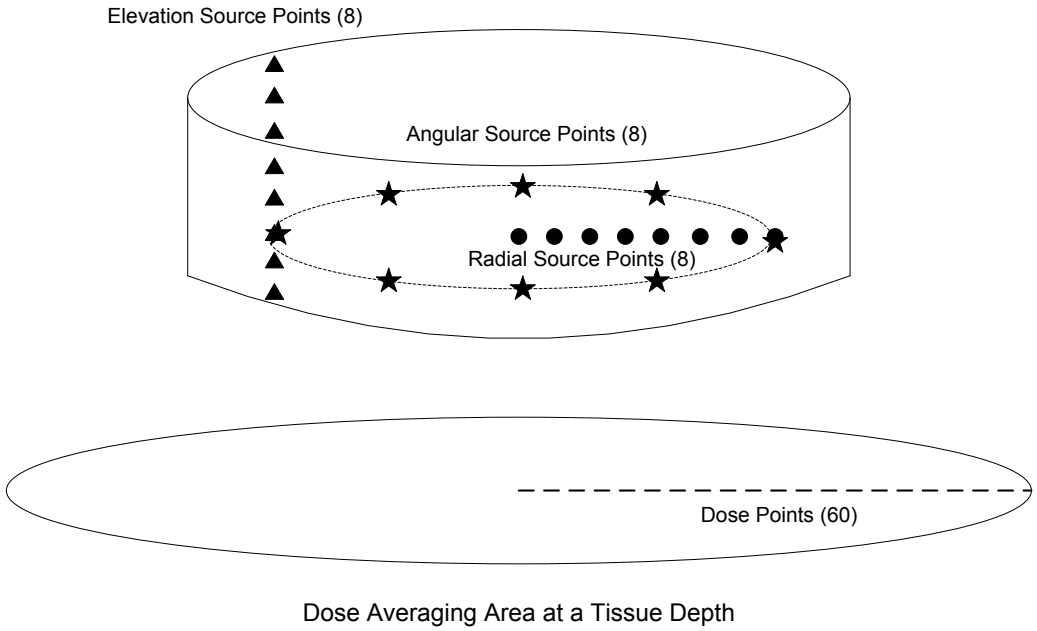

Figure 3-3. Schematic representation of the eight-panel quadrature routine used to calculate dose for a symmetric source (redrawn from Durham 2006).

3.1.3 Homogeneous Dose-Point Kernels. The Monte Carlo transport code, EGSnrc (Ljungberg 2012), was used to determine the radial energy distributions (or DPK's) and X_{90} values for $7.42 < Z \leq 94$ (Figure 3-5, Table 3-1) at electron energies of $0.01 \text{ MeV} \leq E \leq 8 \text{ MeV}$ (30 total values). An isotropic mono-energetic point-source was positioned at the center of concentric spherical shells of the respective media (Figure 3-4). For all simulations, the shell thickness was 5% of the CSDA electron range, as taken from the ESTAR software provided by the National Institute of Standards and Technology (NIST). The last shell was at a radius 150% of the CSDA range to ensure complete absorption of the electron energy (excluding radiative-losses). The maximum energy of 8 MeV covers all beta-particle endpoint energies published in ICRP Publication 107 (2008). The minimum energy of 10 keV was chosen considering the 1 keV lower limit of electron cross-section data available in EGSnrc. Additionally, the CSDA range of a 10 keV electron is nominally 2.5 microns in water.

Monte Carlo simulation with MCNP can be useful to determine energy deposition kernels when the ITS energy indexing algorithm is used and when special care is taken for high-resolution measurements. EGSnrc on the other hand, was not only shown to be step-size independent, but it is significantly faster at transporting electrons than MCNP. For example, MCNP requires 103 minutes of CPU time to measure energy deposition kernels for 1 MeV electrons in water (10^6 particle histories), whereas EGSnrc requires ~9 minutes for the same simulation. This difference becomes even larger as electron energy and material Z increases. For these reasons, EGSnrc is used as the Monte Carlo code of choice for all simulations pertaining to the scaling and scattering models.

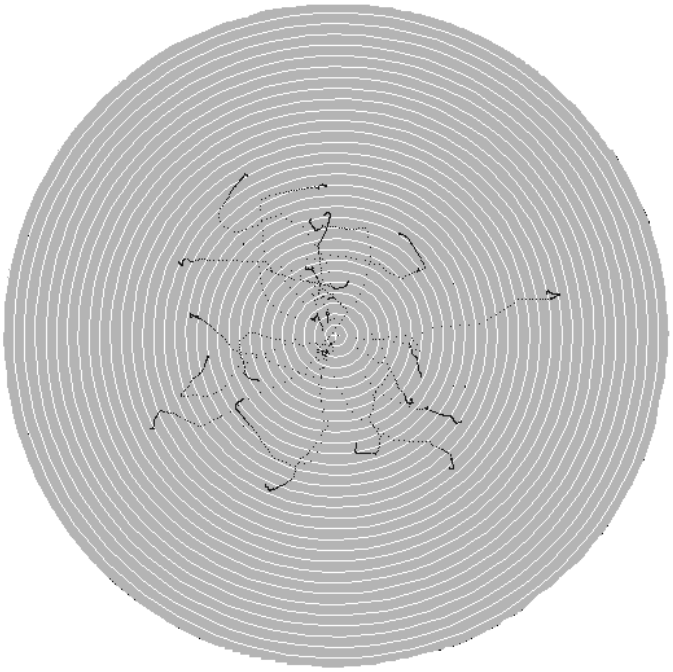

Figure 3-4. Schematic of EGSnrc geometry for determining point-source radial DPK's. Each shell thickness is 5% of the CSDA electron range. Total spherical radius is 150% of CSDA electron range. Simulated electron tracks are represented by the dark dotted lines.

Table 3-1. List of source materials used to develop the scaling model. Material selection covered a wide range of densities and atomic numbers.

Element	*Z*	Density (g cm^{-3})	Element	*Z*	Density (g cm^{-3})
Aluminum	13	2.70	Barium	56	3.59
Titanium	22	4.54	Neodymium	60	7.01
Iron	26	7.87	Gadolinium	64	7.90
Gallium	31	5.91	Ytterbium	70	6.90
Rubidium	37	1.63	Tantalum	73	16.65
Zirconium	40	6.51	Platinum	78	21.45
Ruthenium	44	12.37	Lead	82	11.35
Silver	47	10.50	Actinium	89	10.07
Tin	50	7.31	Plutonium	94	19.84

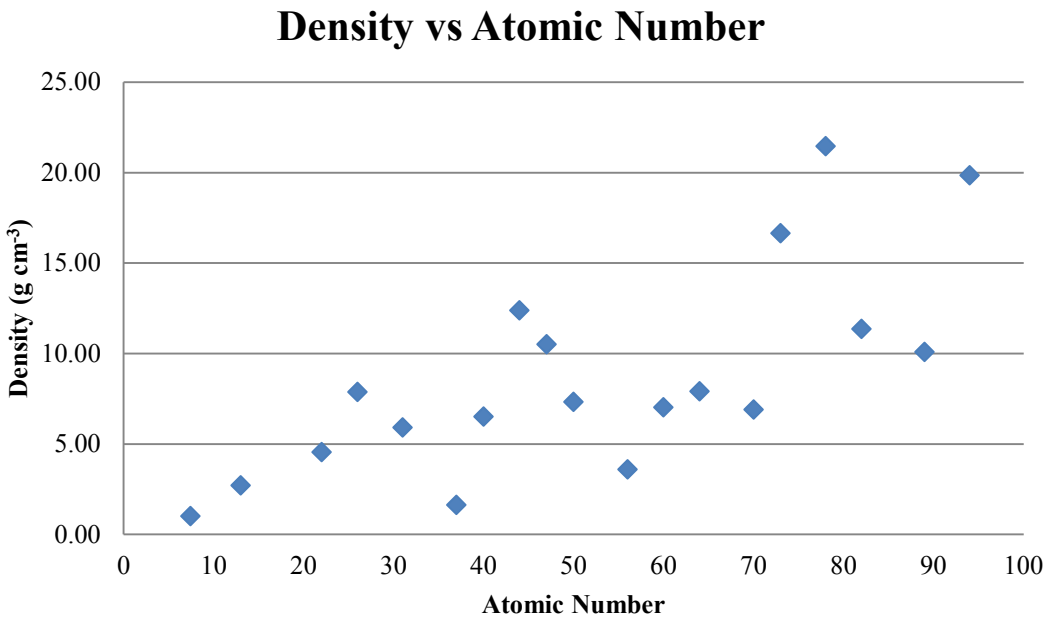

Figure 3-5. Plot demonstrating the wide range of densities and atomic numbers used in development of the scaling model. All materials were solid in nature (except water).

EGSnrc simulations were performed using the EDKnrc user code. The NRC (National Research Council, Canada) user code EDKnrc can be used to calculate Energy Deposition Kernels (EDK) for photons or electrons (mono-energetic or polyenergtic) forced to interact at the center of a spherical geometry (Rogers 2011). The code can output energy deposition kernels in user defined spherical shells.

3.1.4 Non-Homogeneous Dose-Point Kernels. Non-homogeneous point-source DPK's also were determined for $7.42 < Z \leq 94$ at $0.01 \text{ MeV} \leq E \leq 8 \text{ MeV}$ using EGSnrc Monte Carlo simulations using identical transport parameters. The intent of calculating non-homogeneous DPK's is to determine how energy is deposited in water spherical shells after a mono-energetic electron has been emitted from the center of a sphere composed of some medium other than water.

3.1.5 Beta-Particle Dose-Point Kernels. The end goal of the scaling model is the determination of non-homogeneous DPKs from homogeneous DPKs for beta-emitting radionuclides. By determining the depth and energy-scaling parameters for all energies between 0.01 and 8 MeV, it is possible to determine the non-homogeneous beta DPK for any known beta energy spectrum. This is accomplished by integrating over the beta energy spectrum for each source *Z*/thickness using

$$\Phi_{\beta}(R,Z,\rho) = \frac{1}{E_{av}} \int_{0}^{E_{\max}} ESP(R,E,Z,\rho) E\ N(E) \Phi(r,E) dE, \qquad [3.1.13]$$

where r is the *DSP*-adjusted spherical shell radius, E_{max} is the endpoint energy of the beta spectrum, $N(E)dE$ is the fraction of beta-particles emitted per MeV per disintegration that have energies between E and $E+dE$, and

$$E_{av} = \int_0^{E_{\max}} E\, N(E) dE. \qquad [3.1.14]$$

For example, if the nuclide and source material in question are ^{60}Co and iron, the scaling parameters are used to create an n x m array of DPK's for ^{60}Co with source radii ranging from 0 to $a \cdot X_{90}$ of iron and the water radii ranging from 0 to $b \cdot X_{90}$ of water. The parameter a will be based on complete beta-energy absorption in the source material and b will be based on complete beta-energy absorption in water when the source thickness is zero.

Non-homogeneous beta-particle DPK's were determined by incorporating scaling equations into SADCALC. The SADCALC routine utilizes ICRP Publication 107 (2008) beta-particle spectra to calculate homogeneous water DPK's for each beta-particle present in a given dose calculation. Linear interpolation was used to accommodate all source media with $7.42 \leq Z_{eff} \leq 94$.

Non-homogeneous DPK's were calculated for a wide range of beta energies (Table 3-2) and source materials (Table 3-3). Stainless steel and uranium oxide were chosen as they represent common hot particle materials, and tungsten alloy was chosen to demonstrate the model's ability to handle high-density media.

Table 3-2. List of nuclides used in scaling and scattering models.

Nuclide	$\bar{E}$ (MeV)	X_{90} (cm)
^{60}Co	0.0958	0.033
^{90}Sr	0.196	0.083
^{210}Bi	0.307	0.212
^{135}I	0.375	0.239
^{89}Sr	0.583	0.321
^{32}P	0.695	0.363
^{56}Mn	0.832	0.634
^{90}Y	0.934	0.533
^{144}Pr	1.217	0.696

Table 3-3. Source materials used for non-homogeneous beta-particle DPK testing.

Alloy	Z_{eff}	Density (g cm^{-3})
Stainless Steel (SS_302)	25.81	8.06
Tungsten Alloy (Mallory2000)	72.79	18.00
Uranium Oxide	87.88	10.96

3.2 Backscatter Model

A volumetric backscatter model has been developed for VARSKIN 5 to predict the dose perturbations from both source and atmospheric backscattering. The model is applicable for beta-emitting radionuclides in a spherical, cylindrical and slab source geometry, and for source materials with $7.42 < Z_{eff} \leq 94$. Being based on the dose-point-kernel (DPK) concept, VARSKIN 5 relies on the numerical integration of a point kernel over the source volume and the dose region of interest. The medium for which the DPK is defined is typically water, thus allowing for direct comparison with tissue. While the electron scattering contribution has been studied extensively for medical physics applications, it has been limited to point-source assumptions in the past, yet has been expanded to volumetric sources for use in VARSKIN 5. In addition to internal source scatter, electron scattering must also be considered in the medium surrounding the source (i.e., atmospheric scattering).

Inherent to the development of beta DPK's is the assumption of an infinite homogeneous medium. While scaling methods are used to account for the non-homogeneous media which transmit the beta-particles, an additional adjustment is required to correct for the lack of atmospheric scattering in the non-existent water medium. For example, when a DPK is applied to a point-source on an air-water interface, the isotropic nature of DPK's assumes that betas emitted away from the source point have the ability to backscatter in an infinite homogeneous water medium and possibly contribute to the energy deposition at the dose point of interest. This scenario is of particular importance for hot particle skin dosimetry.

In developing the new beta dosimetry model for VARSKIN 5, point-source planar dose profiles were determined using EGSnrc Monte Carlo simulations for the scattering media of water, air, and source materials with $7.42 < Z_{eff} \leq 94$ at electron energies of $0.01 \text{ MeV} \leq E \leq 8 \text{ MeV}$. The planar dose volumes were 1 mg cm^{-2} thick, with a maximum normal depth of 1000 mg cm^{-2}. The dose averaging areas were 1 cm^2 and 10 cm^2, consistent with the monitoring areas recommended by ICRP Publication 103 (2007) and NCRP Statement No. 9 (2001), respectively. The scattering medium was assumed infinite (>> electron range) in both thickness and lateral extent. Pertinent details of EGSnrc can be found in Mangini (2012).

In general, a backscatter factor is found by taking the ratio of the planar dose when the scattering material is present (non-homogeneous case) to that when water is present (homogeneous case). Air scattering corrections are often inversely reported such that they are greater than or equal to one (Cross 1991b, 1992c). Regardless, these backscatter factors will be dependent on electron energy, backscattering medium Z, normal depth, and dose averaging area.

When applied to a beta-emitting nuclide, the backscatter factor for a given dose averaging area takes the form of

$$B_\beta(Z,z) = \frac{\int_0^{E_{\max}} D_{A,S}(Z,z,E)N(E)dE}{\int_0^{E_{\max}} D_W(z,E)N(E)dE}, \qquad [3.2.1]$$

where z is the normal depth, D_W is the dose in the water-water geometry, $D_{A,S}$ is either the dose in the air-water geometry or the dose in the source-water geometry, and $N(E)dE$ is the fraction of beta particles emitted per MeV per disintegration that have energies between E and $E+dE$. Surface functions was used to determine mono-energetic electron planar dose profile curve fits for use in Eq. [3.2.1]. Once planar dose profile curve fits were determined, they were implemented into SADCALC. The ICRP 107 beta spectra were then used to calculate the beta-particle backscatter factor of Eq. [3.2.1]. Linear interpolation was used for all $7.42 < Z \leq 94$.

It is important to remember that it is not possible to determine the absolute volumetric backscatter factor using the same procedures as point-sources. This is due to the largely different attenuation properties of air and water and their impact on the respective dose calculations. Therefore, a number of assumptions and estimations must be made.

The method is based on a selective integration process over the entire source volume. Rather than applying an overall correction factor to final dose calculations, scattering corrections are applied at each step of the numerical integration of dose. If desired, the 'volumetric' correction factor could then be determined by taking the ratio of overall dose with the applied point-source scattering corrections to the overall dose without. Selection criteria are used to determine the proper type and amount of scattering correction for which to account. Scattering corrections are broken down into three components: source-water interface corrections (for the top and bottom of the source), air-water interface corrections (for both the top and the sides of the source), and air-source interface corrections (for the sides of the source).

During the numerical integration process for an 'infinitely large' source (dimensions > range of beta-particle), only source points positioned directly at the source-water interface (i.e., source-skin interface) will require the full application of the source-water scattering data (Figure 3-6). Source points positioned above this interface (Figure 3-7) require a more advance treatment. In this case, there is expected to be an increase in the energy absorption (i.e., dose) from downward scattering taking place in the upper portion of the source, as well as a decrease in dose from upward scattering in the lower portion of the source. If the contribution from downward scattering is greater than the contribution from upward scattering, the dose will be increased for that source-point kernel. Likewise, when the upward contribution is greater, the dose will be decreased. It can be seen from this argument that when the source point is at the top of the source, the application of both air-water and source-water correction results in an effective air-source correction.

Scattering contributions from both upward and downward scattering are determined using Eq. [3.2.2]. The scattering material thicknesses for the top and bottom of the source are given by the normal distances from the source-point to the upper- and lower-most points of the source, respectively. The source backscatter correction factor (BSCF) is then determined by multiplying net scattering effectiveness by the beta-particle source-water scattering correction for point-sources;

$$Source\ BSCF_{top/bottom} = SW(SE_{top} - SE_{bottom}), \qquad [3.2.2]$$

where *SW* is the beta-particle source-water scattering correction for point-sources, SE_{top} is the scattering effectiveness for the top portion of the source, and SE_{bottom} is the scattering effectiveness for the bottom portion of the source. The 'skin depth' at which the scattering factor is determined takes into account the normal density thickness of both the source and tissue through which the beta-particle must traverse.

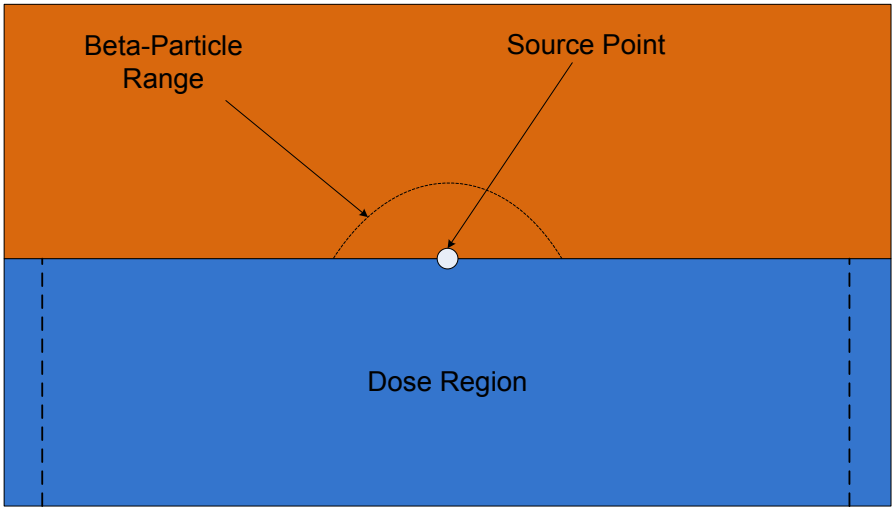

Figure 3-6. Schematic demonstrating conditions in which full source-water scattering corrections are applied. The dimensions of the source (orange) are greater than the range of the beta-particle.

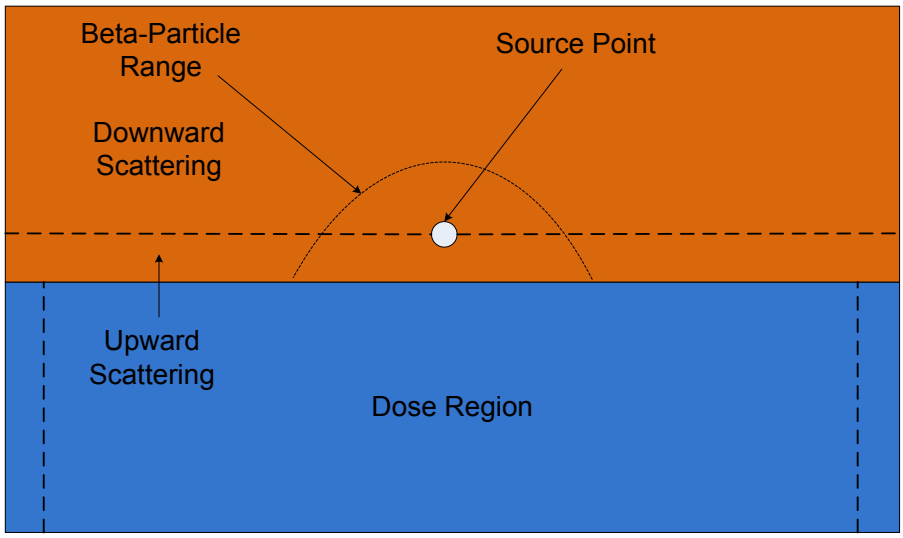

Figure 3-7. Schematic demonstrating conditions in which partial source-water scattering corrections are applied. The lower portion of the source causes upward scattering away from the dose region and the upper portion of the source causes downward scattering towards the dose region.

The point-source factors were developed with the assumption that the source medium is infinite in both height and lateral extent. As such, application to source points near or on the side of the source jeopardizes the accuracy of the results. However, approximations can be made in order to estimate source-scatter corrections for the sides of the source.

When the dimensions of the source are larger than the range of the beta, source points toward the center and the top-center of the source have minimal impact on dose. Therefore, source-points on both sides and the bottom of the source become more important. It is estimated that scattering contributions from the sides of the source will reach a maximum when the scattering media thickness is 1.0 X/X_{90} and greater. Linear interpolation is used for X/X_{90} values less than 1.0.

Unlike source scattering for the top and bottom of the source, during the numerical integration process, the direction of the beta-particle needs to be considered when correcting for side scatter. Side scattering should only be accounted for when the beta-particle's path is directed away from the source and travels through air prior to reaching the dose region. The assumption is that a beta-particle emitted in the 180 degree opposite direction would be permitted to backscatter off of the source's side and still contribute to dose.

The amount of source material directly above the source point (considered the 'lateral' dimension in this case) will also have an impact on the scattering effectiveness. If the source point is located on the very top corner of the source, the probability of a backscattering event toward the dose region is greatly decreased. On the other hand, if the source point is at the very bottom corner of the source, the probability of backscattering event toward the dose region is much greater.

It is estimated that the normal distance to the upper most point of the source must be greater than 0.5 X/X_{90} (or ½ of the 'height' requirement) in order to have 100% scattering effectiveness from the top portion of the source. Therefore, the net scattering correction is given by,

$$Source\ BSCF_{side} = SA\frac{X_{top}}{0.5}(X_{op\_side} - X_{side}), \qquad [3.2.3]$$

where *SA* is the beta-particle source-air scattering correction for point-sources (ratio of source-water to air-water correction factor), X_{side} is the normal distance to the side of the source that the beta travels through, X_{op_side} is the normal distance to the opposite side of the source, and X_{top} is the normal distance to the top of the source. All distances are in terms of X/X_{90}. If X_{top} is greater than 0.5, full scattering correction is applied by setting X_{top} equal to 0.5. Similarly, if X_{side} or X_{op_side} are greater than 1.0, they are set equal to 1.0.

As the energy of the beta-particle decreases and the scattered path angle relative to the air-water interface increases, the probability of the scattered beta depositing energy in the dose area greatly decreases (Figure 3-8). Conversely, high-energy betas are expected to have a contribution extending to the very edge of the dose area when scattered beta-particles enter the dose region at high incident angles. It is assumed that the scattering correction from the top and bottom of the source does not accurately account for such contributions due to its inherent geometry. Without knowing the angle at which a particular beta backscatters and likely enters the dose region at each stage of the integration process, it is very difficult to correctly apply this additional correction factor. Therefore, the angle of incident (Figure 3-9) is used to estimate the frequency at which large angle scattering events occur. The side-scattering correction is only applied when the incident angle is greater than 70 degrees and when the density corrected path length (includes source and air) to the edge of the dose region, or the maximum scattered beta path length, is less than the beta-particle X_{90} distance. The latter limitation prevents the side-scatter correction from being applied to low-energy beta-particles, where this form of scatter is believed unlikely (as explained above).

As with scattering from the top/bottom of the source, the 'skin depth' at which the scattering factor is determined takes into account the normal density thickness of both the source and tissue through which the beta-particle must traverse.

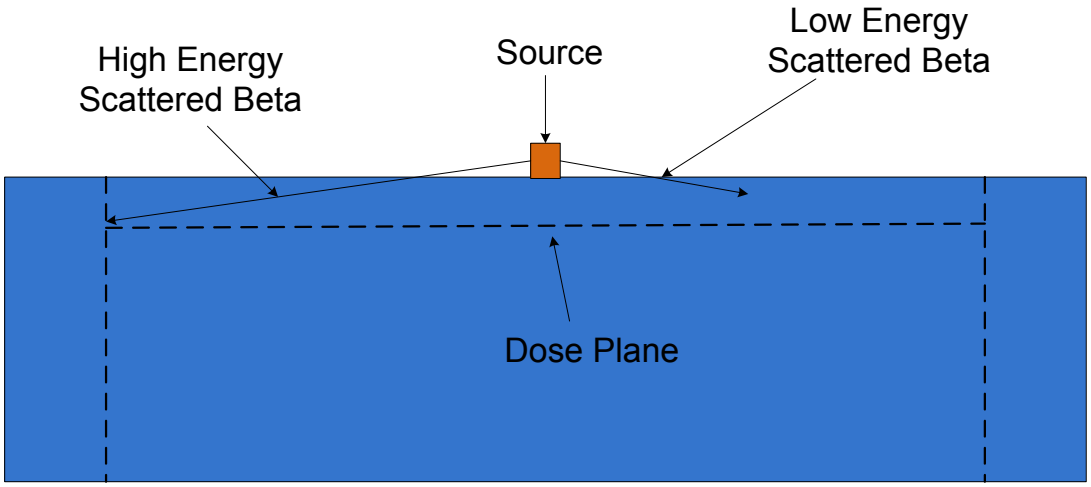

Figure 3-8. Schematic illustrating beta energy limitations of side-scatter corrections. Both scattering paths assume the same incident angle.

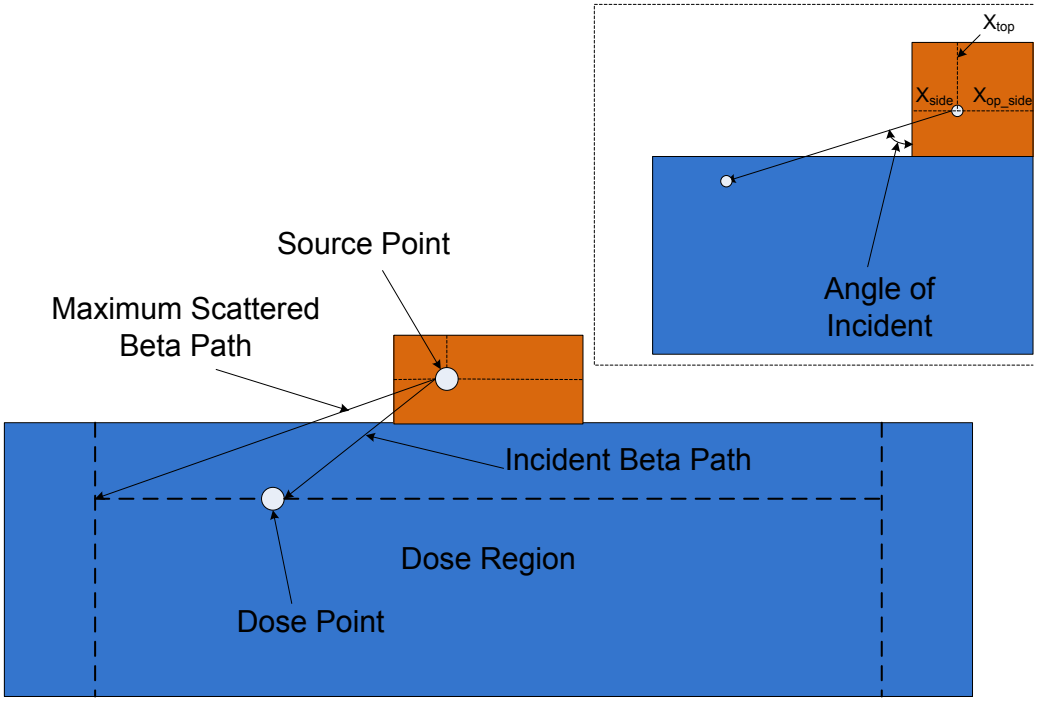

Figure 3-9. Schematic illustrating parameters used to determine the amount of side-scatter correction applied to high-energy beta-particles emitted from large sources.

The application of air-water interface scattering correction factors is more difficult than with a source-water interface. In order to estimate the scattering effectiveness when source material is present between the air-water interface, simple linear interpolation is used.

The two extreme cases are when there is no source material between the air and water boundaries (Figure 3-10) and when the path length out of the top or sides of the source is equal to or greater than the range of the beta. The scattering effectiveness would be 100% and 0%, respectively. The assumption is that if a backscattered beta-particle can escape the source, there is a chance that a dose-contributing scatter event may still occur if water were surrounding the source. This is seen as a conservative estimate as a beta-particle that travels 1.8 X/X_{90} (range estimate, Durham 2006) out of the top of a source will theoretically not be able to backscatter and contribute to dose at any depth.

The overall air BSCF is found using a weighted average. The BSCF's are calculated for all surfaces for which the beta-particle can escape and reach air. Scattering contributions from the top of the source receive a 50% weight and the remaining 50% is evenly divided among the sides of the source. For cylinders and spheres, the shortest distance to the outer surface and the 180 degree opposite distance represent the two side distances (Figure 3-11). For slabs, four sides are used: the normal distances to the *x*-coordinate sides and the normal distances to the *y*-coordinate sides. The scattering reductions (for cylinders and spheres) are therefore given by

$$Air\ BSCF_{top} = AW\ \ 0.5\frac{1.8 - X_{top}}{1.8}, \qquad [3.2.4]$$

$$Air\ BSCF_{side} = AW\ \ 0.25\frac{1.8 - X_{side}}{1.8}, \qquad [3.2.5]$$

and

$$Air\ BSCF_{op\_side} = AW\ \ 0.25\frac{1.8 - X_{op\_side}}{1.8}, \qquad [3.2.6]$$

where AW is beta-particle air-water scattering correction for point-sources, X_{top}, X_{side}, and X_{op_side} are the distances to the top and sides of the source in terms of X/X_{90}.

Unlike the source scattering corrections, no depth adjustments need to be made for materials traversed by the beta-particle prior to entering the dose region. This is due to the fact that corrections are being made for scattering events occurring outside the source. The distance to the air-water interface is considered negligible in terms of beta attenuation (assumed to be completely air). The overall air scattering correction is found by summing the three components above.

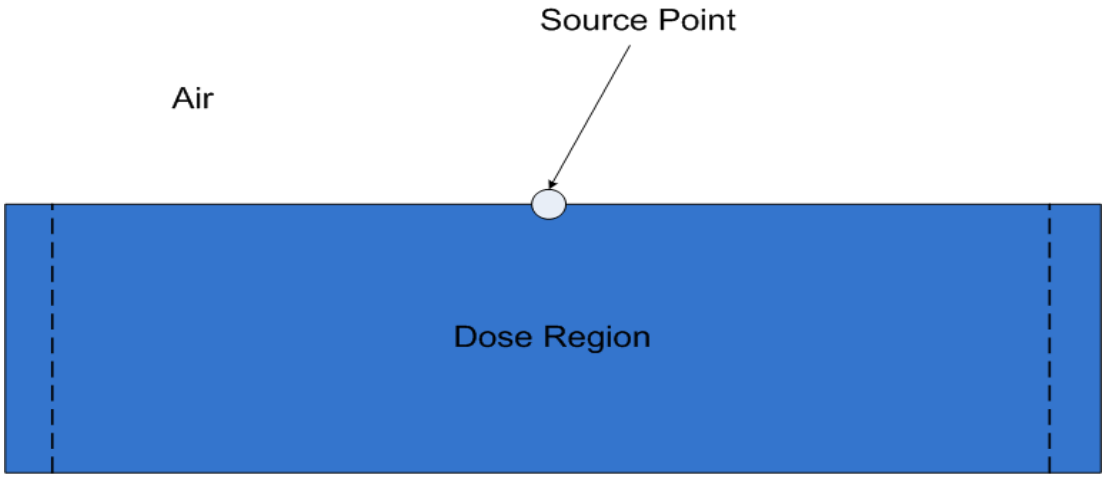

Figure 3-10. Schematic demonstrating conditions in which a full air-water scattering corrections are applied.

All profiles were fit with a 28-parameter Chebyshev Series (LnX-Y, Order 6). While this is a complex fit equation, it allowed for all curves to be fit with the same functional form and a high goodness of fit (R^2 > 0.999). As an example, a second-order Chebyshev is given by,

$$Z = a + bT_1(x') + cT_1(y') + dT_2(x') + eT_1(y') + fT_2(y'), \qquad [3.2.7]$$

where,

$$x' = \ln(x) = \ln(Normal\ Depth\ (cm)) \quad \text{scaled -1 to +1},$$
$$y' = y = \ln(E\ (MeV)) \quad \text{scaled -1 to +1},$$
$$T_n(x') = \cos(n * a * \cos(x')),$$

and Z is the square root of the dose rate per particle (Gy Bq^{-1} s^{-1}).

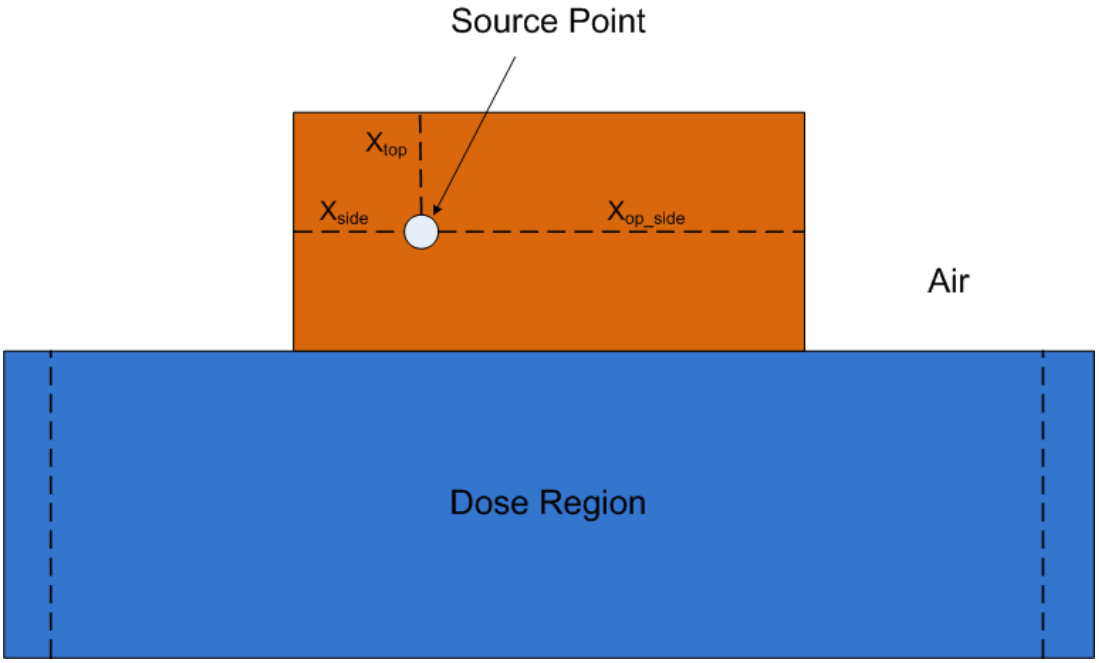

Figure 3-11. Schematic demonstrating conditions in which air-water scattering corrections are applied. When the distance to the top and sides of the source are less than 1.8*X_{90}, a partial air-scattering correction is applied.

3.3 Scaling Models

The DPK scaling model consists of two parameters: a depth-scaling parameter (*DSP*) and an energy-scaling parameter (*ESP*).

3.3.1 Depth Scaling. The depth-scaling model begins with determining the range of the electron in both the homogeneous and non-homogeneous geometries. Given the difficulty of determining an absolute electron range due to energy straggling and a torturous path, the radius at which 99.0% energy deposition occurred was chosen as a range estimate. The difference in ranges between the homogeneous and non-homogeneous data is therefore attributed to the absorption sphere in the non-homogeneous case. For a given absorption radius, the resulting difference in ranges is called the depth-scaling parameter,

$$DSP(R, E_0, \rho, Z) = X_{99\_H} - X_{99\_NH}, \quad [3.3.1]$$

where X_{99_H} is the homogeneous electron range, X_{99_NH} is the non-homogeneous electron range, ρ and Z are the absorption material density and atomic number, respectively.

As an example, consider an iron spherical source (r = 0.0222 cm, Z = 26, ρ=7.874 g cm^{-3}) and an electron energy of 1 MeV. The radius of the iron sphere was chosen to be 0.5X_{90} to allow for sufficient electron self-absorption. Due to the presence of the 0.0222 cm of iron, the electron range in the non-homogeneous shells is 0.120 cm less than the homogeneous range (Figure 3-12). Therefore, for a 1 MeV electron traversing 0.0222 cm of iron, the depth-scaling parameter

will be 0.120 cm. Shifting the homogeneous DPK data to the left by this amount will equate the ranges and provide the necessary depth adjustment (Figure 3-13).

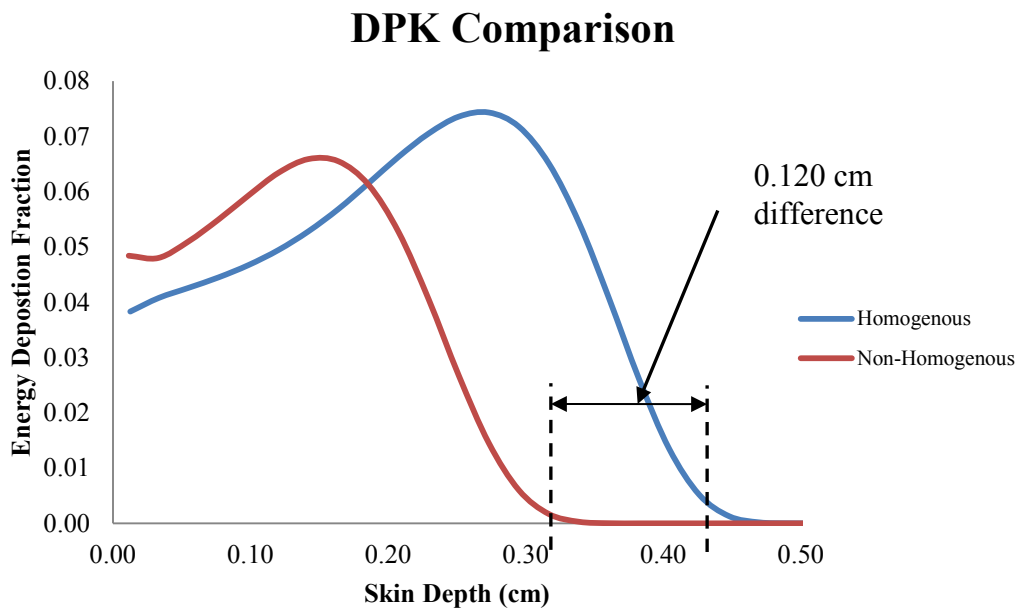

Figure 3-12. Comparison of 1 MeV electron DPK's for the homogeneous water case and the case when the electron traverses iron source material of thickness 0.0222 cm.

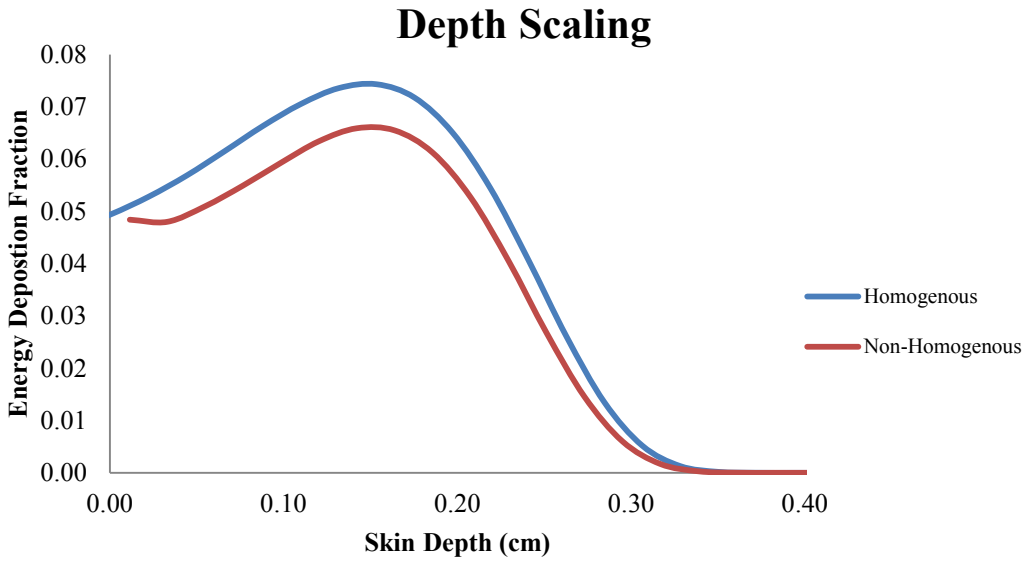

Figure 3-13. Example of depth scaling on the homogeneous DPK curve. The depth-scaling parameter was determined to be 0.120 cm.

When plotted together, the variability with respect to *Z* is difficult to discern as they all follow the same curvature with little separation (Figure 3-14). The variation in *DSP*'s at small radii is greatest with essentially no variability at large radii. Each curve is linear with a slope near unity. This is expected since density thickness is often used to estimate "water equivalent" path length for electrons in non-aqueous media (Cho 2004). The small *Z* dependence, coupled with 18 curve fits, allows for accurate interpolation for any $7.42 < Z \leq 94$.

All curve fits for the *DSP*'s took the form of

$$LN(DSP\ (cm)) = \frac{(a + bx + cx^2 + dx^3 + ey)}{(1 + fx + gx^2 + hx^3 + iy)}, \qquad [3.3.2]$$

where *x* is *LN*(*E* (*MeV*)) and y is $LN(X_x{*}\rho_x\ (g\ cm^{-2}))$. The terms X_x and ρ_x refer to the radius and density of the absorption sphere. The form of Eq. [3.3.2] was chosen because it was the equation that had the largest R^2 value (≥0.9999) and was able to fit all 18 plots. The fit parameters for each function demonstrated a slight *Z* dependence.

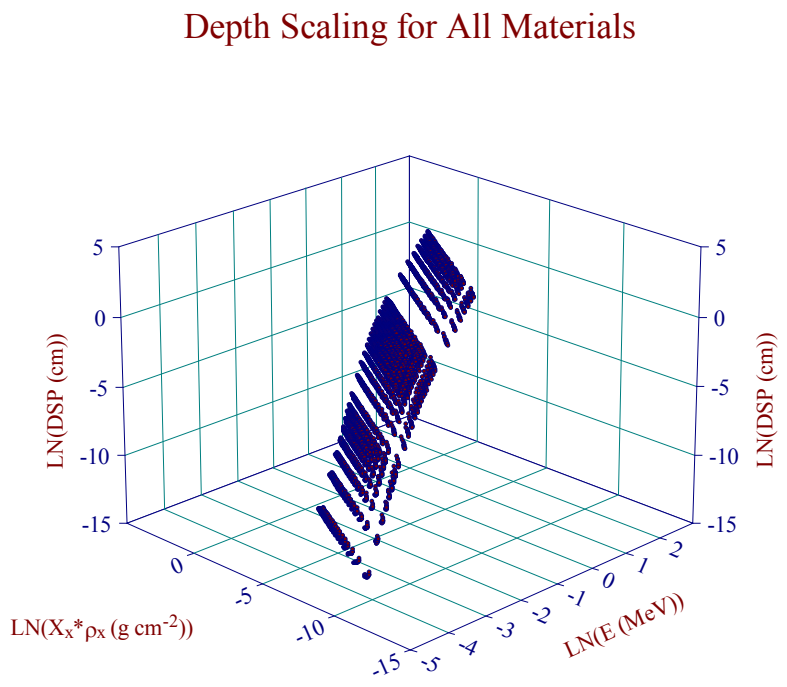

Figure 3-14. TableCurve 3D plot of depth-scaling data for all source materials used in scaling model.

3.3.2 Energy Scaling. The energy-scaling parameter is a direct result of energy conservation at distances within the electron's maximum range, or X_{99} (neglecting radiative loses beyond this distance). Once the homogeneous curve is shifted according to the depth-scaling parameter

(Figure 3-13), the total energy deposition is found for each case. This is performed by summing the homogeneous DPK's for radii between the depth-scaling parameter and the X_{99} distance,

$$4\pi\rho \int_{DSP}^{X_{99}} r^2 \Phi(r, E_0) dr = E_{total}. \qquad [3.3.3]$$

Similarly, the total energy deposition in the non-homogeneous case is found by summing DPK's from 0 to X_{99}. The law of energy conservation requires the two be equal. Therefore, the energy-scaling parameter is found by taking the ratio of the non-homogeneous total to the homogeneous total,

$$ESP(R, E_0, \rho, Z) = \frac{4\pi\rho \int_{0}^{X_{99}} r^2 \Phi_{NH}(r, E_0) dr}{4\pi\rho \int_{DSP}^{X_{99}} r^2 \Phi_{H}(r, E_0) dr}. \qquad [3.3.4]$$

Applying the resulting ratio to the homogeneous DPK equates the total energy depositions in the two geometries. For the example, an energy-scaling parameter of 0.887 is computed. Thus, energy conservation is achieved by multiplying the homogeneous curve by the energy-scaling parameter of 0.887 (Fig 3.3.4).

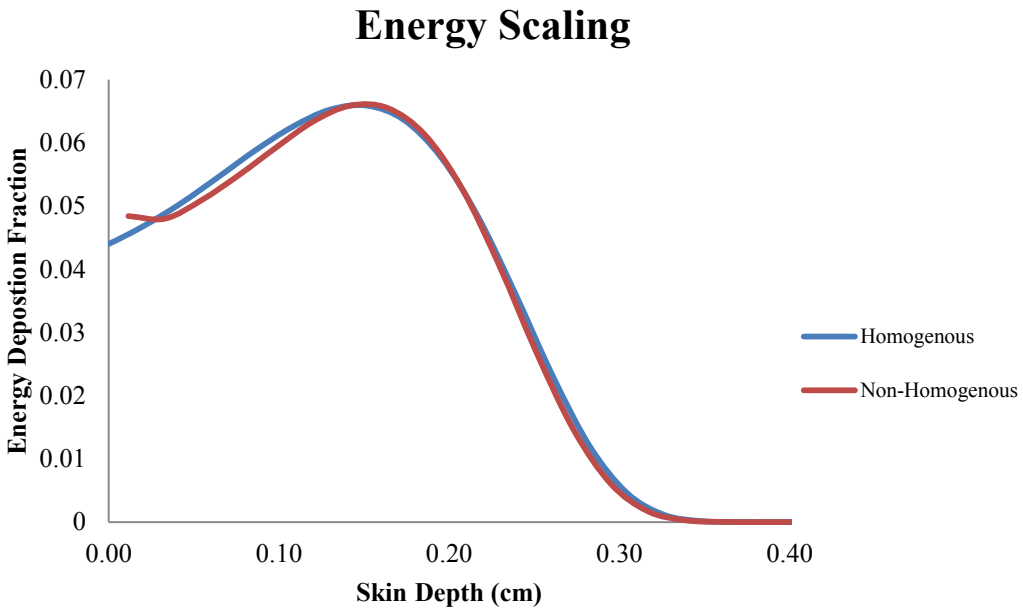

Figure 3-15. Example of energy scaling on the homogeneous DPK curve presented in Figure 3-14. The energy-scaling parameter was determined to be 0.887.

As with the case of depth scaling, the natural logarithm of energy was used to decrease variability over the range of energies examined. The variability associated with the absorption-

sphere radius was minimized by expressing it as a ratio of density thickness to the X_{90} distance in water, $X_x*\rho_x$ / X_{90w}. The natural logarithm of the depth-scaling parameter multiplied by the initial electron energy, $LN(ESP*E_0)$, was chosen as the dependent variable. While the quantity of $ESP*E_0$ has no physical meaning, using it as the dependent variable produced tighter fitting surface plots than simply using *ESP*. Since E_0 is a known quantity, solving for *ESP* is simple.

The variability of the *ESP* curves (Figure 3-16) with respect to *Z* is more pronounced than the *DSP* curves. The variation of *ESP*'s becomes quite large as the absorption-sphere radius increases. As *Z* approaches that of water (Z_{eff} of 7.42), the *ESP* approaches 1.0, as expected. As *Z* increases, the amount of energy reduction following depth scaling increases. Once again, this is expected given the lower profile of high-*Z* non-homogeneous DPK curves for the same absorption-sphere radius (with respect to X/X_{90}). Despite this increased variability, interpolation within surface plots is not seen as an issue.

All curve fits for the *ESP*'s took the form:

$$LN(E*ESP\ (MeV)) = \frac{(a+bx+cx^2+dx^3+ey+fy^2)}{(1+gx+hx^2+iy+jy^2)} \qquad [3.3.5]$$

where *x* is *LN*(*E* (*MeV*)) and *y* is $X_x*\rho_x$ / X_{90w}. The terms X_x and ρ_x refer to the radius and density of the absorption sphere. The above equation was chosen because it was the equation that had the largest R^2 value (≥0.999) and was able to fit all 18 plots. As with the *DSP*'s, fit parameters demonstrated a slight *Z* dependence.

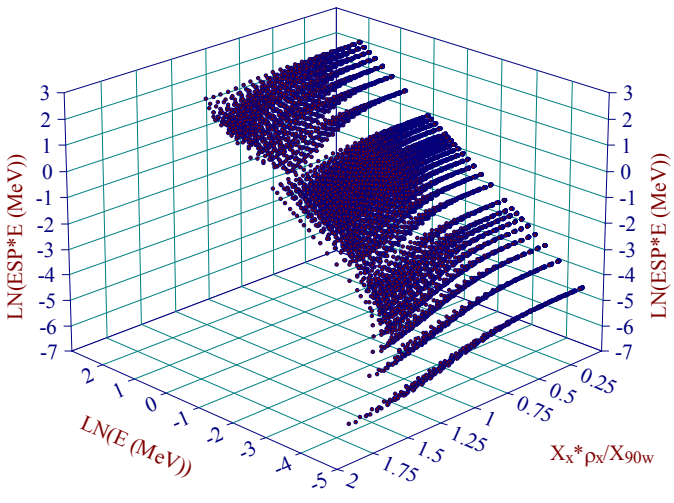

Figure 3-16. TableCurve 3D plot of energy-scaling data for all source materials in scaling model.

Integration of scaling parameters over a particular beta spectrum provides the non-homogeneous DPK for a given source thickness. Comparisons with EGSnrc non-homogeneous DPKs demonstrated excellent agreement over a range of beta-particle energies and high-*Z* source materials by producing nearly identical DPK's for all absorption-sphere radii. In addition, when compared to Cross' (1967, 1968, 1982, 1992a) scaling model and density scaling, the ability to account for spectral hardening is clearly shown. This is in large part due to the scaling model's ability to accurately calculate non-homogeneous DPK's at each mono-energetic electron energy of a given beta-particle spectrum.

3.4 Cover Layer and Air Gap Models

Cover materials and air gaps can be modeled using VARSKIN. The models use the concept of effective path length to determine the beta energy lost in either a cover material or air before it enters the skin. The path length is not the true path traversed by the beta particle; it is merely a mathematical convenience introduced to provide a measure of the energy lost in each layer. To prevent unintended applications of VARSKIN, the air gap is limited to a maximum of 5 cm.

Figure 3-17 illustrates the method used to determine path length within the source and within the cover material. For the pictured cylindrical source, the known values in the figure are the source radius (R_{max}), the horizontal distance from the centerline to the source point (S_{RAD}), the source thickness (S_{THICK}), the cover thickness (C_{THICK}), the skin depth (S_{DEP}), the source and cover densities (Δ_s and Δ_c, respectively), the angular distance from the center of the dose area to the dose point (P_s), and the distance from the skin to the plane of the source point (D_{RAD}).

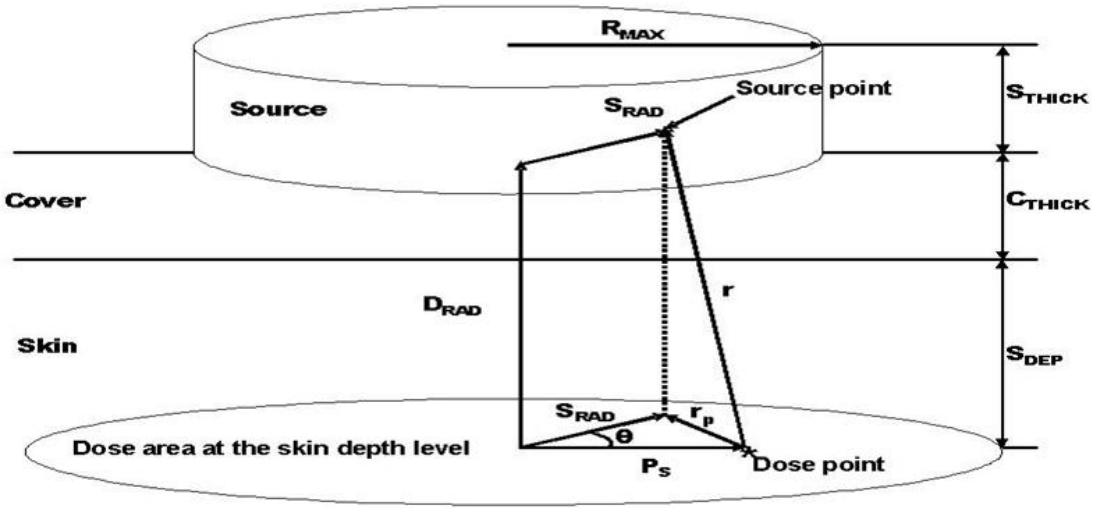

Figure 3-17 Schematic of a generic dose calculation performed by VARSKIN 4 for the cylinder geometry

The quadrature routines are coded to choose values for S_{RAD}; the distance from the centerline to the P_s source point; θ, the angle between S_{RAD} and P_s; and D_{RAD}, the height of the dose point. The first quantity to be calculated is *r*, the physical distance from a source point to a dose point.

To do this, the square of the projected distance, r_p^2, is calculated using the law of cosines:

$$r_p^2 = P_s^2 + S_{rad}^2 - 2P_s S_{rad} cos\theta \quad [3.4.1]$$

The quantity *r* is used in the denominator of the expression in Eq. [3.1.1] and represents the geometric attenuation between the dose point and the source point. This quantity is further analyzed to calculate the modified path length used to evaluate the scaled absorbed dose distribution.

By the law of similar triangles, the ratio to *r* of each of the actual distances along *r* through the source, the cover material, and the tissue is the same as the ratios of the thickness of the cover material to D_{RAD}, the thickness of tissue layer to D_{RAD}, and the remaining distance along *r* to D_{RAD} respectively, provided that the line connecting the dose point and the source point exits through the part of the source that is in contact with the cover material.

Thus, the distance traveled through the cover material is written as the following:

$$r_c = C_{thick} \cdot \left({}^{r}/_{D_{rad}}\right) \quad [3.4.2]$$

The distance traveled through the skin is given by:

$$r_t = S_{dep} \cdot \left({}^{r}/_{D_{rad}}\right) \quad [3.4.3]$$

Finally, the distance traveled through the source is given by:

$$r_s = \left(D_{rad} - C_{thick} - S_{dep}\right) \cdot \left({}^{r}/_{D_{rad}}\right) \quad [3.4.4]$$

For beta dosimetry, the modified path length r_1 is then found using the following equation:

$$r_1 = \frac{(r_s\rho_s + r_c\rho_c + r_t\rho_t)}{\rho_t} \quad [3.4.5]$$

where ρ_t is the density of tissue, assumed to be equal to that of water (1 g cm^{-3}).

For small-diameter sources, the path between the dose point and the source point may pass through the side of the source (e.g., the path may exit the sources and pass through air before passing into skin). Thus, the quantity in Eq. [3.4.5] must be further analyzed to determine the path length within the source and the path length outside the source but above the level of the cover material. The actual path length within the source is multiplied by the source density, and the path length outside the source and above the cover material is multiplied by the density of the material outside the source, assumed to be air.

In spherical geometry, the physical distance from source point to dose point is given by:

$$r_p^2 = P_s^2 + S_{rad}^2 sin^2\phi - 2P_s S_{rad} sin\phi cos\theta \quad [3.4.6]$$

In slab geometry, the physical distance is given by:

$$r = \sqrt{[(X_{source} - X_{dose})^2 + (Y_{source} - Y_{dose})^2 + (Z_{source} - Z_{dose})^2]} \quad [3.4.7]$$

3.5 Volume-Averaged Dose Model

The volume-averaged dose model (shown schematically in Figure 2-8) allows the calculation of dose averaged over a given tissue volume. Any two planes of irradiated skin can be assigned to bound the skin volume. For sources in contact with the skin, the maximum penetration depth for beta particles is equal to the X_{99} distance. Doses averaged over the dose-averaging area are calculated at 10 skin depths between two limits set by the user, and a cubic spline (a third-order piecewise polynomial curve fit) is fit to this depth-dose distribution. When the user specifies the skin depths corresponding to the volume of interest, VARSKIN integrates the depth dose function over the region of interest to obtain the volume-averaged dose.

3.6 Offset Particle Model

The offset particle model allows calculation of skin dose averaged over areas that are not directly beneath the contaminant. This model was developed to determine dose to a single averaging area resulting from multiple hot particles. The offset particle model is available only for the point-source geometry. It requires only one input variable, the distance of the offset. For multiple particle irradiations, the dose from each particle must be calculated separately, with the user running VARSKIN once for each particle. The offset particle model does not calculate the maximum dose to skin from several particles (Section 6.2 outlines the iterative process for determining the maximum dose to the dose-averaging area); rather, the user must manually add doses from each of the sources to a common dose-averaging disk at depth.

3.7 Adding Radionuclides to the VARSKIN 5 Library

Radionuclides are added to the VARSKIN user library through the use of a FORTRAN executable file entitled *Sadcalc.exe*. The purpose of the program, which is an adaptation of a stand-alone program originally called SADDE Mod 2 (Reece, et al., 1989), and modified by Mangini (2012), is to produce data files that contain the information needed to calculate both beta and photon doses. In addition to selecting the nuclide from the master library, the user must specify an effective atomic number (Z_{eff}) to characterize the source material in which the source is incorporated. The default value for Z_{eff} is 7.42 (the effective atomic number of water).

In VARSKIN, beta energy spectra are obtained from the data file *ICRP38.BET*, which is located in the *dat* subdirectory of the VARSKIN folder and contains the maximum energy and the yield information for each of a number of energy bins defined in the file *ENERGY.DAT* (also located in the *dat* subdirectory). The beta yield for the radionuclide is determined by summing each of

the values in *ICRP.DAT*. A file that is associated with the beta spectrum is *ICRP.IDX*, an index file (also located in the *\dat* subdirectory) used to quickly locate data in the large *ICRP.DAT* file. Also included in *ICRP.DAT* is information on any internal conversion or Auger electrons emitted by the radionuclide. The GUI collects the beta spectrum for a selected radionuclide and writes a file entitled *SadInput.dat* which contains the radionuclide name, the yield, the half-life, the maximum beta energy, the beta spectrum, and the energy and yield of any electrons. *Sadcalc.exe* reads this file; adds any electrons to the beta spectrum to form a new spectrum that includes internal conversion and Auger electrons; calculates,, the distance, and ; and then writes these data to the file *sadout.dat*. The GUI reads *sadout.dat*, adds the photon data, and writes the library file with the extension *.rad*. The user enters the name of the file when prompted by the GUI. Note that *sadout.dat* and *sadinput.dat* are internal files and are not intended to be used or modified by the user.

A total of 838 radionuclides are available in the master library, each of which could be added to the VARSKIN user library, and each with its own effective atomic number (i.e., multiple selections of the same nuclide can be made, but with different values of Z_{eff}). Once a radionuclide is added to the library, it is available to be used in all subsequent calculations until the user purposefully removes the radionuclide from the library. Note that not all of the 838 radionuclides emit beta particles, electrons, or photons; some of the radionuclides emit only alpha particles, which do not contribute to skin dose. In that case, the user will be notified that the radionuclide does not emit these types of radiation, and no library file will be produced.

3.8 Photon Dosimetry

The photon dose model first implemented in VARSKIN 4 and unchanged in VARSKIN 5, is an improvement to the basic photon model used in VARSKIN 3. The photon model uses a point kernel method that considers the buildup of CPE, transient CPE, photon attenuation, and off-axis scatter. The photon dose model has many of the basic assumptions carried in the beta dosimetry model, namely that the source can be a point, disk, cylinder, sphere, or slab and that dose is calculated to an averaging disk immediately beneath the surface of skin at a depth specified by the user. Photon dose is calculated for a specific skin averaging area, also specified by the user.

A major problem associated with deterministic photon dosimetry is that of determining the amount of charged particle buildup and electron scatter within shallow depths. Federal law (Title 10 of the *Code of Federal Regulations* (10 CFR) Section 20.1201(b)) states that a dose averaging area of 10 cm^2 is appropriate for skin dosimetry (specifically at the shallow-dose equivalent depth of 0.007 cm in tissue (i.e., 7 mg/cm^2 in unit density material)). Skin dosimetry also involves the calculation or determination of the lens-dose equivalent (at a depth of 0.3 cm) and the deep-dose equivalent (at a depth of 1 cm) in tissue. Throughout this section, the word “depth” is meant to indicate the distance from the skin surface to some point directly beneath a point source, normal to the skin surface.

To begin the explanation of the dose model, we assume the simple instance of a volume of tissue exposed to a uniform fluence, Φ_0, of uncollided photons of energy, E, from a point source in a homogeneous medium. When we ignore attenuation and assume that CPE is established, the dose to any and every point in that volume of tissue is,

$$D(E) = \Phi_0 \cdot E \cdot \left(\frac{\mu_{en}}{\rho}\right)_{tissue} \quad [3.8.1]$$

where $\left(\frac{\mu_{en}}{\rho}\right)_{tissue}$ is the energy-dependent mass energy absorption coefficient for tissue. With this calculation of dose, we essentially assume that the volume is infinitely thin and that interactions occur in two dimensions, normal to a beam of incident photons. The uncollided fluence originating from a point source can be determined by,

$$\Phi_0 = \frac{S}{4\pi d^2} \quad [3.8.2]$$

where *S* has units of photons emitted per nuclear transition (i.e., yield), and *d* is the distance between the source and dose locations, in an infinitely large homogeneous volume. Thus, a point kernel tissue dose per transition at distance, *d*, from a point source can be calculated for radionuclides emitting *i* photons of energy *E* and yield *y*, given that,

$$Dose\left[\frac{\text{Gy}}{\text{nt}}\right] = \frac{k\left[\frac{\text{J·g}}{\text{MeV·kg}}\right]}{4\pi d^2[\text{cm}^2]} \cdot \sum_i \left[y_i \left[\frac{\text{photon}}{\text{nt}}\right] \cdot E_i \left[\frac{\text{MeV}}{\text{photon}}\right] \cdot \left(\frac{\mu_{en}}{\rho}\right)_{i,tissue} \left[\frac{\text{cm}^2}{\text{g}}\right] \right] \quad [3.8.3]$$

where $k = 1.602x10^{-10}\left[\frac{\text{J·g}}{\text{MeV·kg}}\right]$.

If the point source is assumed to rest on the skin surface (with a density interface), and a profile of dose with depth in tissue is of interest, Eq. [3.8.3] must be modified to account for the attenuation of photons in tissue, the electronic buildup, and electron scatter at shallow depths leading to CPE. First, given that attenuation is occurring as photons travel through tissue, photon fluence is decreasing by the factor where μ is the energy-dependent linear attenuation coefficient for tissue (coefficients are taken from International Commission on Radiation Units and Measurements (ICRU) Report 44, 1989). Since tissue typically is assumed to be of unit density (1 g/cm^3), the numerical value of μ (in units of cm^{-1}) is identical to the numerical value of μ/ρ (in units of cm^2/g).

To simplify software coding, analytical expressions are used in VARSKIN 5 (as opposed to using "look-up tables") for a number of dosimetry parameters. An empirical relationship to estimate μ/ρ for tissue as a function of incident photon energy (in megaelectronvolts (MeV)) was developed and is given below. For energies less than or equal to 20 keV,

$$\frac{\mu}{\rho}(E) = \frac{1}{0.0000145 + 3810E^{2.5} + 134400E^3}, \quad [3.8.4]$$

and for energies from 20 keV to 3 MeV,

$$\frac{\mu}{\rho}(E) = e^{\left[-3.22 - 0.11(lnE)^2 + 0.5566\sqrt{E} - 0.7713lnE + \left(0.000721/E^2\right)\right]}. \quad [3.8.5]$$

Figure 3-18 shows a comparison between the ICRU 44 (1989) values of μ/ρ for soft tissue and the functions of Eqs. [3.8.4] and [3.8.5].

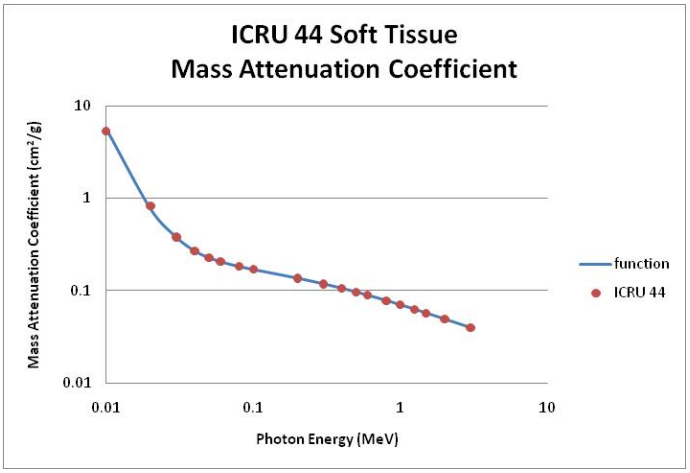

Figure 3-18. ICRU 44 soft tissue mass attenuation coefficients compared to the empirical functions

The function of Eq. [3.8.6] was also developed as part of the VARSKIN 4 enhancements to approximate the energy-dependent value of μ_{en}/ρ for tissue. That function,

$$\frac{\mu_{en}}{\rho}(E) = \frac{a+clnE+e(lnE)^2+g(lnE)^3+i(lnE)^4}{1+blnE+d(lnE)^2+f(lnE)^3+h(lnE)^4+j(lnE)^5}, \qquad [3.8.6]$$

has a different set of coefficients for energies less than or equal to 30 keV and energies from 30 keV to 3 MeV. Table 3-4 provides the coefficients and Figure 3-19 gives the fit of Eq. [3.8.6] to the ICRU 44 (1989) data.

Table 3-4. Coefficients for Eq. [3.8.6]

Coefficient	E ≤ 30 keV	E > 30 keV
a	0.02971	0.03072
b	0.7453	0.4972
c	0.01519	0.009879
d	0.2236	0.1825
e	0.0009557	-0.0002386
f	0.03370	0.07303
g	-0.0001513	0.0006930
h	0.002545	0.01520
i	0.00006018	0.0003239
j	0.00007744	0.001084

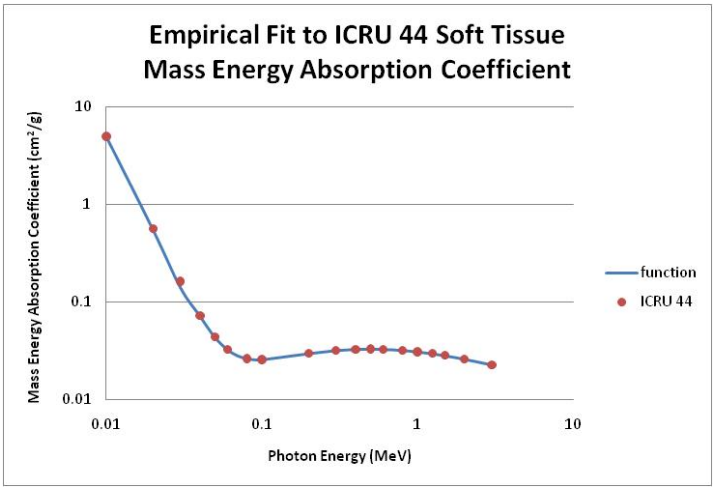

Figure 3-19 ICRU 44 soft tissue mass energy absorption coefficients compared to the functions of Eqs. [3.8.5] and [3.8.6]

In consideration of CPE, Attix (1986) states that the condition exists if, in an infinitely small volume, "…each charged particle of a given type and energy leaving [the volume] is replaced by an identical particle of the same energy entering." For dose at shallow depths to be accurate, the CPE as a function of depth must be determined. The VARSKIN determination of CPE is based on Monte Carlo simulations and the difference between energy released (KERMA) and energy absorbed (dose).

Since energy transfer (KERMA) from photons and energy absorption (dose) from the resulting charged particles does not occur in the same location (Johns and Cunningham, 1983), there is a "buildup region" in which dose is zero at the skin surface and then increases until a depth is reached at which dose and KERMA are equal. The depth at which equilibrium occurs is approximately equal to the range of the most energetic electron created by the incident photons (Johns and Cunningham, 1983). We determined an energy-dependent factor accounting for CPE buildup (f_{cpe}) by Monte Carlo simulation (MCNP5); this factor is the ratio of dose, *D*, to KERMA, *K*, for a particular incident photon energy at a given tissue depth such that,

$$f_{cpe}(E,d) = {}^{D}/_{K} \qquad [3.8.7]$$

When considering CPE and attenuation, a relationship is achieved with depth in a medium in which dose is proportional to KERMA (Attix, 1986); this relationship is referred to as transient charged particle equilibrium (TCPE). Dose reaches a maximum "at the depth where the rising slope due to buildup of charged particles is balanced by the descending slope due to attenuation" (Attix, 1986), and then dose continues to decrease with depth because of subsequent attenuation of photons. At the point where TCPE occurs, dose is essentially equal to KERMA for low-energy photons and the value of f_{cpe} is equal to unity (1). As photon energy

increases over about 1 MeV, this assumption of dose and KERMA equality begins to fail, but not so significantly that it affects deep-dose estimations appreciably. Based on experience with the Monte Carlo simulation of shallow and deep depths, the model used in VARSKIN 4 limits the value of f_{cpe} to 1.05 (i.e., it allows dose to exceed KERMA by a maximum of 5 percent at depth).

A function for f_{cpe} that is dependent on initial photon energy is given as,

$$f_{cpe}(x) = \frac{1}{a+bln(x)+{}^{c}/_{\sqrt{x}}}, \quad [3.8.8]$$

where x (in cm) is a function of energy and is equal to the point kernel distance between source point and dose point, and the coefficients a, b, and c are functions of energy (in keV) as described below:

$$a = 19.78 + 0.1492\,ElnE - 0.008390\,E^{1.5} + 0.00003624\,E^{2} + 3.343\,\sqrt{E}lnE - {}^{10.72\,E}/_{lnE} \quad [3.8.9]$$

$$b = 1.217x10^{-12}E^{4} - 5.673x10^{-9}E^{3} + 7.942x10^{-6}E^{2} - 0.002028E + 0.3296 \quad [3.8.10]$$

$$c = 9.694x10^{-13}E^{4} - 4.861x10^{-9}E^{3} + 7.765x10^{-6}E^{2} - 0.001856E + 0.1467 \quad [3.8.11]$$

The f_{cpe} factor is used for all materials; any buildup in air or thin covers is expected to be insignificant as compared to tissue.

Estimates of f_{cpe} were determined assuming that the line created between the source and dose points was normal to the surface. For a given distance, however, the fractional CPE for point kernel calculations, in which the dose point is located off axis and near the edge of the averaging disk, will vary because of the escape of energetic particles near the air-tissue interface. This loss of energy occurs for more energetic particles, generally from photons of energy greater than a few hundred keV. We have accounted for this off-axis scatter of energy out of tissue, slowing the buildup of equilibrium, by including an off-axis scatter factor, F_{oa}. The factor, taking on values between 0 and 1, is necessary only for point kernel calculations in which the angle between the central axis at the surface and the dose point is greater than 70 degrees from normal, and for photon energies greater than 300 keV; otherwise, F_{oa} is set equal to unity (1). The off-axis scatter factor is calculated from empirical data obtained through Monte Carlo simulation. The factor is represented by,

$$F_{oa} = (-1.57 + 0.000334\,\theta^{2.5} - 0.0000325\,\theta^{3})(0.93 + 0.1R), \quad [3.8.12]$$

where R is the radius of the dose-averaging disk and θ is the off-axis scatter angle (in degrees). Figure 3-20 gives a plot of off-axis correction as a function of scatter angle and the area of the dose-averaging disk. The considerable dip in the function for a 0.1-cm^2 averaging area is an artifact of Eq. [3.8.12] and is not phenomenologically significant.

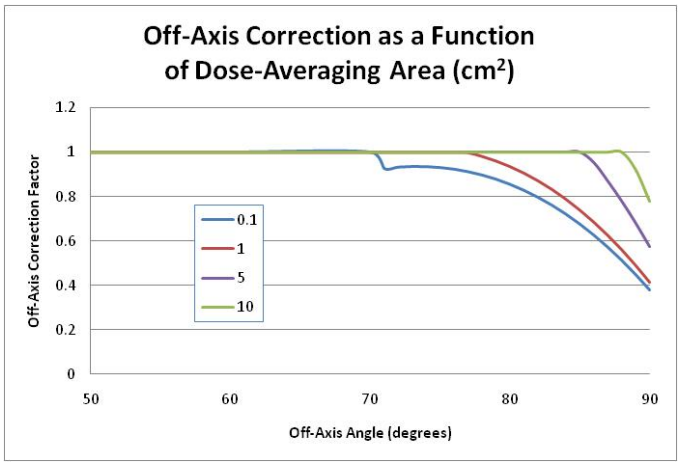

Figure 3-20. Off-axis correction factor as a function of off-axis angle and dose-averaging area. Averaging disks of 0.1, 1, 5, and 10 cm^2 are shown.

Fully accounting for charged particle buildup and attenuation, Eq. [3.8.3] now becomes:

$$Dose\left[\frac{Gy}{nt}\right] = \frac{k}{4\pi d^2} \cdot \sum_i \left[y_i \cdot E_i \cdot \left(\frac{\mu_{en}}{\rho}\right)_{i,tissue} \cdot \left(f_{cpe}\right)_i \cdot \left(F_{oa}\right)_i \cdot e^{-\mu_i d} \right]. \qquad [3.8.13]$$

As stated above, Federal law requires the determination of average dose to skin over an averaging area (e.g., 10 cm^2) at some depth in tissue (e.g., 7 mg/cm^2). To determine average dose at depth from a source at the surface, we must integrate Eq. [3.8.13] over the averaging area. Integrating the exponential, however, results in a solution with imaginary components. Therefore, a stepwise numerical integration of Eq. [3.8.13] is necessary, essentially providing an average of the point kernel dose over combinations of photon emission locations within the volume of the radioactive source and dose point locations within an infinitely thin disk of tissue at depth, *h*, from the surface.

The authors conducted convergence studies to determine which numerical integration method achieved convergence most rapidly for photon dosimetry (i.e., dividing the dose-averaging disk into the fewest number of segments). The studies investigated three segmenting methods (see Figure 3-21): (1) segments determined by equal radii of the dose-averaging disk, (2) segments determined by equal off-axis angles, and (3) segments determined by equal annular area.

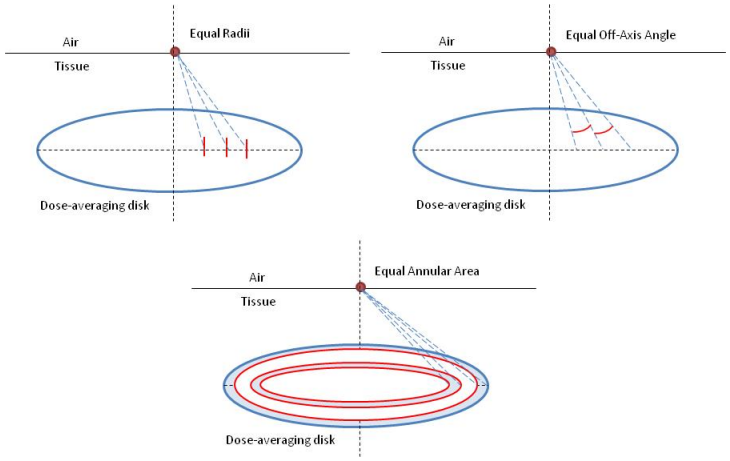

Figure 3-21. Depiction of methods for determining integration segments of the dose-averaging disk

These studies indicated that segments divided according to equal lengths (radii) along the radius of the averaging disk converged with the fewest number of iterations, with segments divided by equal annular area requiring the most iterations. Figure 3-22 shows that convergence was achieved within about 300 iterations for equal lengths along the radius of a 10-cm^2 averaging disk; the VARSKIN 4 numerical integration, therefore, utilizes 300 segments along the radius/diameter. Convergence was achieved with fewer segments when analyzing a smaller averaging disk.

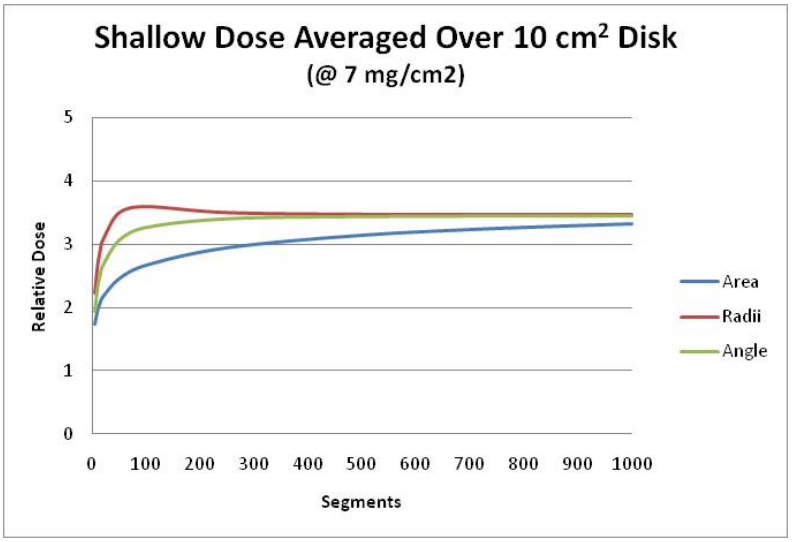

Figure 3-22. Relative dose as a function of the number of segments in a numerical integration (iterations), by method

Therefore, given a point source on the skin, the first task in the integration process is to divide the dose-averaging disk into *N* small segments (annuli), *j*, of uniform incremental radii. If an averaging area, *A*, of radius, *R*, is at some depth, *h*, beneath the surface of skin, a method

based on the convergence study is used in which values of radii, R_j, of the averaging disk are selected such that a radial increment, Δr, is defined,

$$\Delta r = \frac{R}{N} \quad [3.8.14]$$

and

$$R_j = \sum_{j=0}^{N}(j \cdot \Delta r). \quad [3.8.15]$$

If point kernel dose calculations are conducted where dose is estimated to the midpoint of the annulus, each dose must be weighted by w_j, the ratio of the area of the annulus created by, and , to the total area of the disk. Given that R_0 = 0 and R_N = R, the values of w_j are determined by,

$$w_j = \frac{R_j^2 - R_{j-1}^2}{R^2}, \quad [3.8.16]$$

where *j* takes on values from 1 to *N*. We also define r_j, which represents the average of the two radii describing the annulus in each calculation, such that,

$$r_j = \frac{R_j - R_{j-1}}{2}. \quad [3.8.17]$$

Once all values of are determined, then the dose per nuclear transition for a given point source radionuclide with *i* emissions, averaged over an infinitely thin disk of radius *R*, at normal depth in tissue *h* and radius r_j, is calculated by,

$$\dot{D}(h,R)\left[\frac{\mathrm{Gy}}{\mathrm{nt}}\right] = \frac{k}{4\pi} \cdot \sum_{j=1}^{N} \frac{w_j}{d_j^2}\left[\sum_i \left[y_i \cdot E_i \cdot \left(\frac{\mu_{en}}{\rho}\right)_i \cdot \left(f_{cpe}\right)_{i,j} \cdot (F_{oa})_{i,j} \cdot e^{-\mu_i d_j}\right]\right], \quad [3.8.18]$$

where $d_j = \sqrt{(h^2 + r_j^2)}$.

3.9 Attenuation Coefficients for Cover Materials

For photon dose calculations, the cover materials (and associated attenuation coefficients) are "forced" to be either latex or cotton. This determination is made by the density entry, i.e., if the density is less than 1.25 g/cm^3, then latex is assumed, if greater, cotton is assumed. These are the two most likely materials used for cover. It is noted that the cover attenuation is minor and this decision should be insignificant for the dose calculation.

An empirical function of energy was used for attenuation coefficients for cotton and latex, namely:

$$\mu_{cotton/latex} = e^{(a+b\sqrt{E}\cdot\ln(E)+c\sqrt{E})} \quad [3.9.1]$$

where a = -1.0132, b = 0.31505, and c = -1.6086 for cotton, and a = -1.0286, b = 0.32189, and c = -1.6217 for latex. Coefficients for air were determined from,

$$\mu_{air} = \left(\left(a + \frac{b}{\sqrt{E}}\right) + \left(c \cdot \frac{\ln(E)}{E}\right) + \left(\frac{d}{E}\right) + \left(\frac{e}{E^{1.5}}\right) + \left(f \cdot \frac{\ln(E)}{E^2}\right) + \left(\frac{g}{E^2}\right)\right) * 0.001168 \qquad [3.9.2]$$

where a = 0.027413, b = -0.12826, c = 0.11227, d = 0.060526, e = 0.12508, f = -0.0030978, and g = -0.021571. Both of these functions track very well with data from ICRP 44.

3.10 Off-Axis Calculation of Dose

The model described thus far is constructed under the assumption that the source of photons is a point, located directly above and on axis with the averaging disk, and that there is symmetry in dose calculations along a radius of the dose-averaging disk (Figure 3-23).

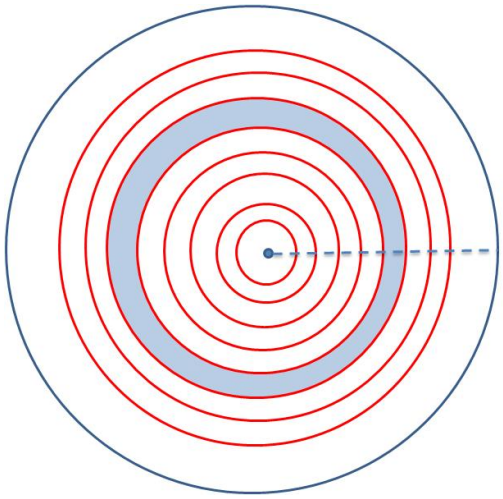

Figure 3-23. Dose-averaging disk with the source point located on axis

To extend the model to handle point kernel calculations for volumetric sources, or for multiple point sources, we must consider the case where the point source is off axis yet still over the dose-averaging disk (Figs. 3.10.2 and 3.10.3) and the case where the point source is completely removed from the dose-averaging disk (Figs. 3.10.4 and 3.10.5).
The implication is simply a geometric determination of the distance between source and dose points in each point kernel calculation and an area-weighted factor for the symmetric dose location on the averaging disk.

In the first case, where the point source is off axis yet still over the dose area, there is symmetry along a diameter of the dose-averaging disk. The average of the point kernel doses will be

determined by a weighting of doses calculated along the diameter. The calculation begins by projecting the dose point to the averaging disk, normal to the skin surface (see Figure 3-24).

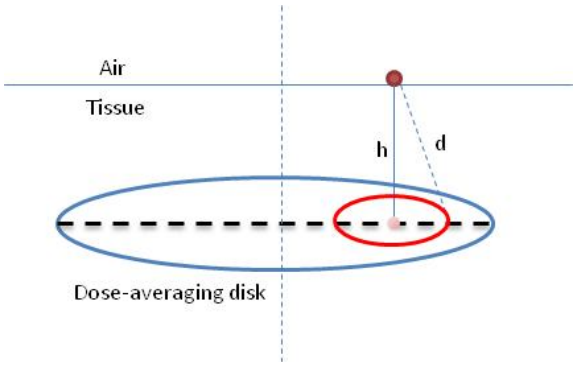

Figure 3-24. Dose-averaging disk located at depth h beneath an offset point source

The averaging disk then is divided, as described above, into a series of concentric annuli, about the projected dose point, until the radius of the annuli reaches the nearest edge of the averaging disk (Figure 3-25). At this point, the weighting model transitions to a series of arcs passing through the averaging disk; these arcs are created by differential radii of two intersecting circles (Figure 3-26). The model creates a total of 300 annuli and arcs. Point kernel dose is calculated along the diameter in each of the 300 segments defined by the differential annuli and arcs and then weighted based on the fractional area of each segment.

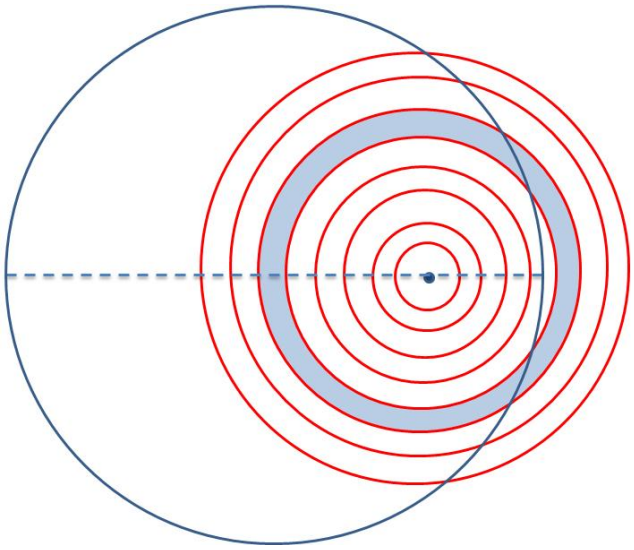

Figure 3-25. Dose-averaging disk with the source point located off axis, yet still over the averaging disk

The weight (fractional area) of each annulus to the total is straightforward, in that,

$$w_i = \frac{\pi(r_i^2 - r_{i+1}^2)}{\pi R^2} = \frac{r_i^2 - r_{i+1}^2}{R^2}. \qquad [3.10.1]$$

The weight of each arc is determined by a method considering intersecting circles. In the case of Figure 3-26, the area of the "lens" created by the two intersecting circles is given by:

$$A_i = r^2 cos^{-1}\left(\frac{d^2+r^2-R^2}{2dr}\right) + R^2 cos^{-1}\left(\frac{d^2+R^2-r^2}{2dR}\right)$$
$$-\frac{1}{2}\sqrt{(-d+r+R)(d+r-R)(d-r+R)(d+r+R)}. \qquad [3.10.2]$$

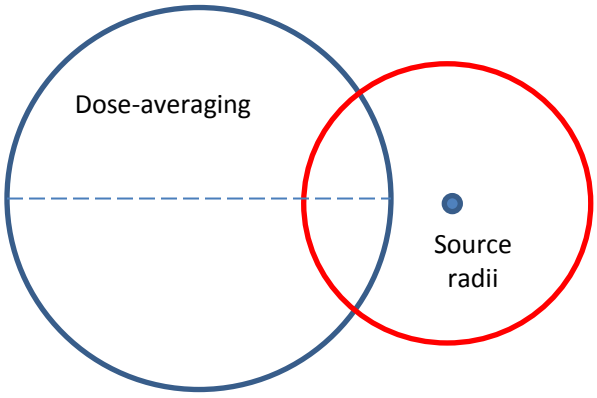

Figure 3-26. Relationship between the source-averaging disk and one of the radii for dose calculation. A "lens" is created by the intersection of the two circles.

The area of the arc formed (Figure 3-26) by two concentric circles (two radii from the point source) that overlap another circle (the averaging disk) is the difference in the area calculations of Eq. [3.10.1]. The arc weight is then the ratio of the arc area to the total area of the averaging disk. In the case where the source projection does not fall on the dose-averaging disk (Figure 3-27), the weighting scheme is based solely on arcs.

The numerical integration is conducted from the point source to each of 300 locations along the diameter of the averaging disk (or along the radius if the source point is directly on axis with the disk). Then, for volumetric sources, point source locations are chosen in equal symmetric increments at 15 point locations in each of the three dimensions within the source volume, relative to the averaging-disk diameter. For each volumetric source dose estimate, 1,000 calculations of dose from each of 15 x 15 x 15 source point locations are executed (1 million dose calculations).

The new VARSKIN 4 photon dosimetry model accounts for attenuation in cover materials and air. As with the beta dosimetry model, up to five layers above the skin are allowed, with the air layer only acceptable just above the skin surface. For photon calculations, the other material layers are restricted to cotton and/or latex, and the source material is assumed to have the same characteristics as air. This latter assumption is not significant for very small volumetric sources and for photon energies above about 50 keV. For example, if we examine the ratio of air attenuation to lead, tin, copper, aluminum, and water attenuation, the greatest difference is obviously at low photon energies with higher-Z materials (i.e., instances of higher interaction probability).

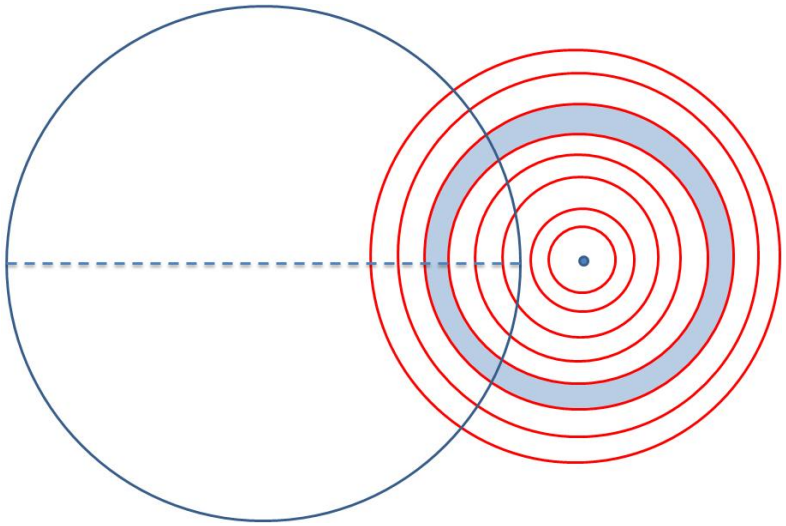

Figure 3-27. Dose-averaging disk from above with the source point located off axis, far enough removed to be off the averaging disk

The data indicate that, for volumetric sources with a maximum linear dimension less than about 100 microns, the assumption that the source material is similar to air is of no consequence whatsoever for photon energies between 10 keV and 3 MeV. As the source particle dimensions increase in size, an assumption of air for the source material can be quite significant for very low photon energies (e.g., energies less than about 40 keV). The significance, however, is one of conservatism in that more low-energy photons than actual will be modeled as striking the skin surface when source dimensions are large. The analysis of attenuation also shows that the assumption of air and water (tissue) being similar, in terms of attenuation, over very short distances (i.e., less than 5 mm) is a good assumption.

4 VALIDATION AND VERIFICATION

To validate the new photon and beta dosimetry models incorporated into VARSKIN, results were compared to the general purpose radiation transport codes, MCNP5 and EGSnrc. The two software packages are Monte Carlo transport codes which simulate movement and interaction of particles in material (Los Alamos National Laboratory, 2003; Ljungberg et al. 2012).

4.1 Comparison with A General Monte Carlo N-Particle Transport Code (MCNP)

For the simulations, we used MCNP5 for photon comparisons and EGSnrc for electron comparisons. With each code, various source geometries were modeled close to the skin. The fundamental geometry, illustrated in Figure 4-1, involves an infinite volume of air located above an infinite volume of tissue. Composition of these materials was taken from National Institute of Standards and Technology standards for each material. Each of the sources was situated 1 μm above the skin and above the perpendicular bisect of the volume of tissue over which the dose is calculated.

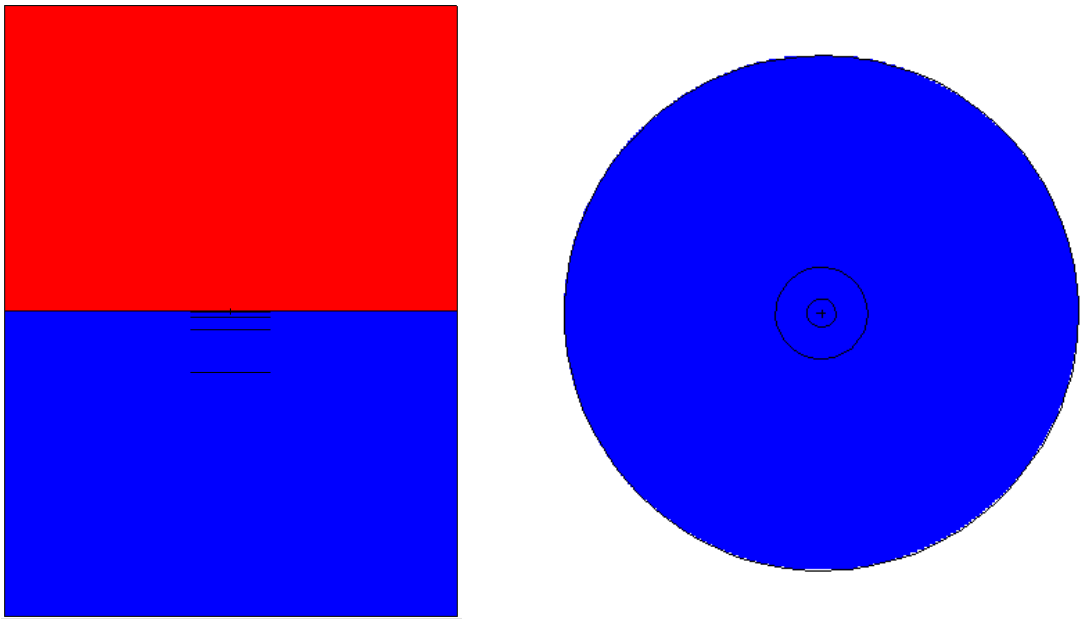

Figure 4-1. Horizontal (left) and vertical (right) cross-sectional views of the MCNP5 geometry

As illustrated in Figure 4-2, the dose per particle (photon or electron) was calculated for each of the sources at tissue depths of 7, 100, 300, and 1,000 mg/cm^2. The density thicknesses of 7, 300, and 1,000 mg/cm^2 correspond to the depth required by 10 CFR Part 20, "Standards for Protection against Radiation," for calculation of doses to the skin, lens of the eye, and the deep dose, respectively. Although the value of 100 mg/cm^2 does not correspond to a regulatorsignificant density thickness, results at that depth are provided as an indication of accuracy at an intermediate, yet shallow, depth.

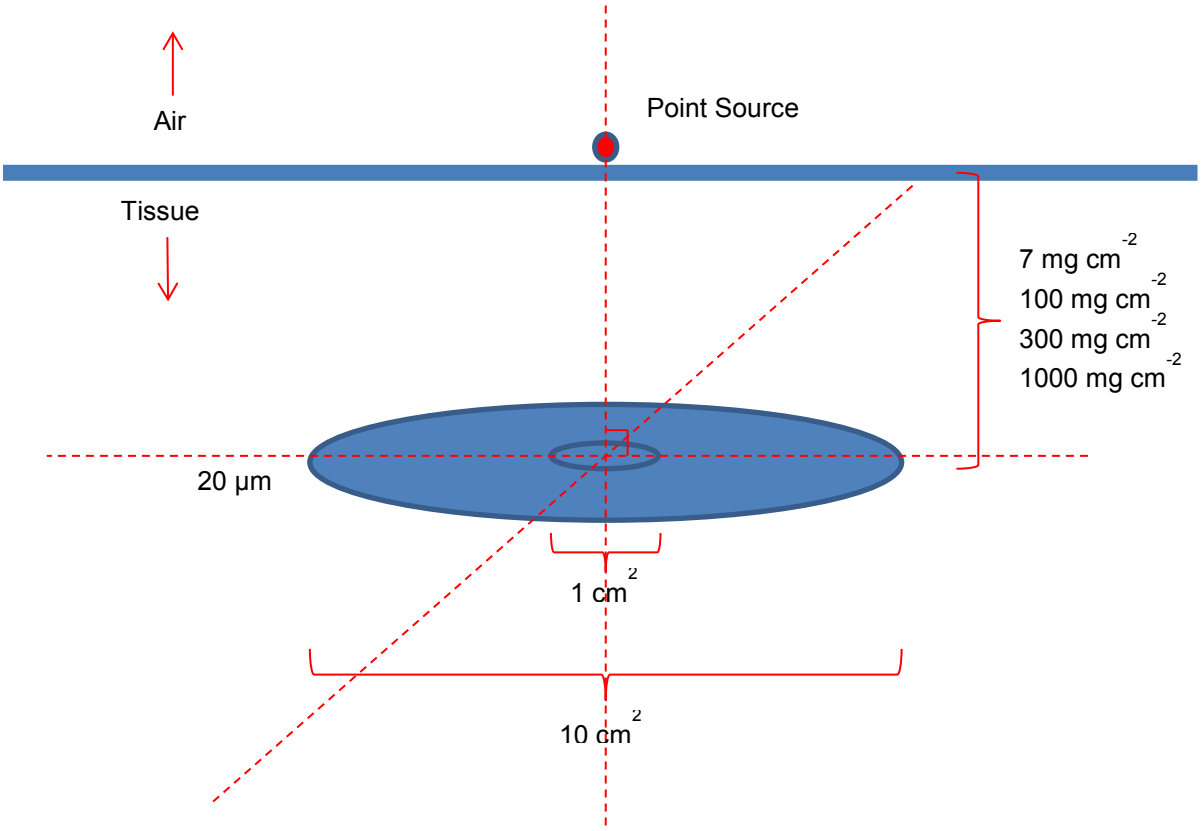

Figure 4-2. Illustration of the point source geometry of the tissue volumes of interest at various density thicknesses in tissue

At each density thickness, the dose to two volumes of tissue, $2x10^{-3}$ cm^3 and $2x10^{-2}$ cm^3, was calculated. These dimensions correspond to cylindrical volumes within tissue, each having a thickness of 20 µm and a cross-sectional area of 1 cm^2 and 10 cm^2, respectively. The value of 20 µm was selected for use to create a volume large enough that uncertainties resulting from low numbers of particles interacting in the volume would not be an issue. Sherbini et al. (2008) showed that at thicknesses greater than 10 µm, any effects of dose averaging over increasingly smaller volumes are avoided.

Energy deposited in the volume of interest was calculated for dose estimation. The number of particle histories executed was sufficiently high to maintain statistical errors below 6 percent, with the majority producing an error of approximately 3 percent. Dose rate was calculated for a simulated source strength of 1 µCi, with a yield of 100 percent at a given energy ranging from 25 keV to 3 MeV. While this is not specific to any particular nuclide, it demonstrates the energy dependence of each methodology and also shows which current models are accurate predictors (as compared to MCNP5/EGSnrc) and which are not.
Appendix A provides results for beta dosimetry comparisons, with Appendix B providing similar results, but for photon dosimetry. The appendices are arranged as follows.

For beta dosimetry, results of the V&V exercise are provided in seven geometries: (1) point source; (2) 0.5 mm diameter 2D disk source; (3) 1 mm diameter 2D disk source; (4) 5 mm diameter 2D disk source; (5) 1 mm diameter by 1 mm height cylindrical source; (6) 1 mm diameter spherical source; and (7) 1 mm cube slab source. For each geometry, dose estimates from VARSKIN 5 as a function of electron energy were compared with EGSnrc and MCNP5 results at depths of 7, 100, 300, and 1000 mg/cm^2. Additionally, comparisons with four beta-emitting nuclides (^{28}Al, ^{42}K, ^{66}Cu, and ^{138}Cs) were conducted to show how the current VARSKIN beta dose predictions compare to previous estimates. VARSKIN 5 estimates of dose compare very well with EGSnrc and MCNP5, although MCNP5 estimates are slightly higher at deeper depths.

For photon dosimetry, V&V focused on seven geometries, including: (1) point source; (2) 1 mm diameter 2D disk source; (3) 1 mm diameter by 1 mm height cylindrical source; (4) 1 mm cube slab source; (5) 1 mm diameter spherical source; (6) point source with an air gap and a cotton cover; and (7) point source that is 1 cm off axis. Dose estimates from VARSKIN 5 as a function of electron energy were compared with MCNP5 results at depths of 7, 100, 300, and 1000 mg/cm^2 for each of the geometries considered. VARSKIN is shown to be a very good predictor at various tissue depths when the point- and disk-source geometries are modeled. VARSKIN consistently overpredicts dose (compared to MCNP5) in the cylindrical, slab, and spherical geometries at energies greater than about 200 keV.

4.2 Shallow Dose Comparisons

VARSKIN 4 was released after an enhancement to the photon dosimetry model (without changes to the beta dosimetry model), and VARSKIN 5 includes enhancements to the beta dosimetry model (without photon dosimetry changes). Comparisons of dose calculated using VARSKIN 3.1, 4 and 5 are given below to demonstrate how the three versions differ in dose estimation for the few scenarios considered.

4.2.1 Point Source on the Skin. In this test, calculations were completed for the case of a ^{60}Co point source placed directly on the skin (i.e., no material and no air gap between the source and skin). For a 1-μCi hot particle and a 1-hour exposure time, the beta and photon dose averaged over 1 cm^2 at a depth of 7 mg/cm^2 was calculated. Table 4-1 shows the results of this calculation. Changes to beta dosimetry indicate a reduction of about 10% at this shallow depth, due primarily to changes in the calculation of specific absorbed dose distribution. Photon dose estimates changed dramatically because of the inclusion of charged particle buildup and photon attenuation.

Table 4-1. Comparison between Beta and Photon Shallow Dose Calculations from VARSKIN 3.1, 4, and 5 for a 1-µCi Point Source of Co-60 Exposing the Skin for 1 Hr

Nuclide	V3.1 β Dose (mGy)	V4 β Dose (mGy)	V5 β Dose (mGy)	V3.1 γ Dose (mGy)	V4 γ Dose (mGy)	V5 γ Dose (mGy)
Co-60	37.6	37.6	34.5	3.29	0.79	0.79

4.2.2 Point Source on Cover Material. Dose calculations at 7 mg/cm^2 were also performed for ^{60}Co, ^{137}Cs/^{137m}Ba, and ^{90}Sr/^{90}Y with three different cover material configurations. In each case, a 1-µCi point source and an exposure time of 1 hour were assumed with no air gap between the layers of cover material. Doses were calculated for a 1-cm^2 averaging disk. Table 4-2 shows the results of this calculation. Changes to beta dosimetry are shown to either increase or decrease, due to model enhancements that impact particle track lengths, energy loss, backscatter characteristics, conversion electron consideration, etc. Photon dose at shallow depths for the scenario considered decreases by about a factor 2 after model enhancement, again, primarily due to the consideration of charged particle buildup and photon attenuation.

Table 4-2. Comparison between VARSKIN 3.1, 4 and 5 of the Shallow Dose for Various Cover Material Configurations

Nuclide	Air Gap (cm)	Cover Material	V3.1 β Dose (mGy)	V4 β Dose (mGy)	V5 β Dose (mGy)	V3.1 γ Dose (mGy)	V4 γ Dose (mGy)	V5 γ Dose (mGy)
Co-60	0.2	M_1	1.96	1.96	1.69	0.571	0.292	0.292
Cs-137/ Ba-137m	0.2	M_1	14.0	14.0	12.1	0.199	0.0969	0.0969
Sr/Y-90	0.2	M_1	32.6	32.6	27.0	0	0	0
Co-60	0.2	$M_1 + M_1$	0	0	0.0643	0.558	0.258	0.258
Cs-137/ Ba-137m	0.2	$M_1 + M_1$	4.75	4.75	5.91	0.181	0.0842	0.0842
Sr/Y-90	0.2	$M_1 + M_1$	20.7	20.7	18.6	0	0	0
Co-60	1.0	M_1	0.813	0.813	0.634	0.0797	0.0429	0.0429
Cs-137/ Ba-137m	1.0	M_1	2.79	2.79	2.25	0.0277	0.0129	0.0129
Sr/Y-90	1.0	M_1	5.37	5.37	4.35	0	0	0
Co-60	1.0	$M_1 + M_1$	0	0	0.0335	0.0836	0.0404	0.0404
Cs-137/ Ba-137m	1.0	$M_1 + M_1$	1.40	1.40	1.35	0.0270	0.0121	0.0121
Sr/Y-90	1.0	$M_1 + M_1$	3.95	3.95	3.42	0	0	0
Co-60	1.0	$M_1 + M_2$	0	0	0.00704	0.0876	0.0400	0.0400
Cs-137/ Ba-137m	1.0	$M_1 + M_2$	0.770	0.770	0.939	0.0271	0.0120	0.0120
Sr/Y-90	1.0	$M_1 + M_2$	3.26	3.26	2.96	0	0	0
Co-60	5.0	$M_1 + M_2$	0	0	0.00038	0.00453	0.00205	0.00205
Cs-137/ Ba-137m	5.0	$M_1 + M_2$	0.0384	0.0384	0.0476	0.00138	0.00061	0.00061
Sr/Y-90	5.0	$M_1 + M_2$	0.167	0.167	0.151	0	0	0

M_1—Cover material = thickness of 0.37 mm, density of 0.70 g/cm^3.
M_2—Cover material = thickness of 0.40 mm, density of 1.1 g/cm^3.

4.2.3 Distributed Beta Contamination on Skin.

Calculations were performed for the same three nuclides using VARSKIN 3.1, 4 and 5 to compare specifically the beta dose estimate for a distributed disk source on the skin over an exposure period of 1 hour (Table 4-3). The beta dose at a depth of 7 mg/cm^2 was calculated for a simulated contamination scenario with a concentration of 1 μCi/cm^2 distributed over a circular area of 100 cm^2. A dose-averaging area of 1 cm^2 was assumed. The results were compared to values published by Rohloff and Heinzelmann (1986) and by Kocher and Eckerman (1987). The results from VARSKIN and published values are somewhat different than expected, however, comparisons with Monte Carlo simulation (Appendix B) are shown to be quite good.

Additional comparisons were made for shallow beta dosimetry assuming a 1-hour exposure from a source modeled as an infinitely thin, uniformly contaminated (1 μCi/cm^2) two-dimensional disk with a diameter of 2 cm. Doses were calculated at different depths in the skin and compared to similar values in the literature. Tables 4-4 and 4-5 show that the results are in fair agreement, although the VARSKIN results are lower than the published values.

Table 4-3. Comparison between VARSKIN 3.1, 4 and 5 of the Beta Dose (mGy) for a 1-hr Exposure to Distributed Contamination on the Skin

Nuclide	V3.1	V4	V5	Rohloff et al. (1986)	Kocher et al. (1987)
Co-60	37.7	37.7	34.5	32.4	41.8
Cs-137	51.2	51.2	47.6	-	59.1
Sr/Y-90	123.4	123.4	104.2	121	156

Table 4-4. Dose (mGy) for Various 1 μCi/cm^2 Distributed Disk Sources and a 1-hr Exposure Time (dose calculated at a depth of 7 mg/cm^2 and averaged over 1 cm^2)

Method	C-14	P-32	I-131	Sr-90	Y-90
VARSKIN 3.1	11.2	66.3	52.5	54.7	68.2
VARSKIN 4	11.2	66.3	52.5	54.7	68.2
VARSKIN 5	11.1	58.6	48.4	49.7	59.4
Delacroix (1986)	10.7	91.5	64.2	69.9	91.8
Kocher and Eckerman (1987)	12.2	88.7	63.4	67.6	88.7
Piechowski (1988)	12	70	60	59	75

Table 4-5. Dose (mGy) vs. Depth for a 1 μCi/cm^2 Distributed Disk Source of Y-90 and a 1-hr Exposure Time (dose averaged over 1 cm^2)

Method	4 mg/cm^2	7 mg/cm^2	10 mg/cm^2	40 mg/cm^2
VARSKIN 3.1	79.0	68.2	61.4	40.7
VARSKIN 4	79.0	68.2	61.4	40.7
VARSKIN 5	65.7	59.4	55.3	38.2
Delacroix (1986)	104.6	91.8	83.7	52.4
Kocher and Eckerman (1987)	101.4	88.7	—	50.7

5 VARSKIN LIMITATIONS

VARSKIN calculates skin dose to an infinitely thin disk at depth in tissue for comparison to the NRC limit of 0.5 gray (Gy) for both point and distributed sources (NRC, 2006). VARSKIN can calculate the dose to averaging areas from a minimum of 0.01 cm^2 to a maximum of 100 cm^2. Users are cautioned that VARSKIN is designed to calculate the dose to skin from skin contamination. Using VARSKIN to perform calculations that are beyond the intended application of the code may result in erroneous dose estimates. This section discusses the known limitations of VARSKIN and establishes the limits over which the code has been tested.

The first item of note is not a limitation, but a code design decision, and involves the treatment of radioactive progeny. In VARSKIN, radioactive progeny are not included with the parent radionuclide and must be entered explicitly, i.e., selecting ^{137}Cs gives you only that nuclide, ^{137m}Ba is not included unless it is specifically called. The user is additionally cautioned to consider the half-life of the progeny when selecting the appropriate dose contribution (decay-corrected or not) from daughter products. As an example, for the case of ^{144}Ce and its daughter, ^{144}Pr (with a short half-life), the dose result from the daughter product must be taken from the non-decay corrected calculation. If the user takes the decay-corrected dose in this case, the dose would be significantly underestimated. The limitation that must be recognized by the user in this case is that VARSKIN uses the decay characteristics of each nuclide, whether that nuclide is in secular equilibrium with a parent, or not.

Dose calculations involving air gaps greater than 5 cm have not been tested and are, therefore, not allowed. It is likely that erroneous results may be obtained for large air gaps because the code does not account for multiple scattering events in air. These events may result in the dose being delivered to an area greater than that determined using VARSKIN and can lead to inaccurate results. VARSKIN is limited such that calculations for air gaps greater than 5 cm are not possible and a warning message is displayed.

VARSKIN has not been tested extensively for dose-averaging areas other than 1 and 10 cm^2. However, because of the nature of the calculations performed by VARSKIN, there is no reason to believe that doses to areas less than or greater than 10 cm^2 will result in errors. A quick and limited study of dose results as a function of averaging disk area shows that the code appears to be stable and linear in this regard from 0.01 to 100 cm^2.

5.1 Beta Dosimetry

VARSKIN has been shown to be reliable for particulate sources that have dimensions less than eight times the X_{99} distance of the radionuclide in tissue. The X_{99} distance is essentially 99 percent of the range of beta particles in tissue emitted by nuclides in the source term. When the physical size of the source approaches this value, VARSKIN may give unreliable results. A user who wants to model sources larger than this limit may wish to begin with smaller sources and increase the source size gradually to ensure that spurious results are not being generated.

Modeling a source of this size is generally not necessary, however, as most of the source does not contribute to beta skin dose because of self-shielding. If the source dimensions selected are too large, VARSKIN prompts the user with a warning of the potential for inaccurate results. The X_{99} distance is included on the printout of a calculation to assist the user in determining the appropriateness of input source dimensions.

The VARSKIN 5 V&V results indicate discrepancies between VARSKIN 5 and EGSnrc for beta dosimetry on scenarios involving volumetric sources and intermediate electron energies. The V&V results for low-energy electrons at shallow depths are similar to the results seen at all depths where the electron is reaching its maximum range (even for the point-sources to a certain degree). These larger deviations are apparent at the tail end of the beta-dose profiles, as well (Mangini, 2012). Either way, it is clear from these results that the accuracy of VARSKIN5 decreases as the electron reaches its maximum depth. In dose calculations for a distribution of electrons, this effect is still present since, approaching the deeper depths, the deposited energy is occurring at the tail end of the electron range.

5.1.1 DPK's and Scaling Model.

DPK's have always underestimated dose at depths approaching the range of the electron. Monte Carlo is the standard and DPK models begin to fail when energy and range straggling becomes more and more important at greater depths. The effects of straggling are dominant at that part of the electron path. We suspect that the scaling model is not a contributor to the discrepancies noted. In fact, the accuracy of the scaling model is highest towards the end of the electron path. The interface between the source material and water is where the model has its largest deviations. This is likely not the cause, as dose at deeper depths will be dominated by electrons traversing very little of the source material (i.e., 0.25 X/X90); the model is extremely accurate in this case.

5.1.2 Scattering Model.

In developing the scattering model, the Monte Carlo (EGSnrc) data used for the model all had a percent error less than 5%. Simulations with a greater error were eliminated with a dose contribution of zero. However, once the curve fits in SADCALC were developed for the dose profiles, the error in the predicted dose values from the curve fits became extremely unreliable at very low dose values and the deeper depths. In examining the raw data used to create the scattering model and dose profiles, it became apparent that the dose values reached an asymptote of about $1x10^{-12}$ (Gy per electron). At these dose values the standard error of the Monte Carlo simulations begins to exceed 5%. The VARSKIN 5 code was modified to set all dose contributions to zero if the calculation resulted in something less than $1x10^{-12}$ Gy/electron. This patch is justified since the model begins to fail at such low doses (and the standard error from Monte Carlo calculations is very high). When averaging over a beta spectrum, these contributions to the BSCF and dose are negligible. Setting dose to zero at these depths is executed for both the source scattering profile and the water scattering profile, thereby setting the BSCF equal to one (1). Nonetheless, for doses just greater than $1x10^{-12}$ Gy/electron, the VARSKIN model will be rather inaccurate for dose calculations at the end of the electron range.

5.2 Photon Dosimetry

The photon dosimetry model assumes that all volume sources are made of air. This assumption results in greater accuracy when modeling larger, less dense sources (a gas cloud, for example). However, when modeling volumetric sources of greater density, VARSKIN 4 is optimized for small dimensions (less than about a millimeter). This optimization is the result of a tradeoff between attenuation and charge particle buildup within the source itself. Care should be exercised when modeling large-volume sources.

6 SPECIAL TOPICS FOR ACCURATE USE OF VARSKIN

VARSKIN is designed to be very flexible while maintaining a high level of accuracy. However, the code can be misused, particularly when modeling infinitely large sources (i.e., sources with physical dimensions greater than the X_{99} distance for the source radionuclides). This section describes this possible misuse of VARSKIN and how it can be avoided. This section also describes a method to determine the maximum dose to an area from multiple hot particles.

6.1 Infinite Sources

When modeling infinite or semi-infinite sources (e.g., an enveloping cloud) with VARSKIN, the tendency is to choose very large dimensions for the source. This approach will result in the calculation of a grossly inaccurate dose or a zero dose because the integration routine becomes unstable. The correct method is to determine the maximum penetration distance (i.e., the X_{99} distance) and set the source dimensions accordingly.

The X_{99} distance can be found by running a simple calculation for the radionuclide of interest and looking at the printout for the value. The maximum source radius (r_{max}) and the side lengths are then determined using the equation,

$$r_{max} = r_{dos} + \left({}^{X_{99}}/_{\rho_{min}}\right)\rho_w, \qquad [6.1.1]$$

where r_{dos} is the radius of the dose-averaging area (in cm), is the density of water, and is the smallest density of the covering material, source, air (if an air gap is included), or tissue. Using the density of the least dense material will ensure that the dose-averaging area includes contributions from the entire source. If an air gap is included, using the VARSKIN default value for the density of air (0.001293 g/cm^3) is appropriate. If no cover material is specified, using tissue density is the best choice.

When modeling infinite sources, the use of the cylinder source geometry is recommended. When using the cylinder source geometry, the source thickness, Δt_{max}, should be determined using the equation,

$$\Delta t_{max} = \frac{X_{99}\rho_w}{\rho_s}, \qquad [6.1.2]$$

where ρ_s is the source density.

6.2 Maximum Dose from Multiple Contamination Sources

Determining the maximum dose to the dose-averaging area for multiple contaminations requires multiple calculations. These calculations require elements that are not available in VARSKIN but can be accomplished manually, as described below.

Before attempting to run the offset particle model, the user should determine the size of the irradiation area directly beneath each of the contaminated areas. Note that the size of sources

does not need to be the same for each particle. By comparing these areas for each source, it may be possible to eliminate one or more of the contaminated areas because no overlapping fields are associated with them. For contaminated areas with overlapping fields, the doses and their relative positions should then be plotted on a sheet of graph paper, leaving plenty of room between the sources for results from additional calculations.

Next, calculations using the offset particle model should be performed for locations midway between any two contaminated areas. For more than two sources that are not in a straight line, a central location should be chosen, and the dose at this point should be calculated using the offset particle model. Thus, for three contaminated areas in a triangular formation, a total of four calculations should be performed. The value of the offset should be chosen to be one-half of the distance between any two sources, with one additional dose calculation performed in the center of the triangle.

After these calculations have been performed, it is left to the user's discretion to determine the most probable area of highest dose based on the distribution of dose on the graph paper. After determining this area, the user can perform a final calculation for each particle by using the offset particle model. An accuracy of greater than 20 percent should not be anticipated.

7 REFERENCES

Attix, F.H. Introduction to Radiological Physics and Radiation Dosimetry. New York, NY: John Wiley & Sons. 1986.

Berger, M.J. "Distribution of Absorbed Dose Around Point Sources of Electrons and Beta Particles in Water and Other Media." Medical Internal Radiation Dose Committee, Pamphlet No. 7. *Journal of Nuclear Medicine*. Vol. 12, Supplement No. 5. pp. 5–22. 1971.

Berger, M.J., J.S. Coursey, M.A. Zucker, and J. Change. "Stopping-Power and Range Tables for Electrons, Protons, and Helium Ions." ESTAR, PSTAR, and ASTAR databases. Washington, DC: National Institute of Standards and Technology. <http://physics.nist.gov/PhysRefData/Star/Text/contents.html> (February 14, 2006).

Cross, W.G., N.O. Freedman, and P.Y. Wong. "Tables of Beta-Ray Dose Distributions in Water." AECL 10521, CA9200298. Chalk River, Ontario, Canada: Chalk River Laboratories, Dosimetric Research Branch. 1992.

Delacroix, D. "Beta Particle and Electron Absorbed Dose Calculations for Skin Surface Contaminations" (in French). DCES/SPR/SRI/86–656. Paris, France: Commissariat à l'Energie Atomique. 1986.

Durham, J.S. "VARSKIN 3: A Computer Code for Assessing Skin Dose from Skin Contamination." NUREG/CR-6918. Washington, DC: U.S. Nuclear Regulatory Commission. 2006.

Durham, J.S. "VARSKIN Mod 2 and SADDE Mod 2: Computer Codes for Assessing Skin Dose from Skin Contamination." NUREG/CR-5873, PNL-7913. Washington, DC: NRC. 1992.

Durham, J.S., and M.W. Lantz. "Determination of Gamma Dose Rates and Charged Particle Equilibrium from Hot Particles." *Radiation Protection Management*. Vol. 8, No. 3. pp. 35–41. 1991.

International Commission on Radiation Units and Measurements. "Tissue Substitutes in Radiation Dosimetry and Measurement." ICRU Report 44. Bethesda, MD: International Commission on Radiation Units and Measurements. 1989.

International Commission on Radiological Protection. "The Biological Basis for Dose Limitation in the Skin." Publication 59. Oxford, England: Pergamon Press. 1991.

International Commission on Radiological Protection. "Radionuclide Transformations." Publication 38. Oxford, England: Pergamon Press. 1983.

International Commission on Radiation Protection. "Nuclear Decay Data for Dosimetric Calculations." Publication 107. Ann. ICRP 38 (3). 2008

Johns, H.E., and J.R. Cunningham. The Physics of Radiology. 4th Edition. Springfield, IL:

Charles C. Thomas. 1983.

Kawrakow, I., & Rogers, D. W. (2000). The EGSnrc code system: Monte Carlo simulation of electron and photon transport. *Technical Report* PIRS-701. Ottawa, Canada: National Research Council of Canada.

Kocher, D.C., and K.F. Eckerman. "Electron Dose-Rate Conversion Factors for External Exposure of the Skin from Uniformly Deposited Activity on the Body Surface." *Health Physics*. Vol. 53. pp.135–141. 1987.

Lantz, M.W., and M.W. Lambert. "Charged Particle Equilibrium Corrections for the Gamma Component of Hot Particle Skin Doses." *Radiation Protection Management*. Vol. 7, No. 5. pp. 38–48. 1990.

Ljungberg, M., S.E. Strand, and M.A. King. Monte Carlo Calculations in Nuclear Medicine, Second Edition. CRC Press. pp. Chapter 10, 175–195. ISBN 9781439841099. 2012.

Los Alamos National Laboratory, X-5 Monte Carlo Team. "MCNP—A General Monte Carlo N-Particle Transport Code, Version 5. LA-CP-03-0245. Los Alamos, NM: LANL. 2003.

Mangini, C.D. "Beta-particle backscatter factors and energy-absorption scaling factors for use with dose-point kernels." Doctoral Dissertation. Oregon State University. December 2012.

NIST website, http://physics.nist.gov/PhysRefData/Star/Text/ESTAR.html).

Piechowski, J. "Dosimetry and Therapy of Skin Contaminations" (in French). CEA–R–5441. Paris, France: Commissariat à l'Energie Atomique. 1988.

Radiation Safety Information Computational Center. "MCNP4c2, Coupled Neutron, Electron Gamma 3-D Time-Dependent Monte Carlo Transport Calculations." CCC–701. Oak Ridge, TN: RSICC. 2001.

Radiation Safety Information Computational Center. "NUCDECAY: Nuclear Decay Data for Radiation Dosimetry Calculations for ICRP and MIRD." CCC–701. Oak Ridge, TN: RSICC. 1995.

Reece, W.D., S.D. Miller, and J.S. Durham. "SADDE (Scaled Absorbed Dose Distribution Evaluator), A Code to Generate Input for VARSKIN." NUREG/CR–5276. Washington, DC: NRC. 1989.

Rogers, D. W. O. (2006). Fifty years of Monte Carlo simulations for medical physics. *Physics in Medicine and Biology, 51*, R287-R301.

Rohloff, F. and M. Heinzelmann. "Calculation of Dose Rates for Skin Contamination by Beta Radiation." *Radiation Protection Dosimetry*. Vol. 14. pp. 279–287. 1986.

Sherbini, S., J. DeCicco, A.T. Gray, and R. Struckmeyer. "Verification of the Varskin Beta Skin Dose Calculation Computer Code," *Health Physics.* Vol. 94. pp. 527–538. 2008.

Spencer, L. V. (1955). Theory of electron Penetration. *Physical Review, 98*, 1597-1615.

Spencer, L. V. (1959). Energy Dissipation by Fast Electrons. *National Bureau of Standards Monograph 1.*

Traub, R.J., W.D. Reece, R.I. Scherpelz, and L.A. Sigalla. "Dose Calculation for Contamination of the Skin Using the Computer Code VARSKIN." NUREG/CR–4418. Washington, DC: NRC. 1987.

U.S. Nuclear Regulatory Commission. News Release No. 02-039. http://www.nrc.gov/reading-rm/doc-collections/news/2002/02-039.html. April 2, 2002. Last Accessed March 2006.

APPENDIX A

Supporting Figures from Section 5

GEOMETRY 1:
POINT SOURCE

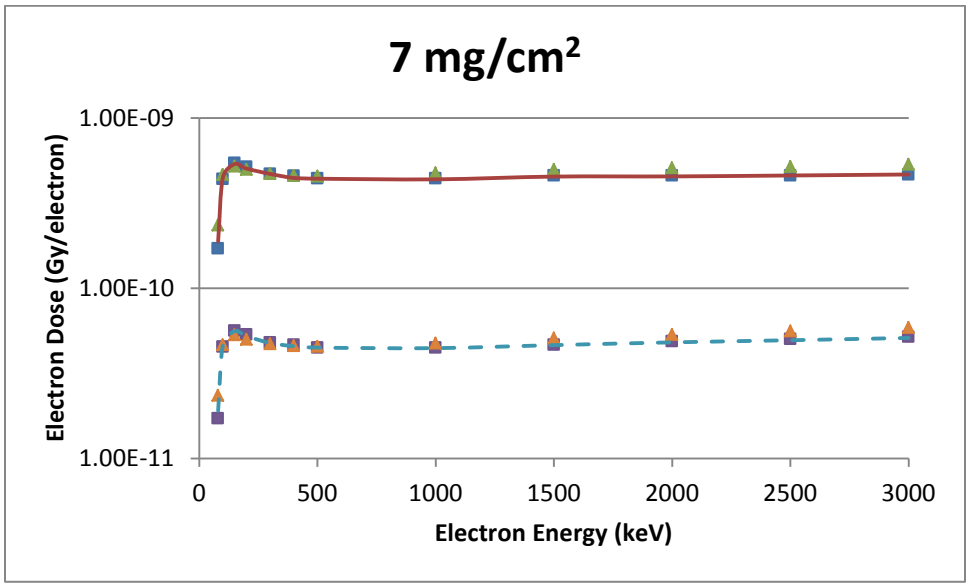

Figure A.1.1. A point source geometry comparison of VARSKIN 5 (boxes), MCNP5 (triangles) and EGSnrc (lines) predicted dose per initial electron as a function of electron energy in tissue at a density thickness of 7 mg/cm^2 and a 20 μm thick tissue volume cylinder of area 1 cm^2 (solid line) and 10 cm^2 (dashed line).

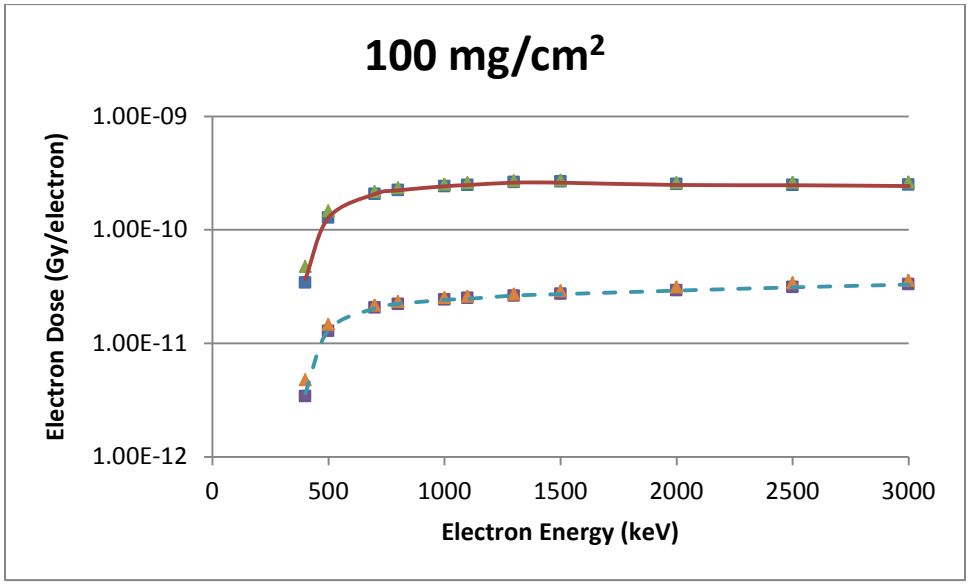

Figure A.1.2. A point source geometry comparison of VARSKIN 5 (boxes), MCNP5 (triangles) and EGSnrc (lines) predicted dose per initial electron as a function of electron energy in tissue at a density thickness of 100 mg/cm^2 and a 20 μm thick tissue volume cylinder of area 1 cm^2 (solid line) and 10 cm^2 (dashed line).

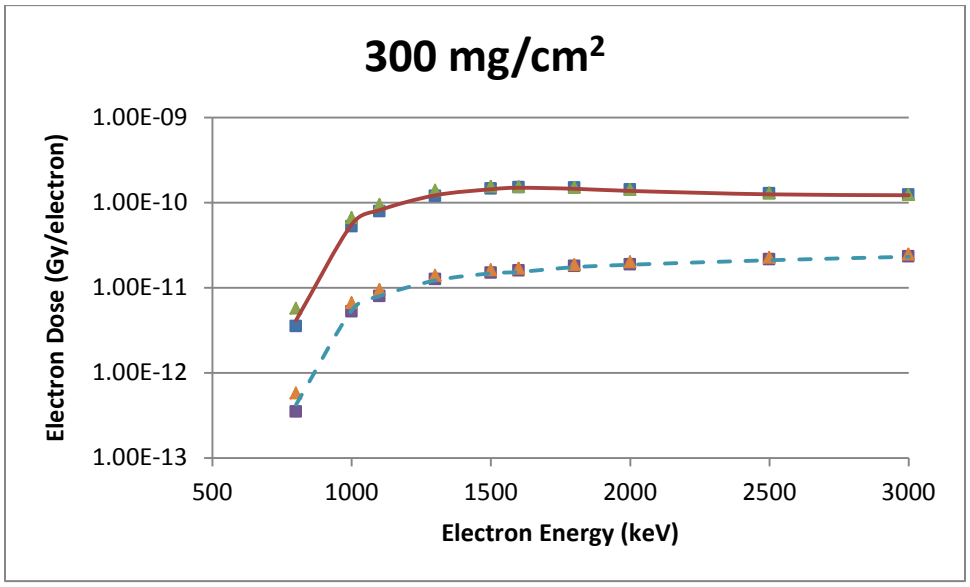

Figure A.1.3. A point source geometry comparison of VARSKIN 5 (boxes), MCNP5 (triangles) and EGSnrc (lines) predicted dose per initial electron as a function of electron energy in tissue at a density thickness of 300 mg/cm^2 and a 20 μm thick tissue volume cylinder of area 1 cm^2 (solid line) and 10 cm^2 (dashed line).

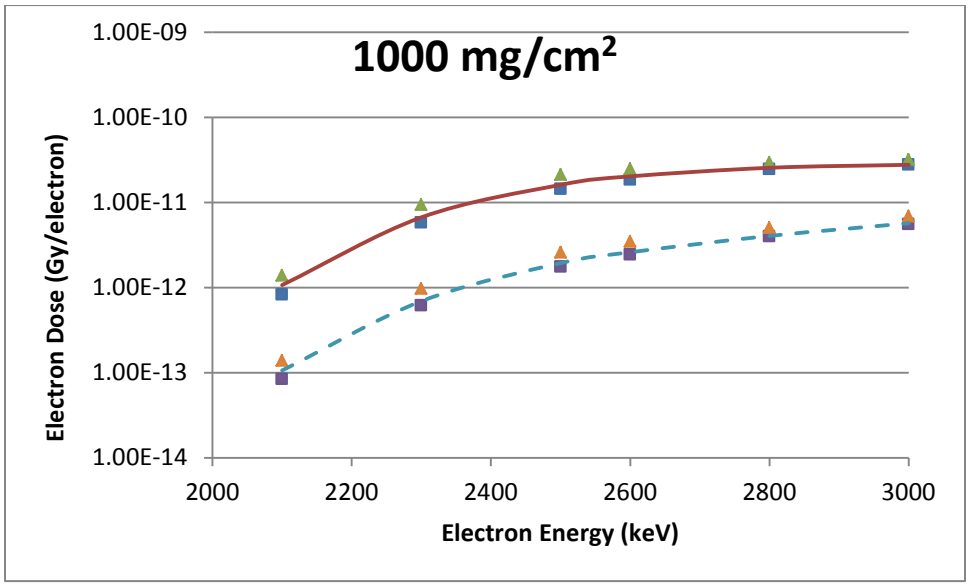

Figure A.1.4. A point source geometry comparison of VARSKIN 5 (boxes), MCNP5 (triangles) and EGSnrc (lines) predicted dose per initial electron as a function of electron energy in tissue at a density thickness of 1000 mg/cm^2 and a 20 μm thick tissue volume cylinder of area 1 cm^2 (solid line) and 10 cm^2 (dashed line).

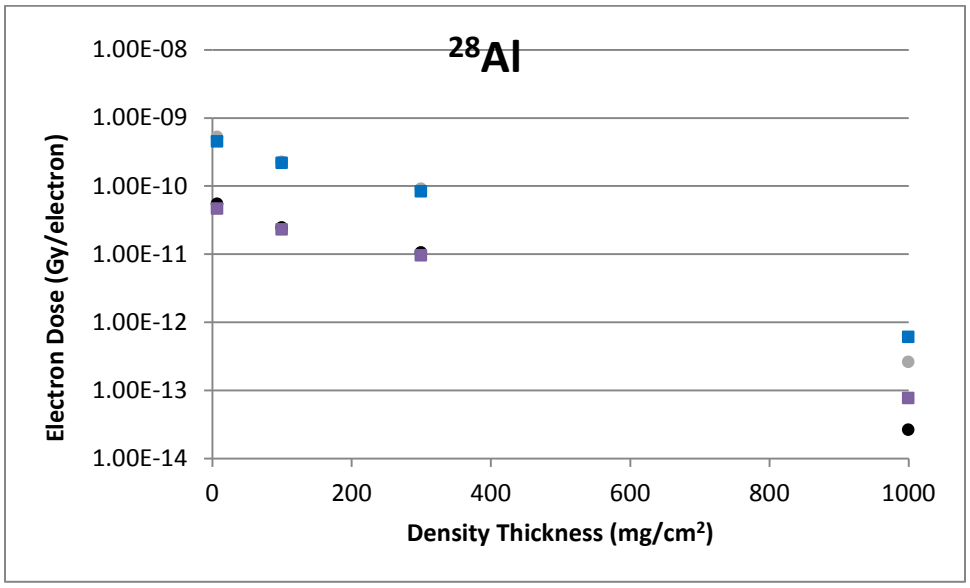

Figure A.1.5. A point source geometry comparison of VARSKIN 5 (boxes) and VARSKIN 4 (circles) predicted dose per initial beta from ^{28}Al as a function of density thickness in tissue and a tissue volume cylinder of area 1 cm^2 (upper) and 10 cm^2 (lower), with a thickness of 20 µm

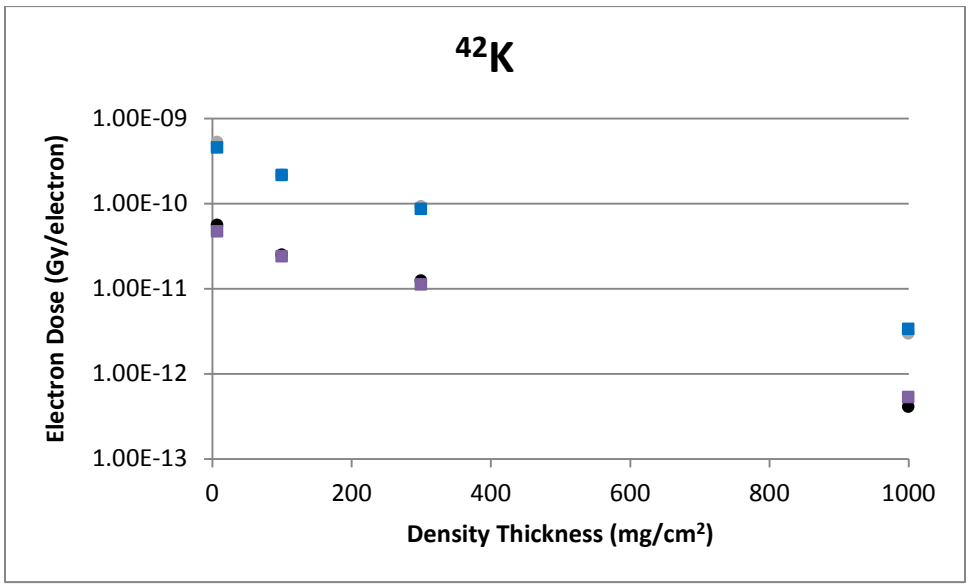

Figure A.1.6. A point source geometry comparison of VARSKIN 5 (boxes) and VARSKIN 4 (circles) predicted dose per initial beta from ^{42}K as a function of density thickness in tissue and a tissue volume cylinder of area 1 cm^2 (upper) and 10 cm^2 (lower), with a thickness of 20 µm

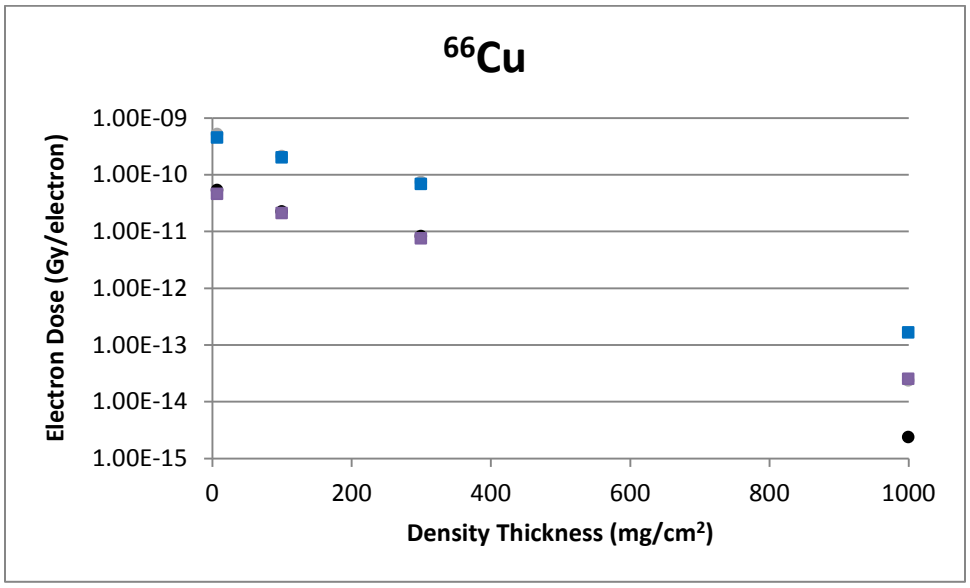

Figure A.1.7. A point source geometry comparison of VARSKIN 5 (boxes) and VARSKIN 4 (circles) predicted dose per initial beta from ^{66}Cu as a function of density thickness in tissue and a tissue volume cylinder of area 1 cm^2 (upper) and 10 cm^2 (lower), with a thickness of 20 µm

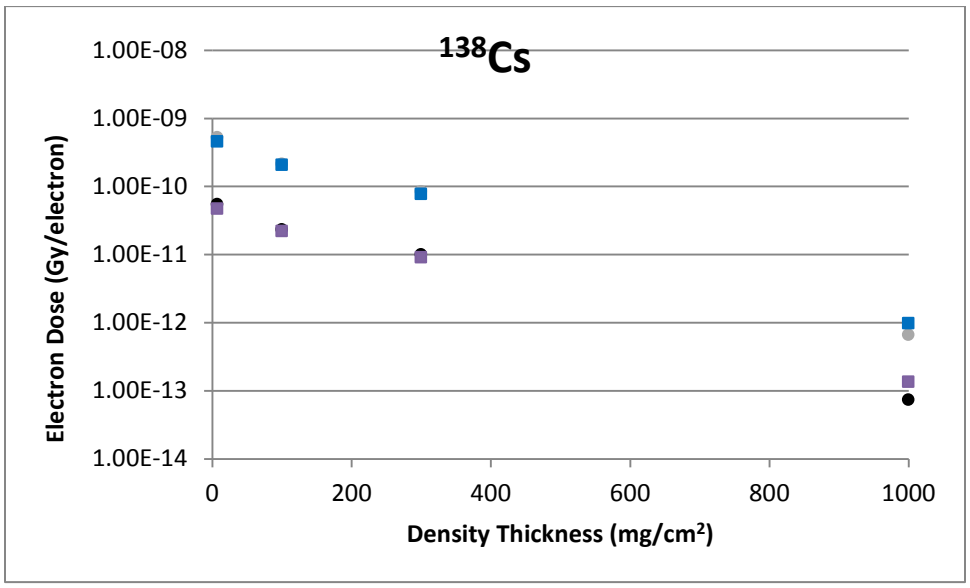

Figure A.1.8. A point source geometry comparison of VARSKIN 5 (boxes) and VARSKIN 4 (circles) predicted dose per initial beta from ^{138}Cs as a function of density thickness in tissue and a tissue volume cylinder of area 1 cm^2 (upper) and 10 cm^2 (lower), with a thickness of 20 µm

GEOMETRY 2:
DISK SOURCE (0.5 mm dia)

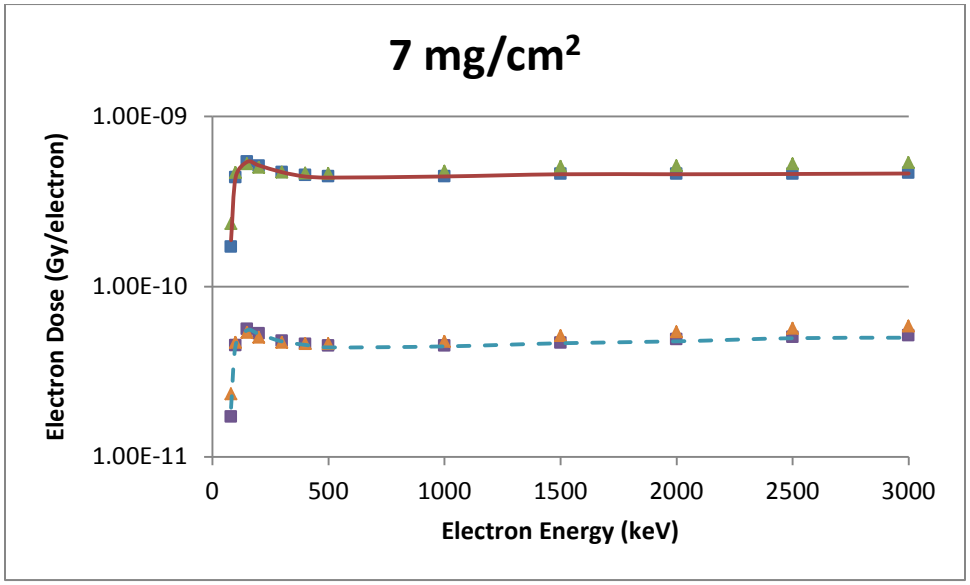

Figure A.2.1. A 0.5 mm diameter disk source geometry comparison of VARSKIN 5 (boxes), MCNP5 (triangles) and EGSnrc (lines) predicted dose per initial electron as a function of electron energy in tissue at a density thickness of 7 mg/cm^2 and a tissue volume cylinder of area 1 cm^2 (solid line) and 10 cm^2 (dashed line), with a thickness of 20 µm

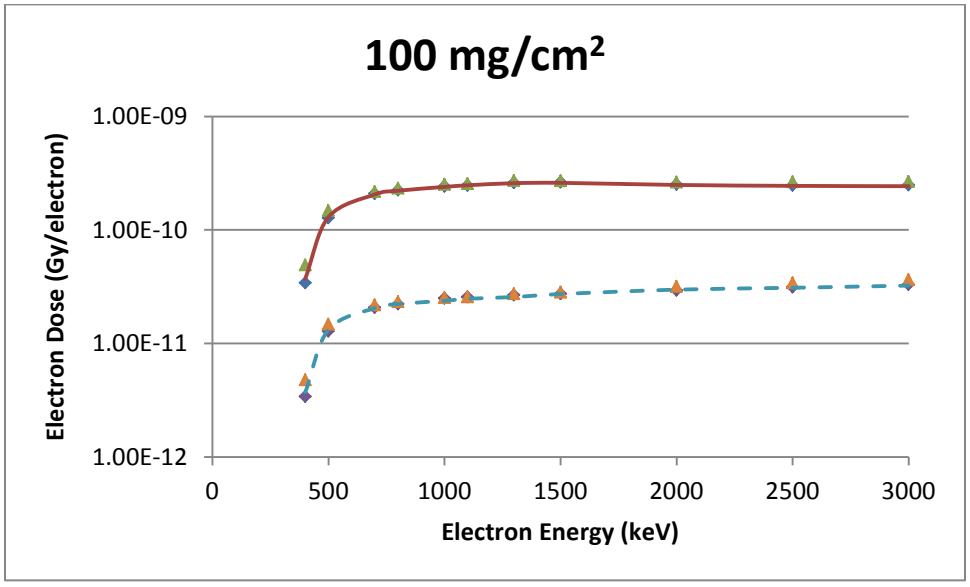

Figure A.2.2. A 0.5 mm diameter disk source geometry comparison of VARSKIN 5 (boxes), MCNP5 (triangles) and EGSnrc (lines) predicted dose per initial electron as a function of electron energy in tissue at a density thickness of 100 mg/cm^2 and a tissue volume cylinder of area 1 cm^2 (solid line) and 10 cm^2 (dashed line), with a thickness of 20 µm

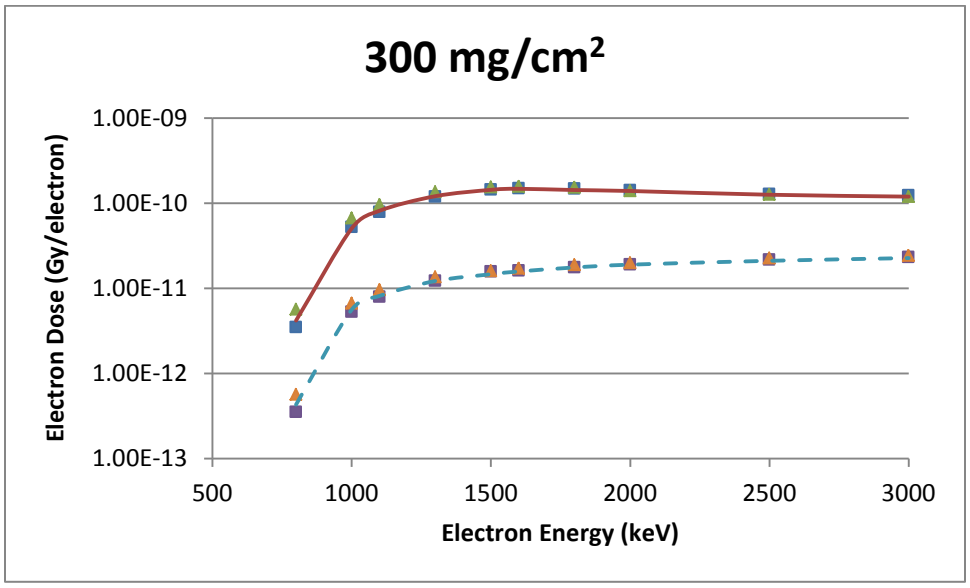

Figure A.2.3. A 0.5 mm diameter disk source geometry comparison of VARSKIN 5 (boxes), MCNP5 (triangles) and EGSnrc (lines) predicted dose per initial electron as a function of electron energy in tissue at a density thickness of 300 mg/cm^2 and a tissue volume cylinder of area 1 cm^2 (solid line) and 10 cm^2 (dashed line), with a thickness of 20 µm

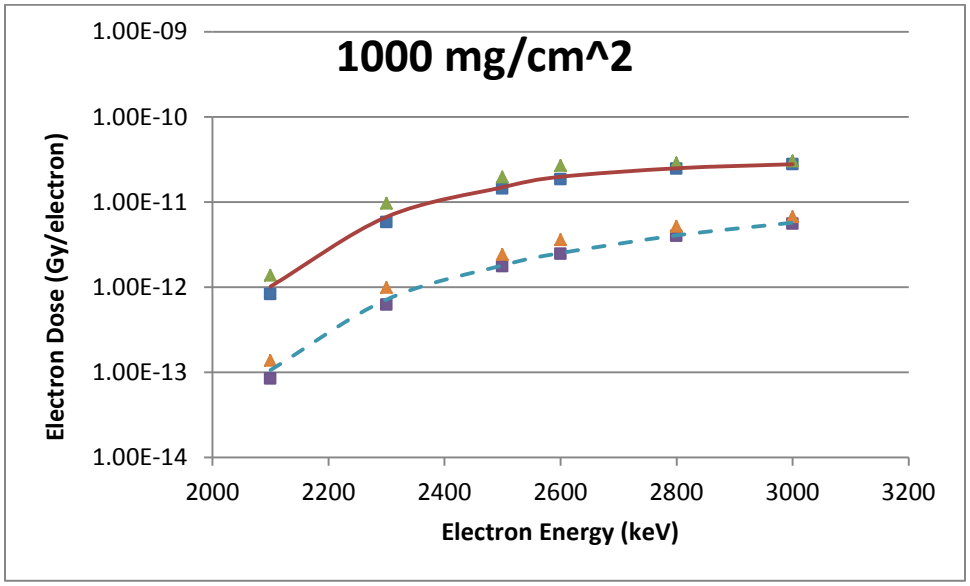

Figure A.2.4. A 0.5 mm diameter disk source geometry comparison of VARSKIN 5 (boxes), MCNP5 (triangles) and EGSnrc (lines) predicted dose per initial electron as a function of electron energy in tissue at a density thickness of 1000 mg/cm^2 and a tissue volume cylinder of area 1 cm^2 (solid line) and 10 cm^2 (dashed line), with a thickness of 20 µm

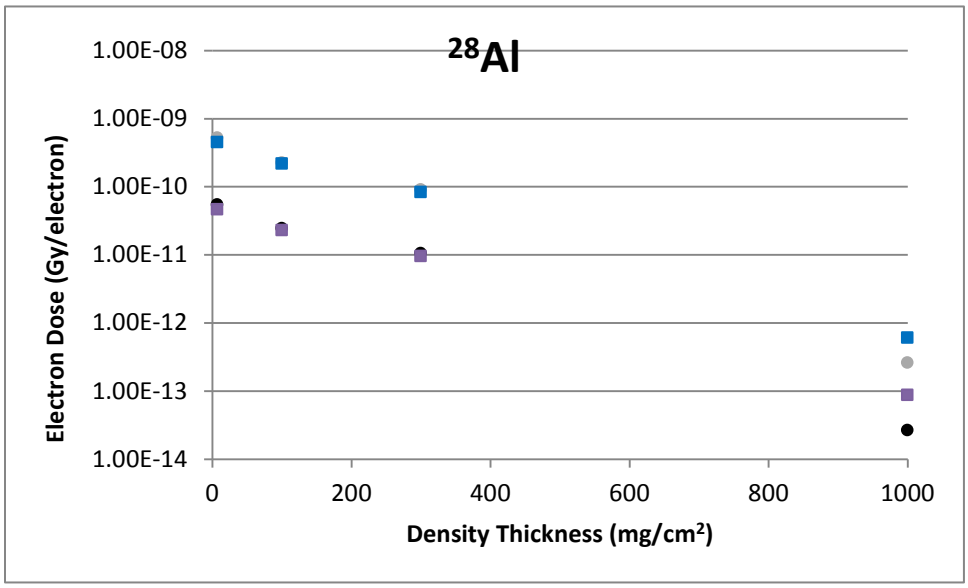

Figure A.2.5. A 0.5 mm diameter disk geometry comparison of VARSKIN 5 (boxes) and VARSKIN 4 (circles) predicted dose per initial beta from ^{28}Al as a function of density thickness in tissue and a tissue volume cylinder of area 1 cm^2 (upper) and 10 cm^2 (lower), with a thickness of 20 µm

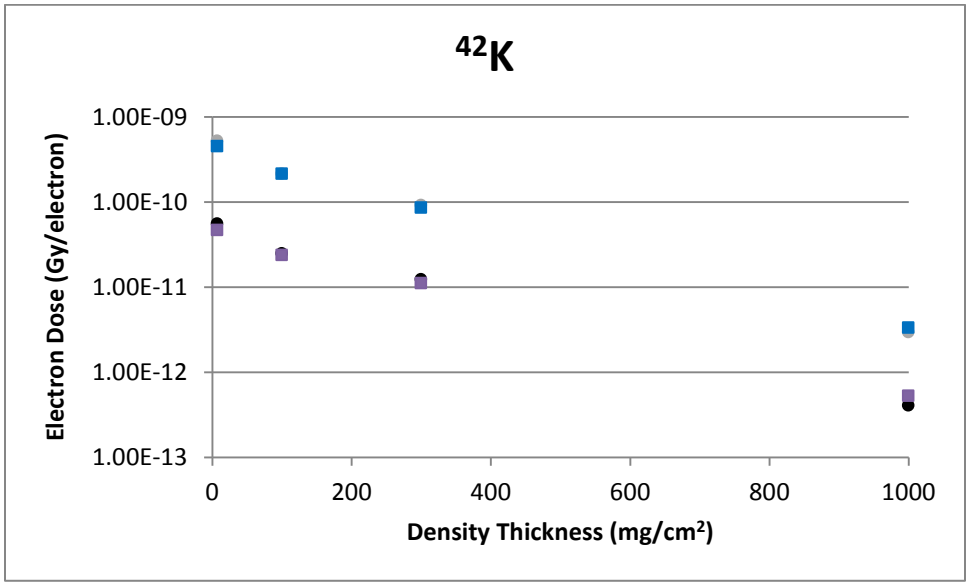

Figure A.2.6. A 0.5 mm diameter disk geometry comparison of VARSKIN 5 (boxes) and VARSKIN 4 (circles) predicted dose per initial beta from ^{42}K as a function of density thickness in tissue and a tissue volume cylinder of area 1 cm^2 (upper) and 10 cm^2 (lower), with a thickness of 20 µm

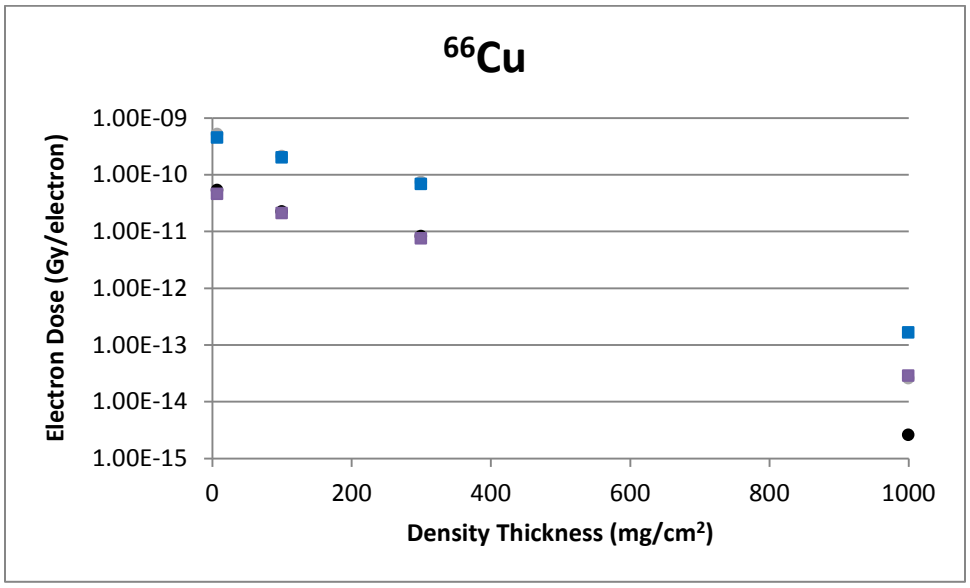

Figure A.2.7. A 0.5 mm diameter disk geometry comparison of VARSKIN 5 (boxes) and VARSKIN 4 (circles) predicted dose per initial beta from ^{66}Cu as a function of density thickness in tissue and a tissue volume cylinder of area 1 cm^2 (upper) and 10 cm^2 (lower), with a thickness of 20 µm

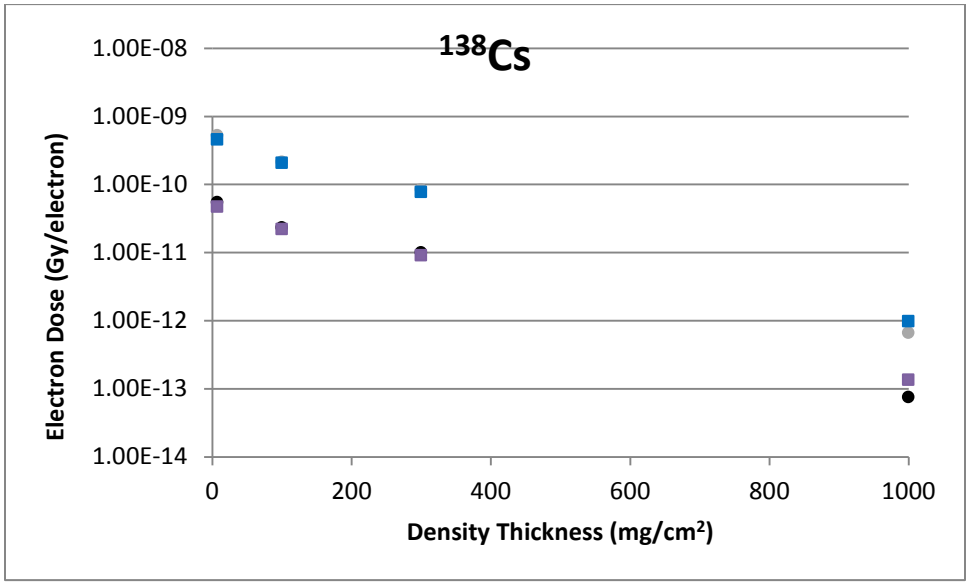

Figure A.2.8. A 0.5 mm diameter disk geometry comparison of VARSKIN 5 (boxes) and VARSKIN 4 (circles) predicted dose per initial beta from ^{138}Cs as a function of density thickness in tissue and a tissue volume cylinder of area 1 cm^2 (upper) and 10 cm^2 (lower), with a thickness of 20 µm

GEOMETRY 3:
DISK SOURCE (1 mm dia)

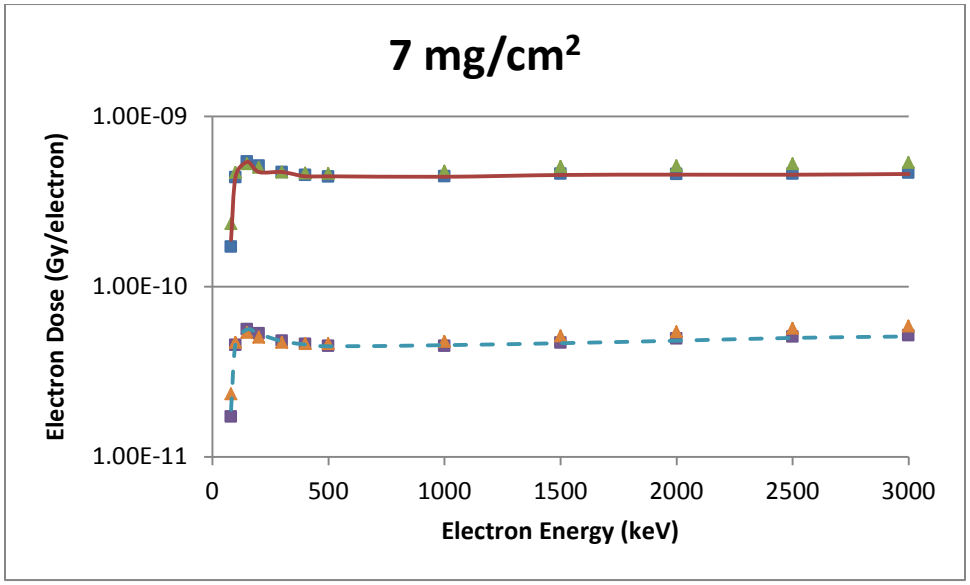

Figure A.3.1. A 1 mm diameter disk source geometry comparison of VARSKIN 5 (boxes), MCNP5 (triangles) and EGSnrc (lines) predicted dose per initial electron as a function of electron energy in tissue at a density thickness of 7 mg/cm^2 and a tissue volume cylinder of area 1 cm^2 (solid line) and 10 cm^2 (dashed line), with a thickness of 20 µm

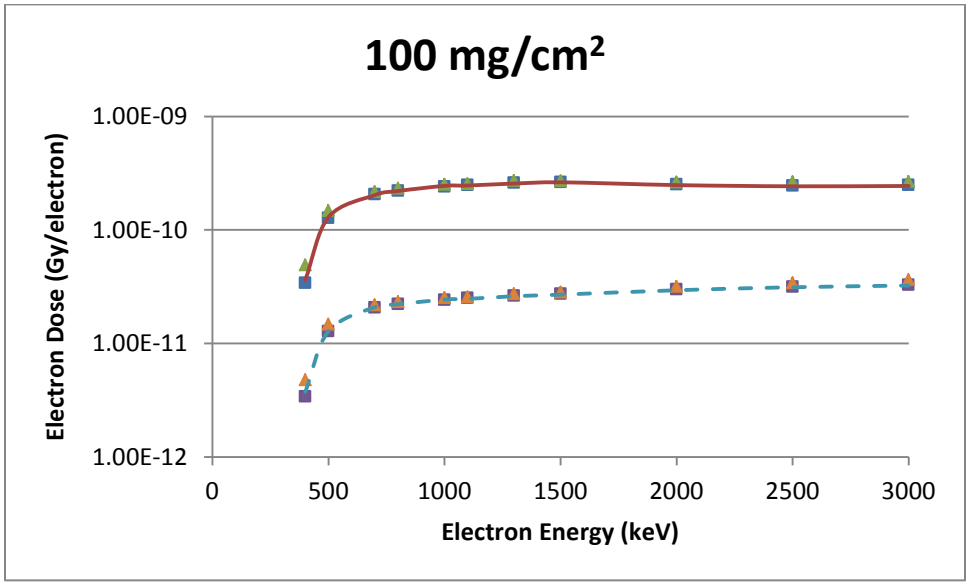

Figure A.3.2. A 1 mm diameter disk source geometry comparison of VARSKIN 5 (boxes), MCNP5 (triangles) and EGSnrc (lines) predicted dose per initial electron as a function of electron energy in tissue at a density thickness of 100 mg/cm^2 and a tissue volume cylinder of area 1 cm^2 (solid line) and 10 cm^2 (dashed line), with a thickness of 20 µm

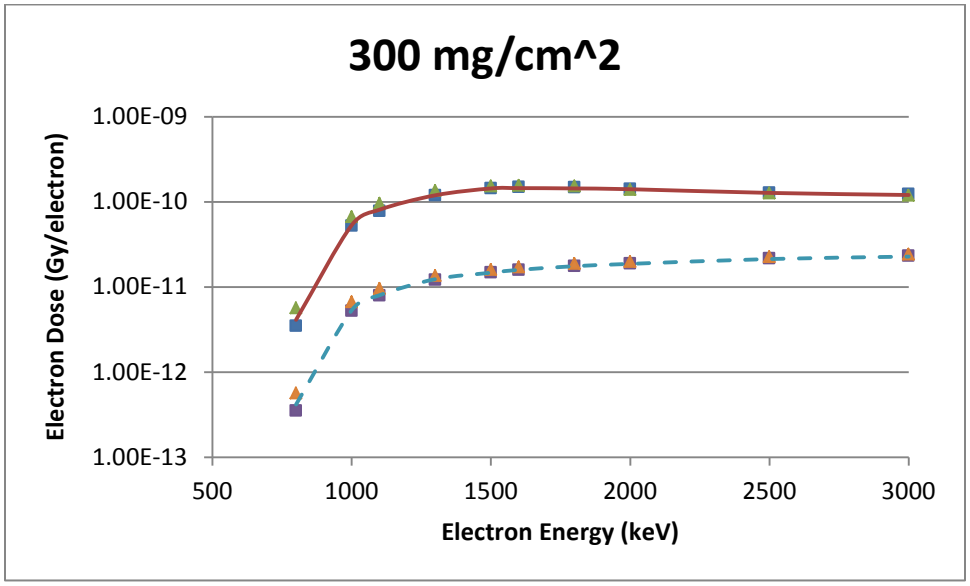

Figure A.3.3. A 1 mm diameter disk source geometry comparison of VARSKIN 5 (boxes), MCNP5 (triangles) and EGSnrc (lines) predicted dose per initial electron as a function of electron energy in tissue at a density thickness of 300 mg/cm^2 and a tissue volume cylinder of area 1 cm^2 (solid line) and 10 cm^2 (dashed line), with a thickness of 20 μm

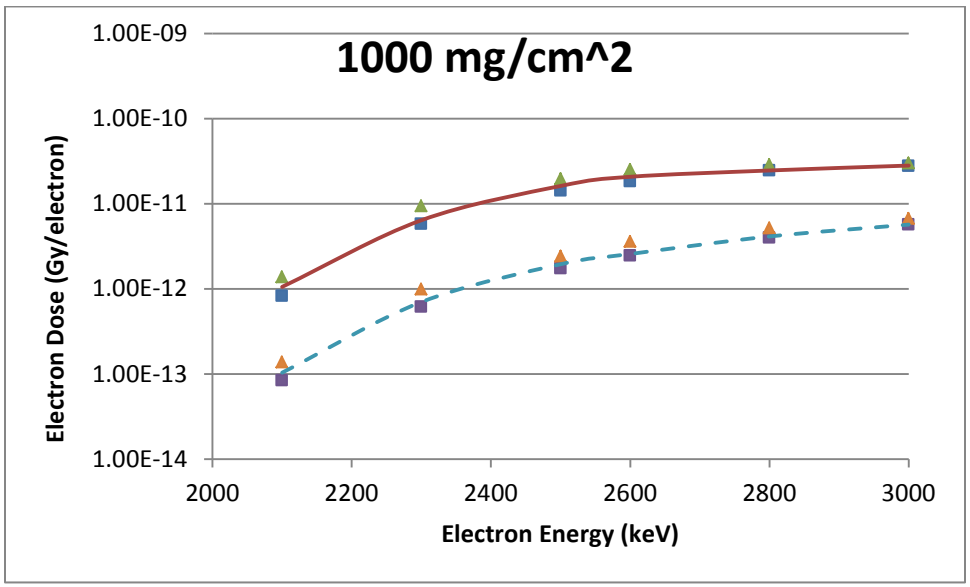

Figure A.3.4. A 1 mm diameter disk source geometry comparison of VARSKIN 5 (boxes), MCNP5 (triangles) and EGSnrc (lines) predicted dose per initial electron as a function of electron energy in tissue at a density thickness of 1000 mg/cm^2 and a tissue volume cylinder of area 1 cm^2 (solid line) and 10 cm^2 (dashed line), with a thickness of 20 μm

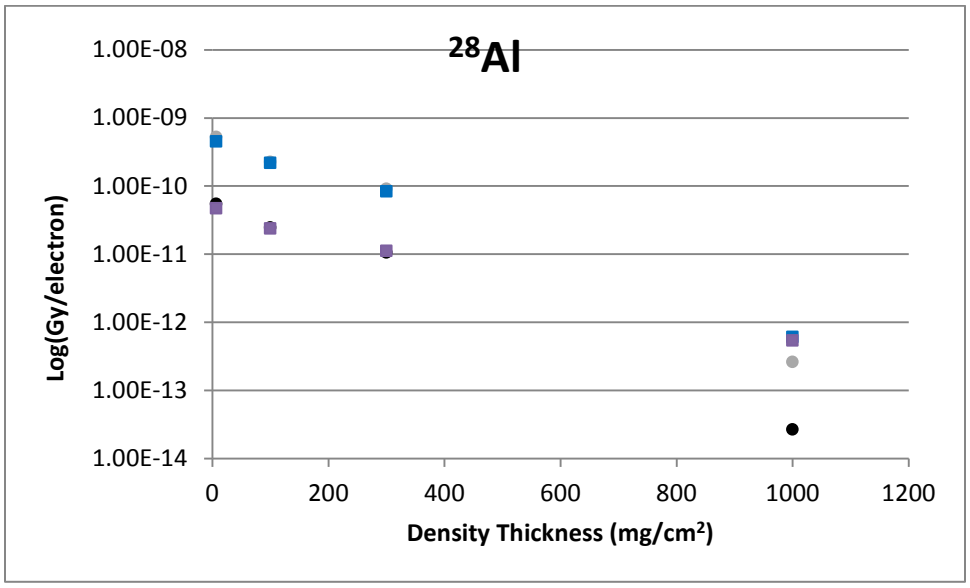

Figure A.3.5. A 1 mm diameter disk geometry comparison of VARSKIN 5 (boxes) and VARSKIN 4 (circles) predicted dose per initial beta from ^{28}Al as a function of density thickness in tissue and a tissue volume cylinder of area 1 cm^2 (upper) and 10 cm^2 (lower), with a thickness of 20 µm

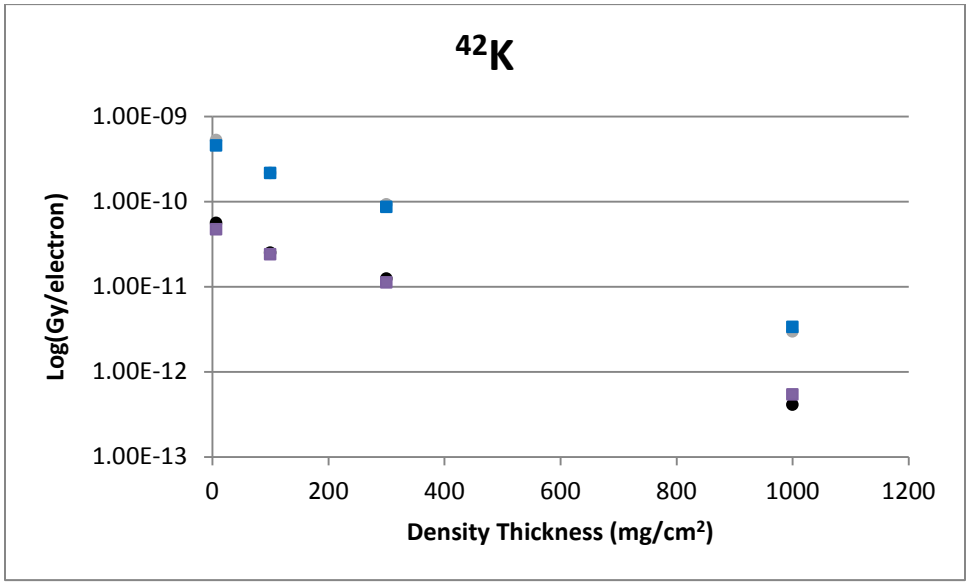

Figure A.3.6. A 1 mm diameter disk geometry comparison of VARSKIN 5 (boxes) and VARSKIN 4 (circles) predicted dose per initial beta from ^{42}K as a function of density thickness in tissue and a tissue volume cylinder of area 1 cm^2 (upper) and 10 cm^2 (lower), with a thickness of 20 µm

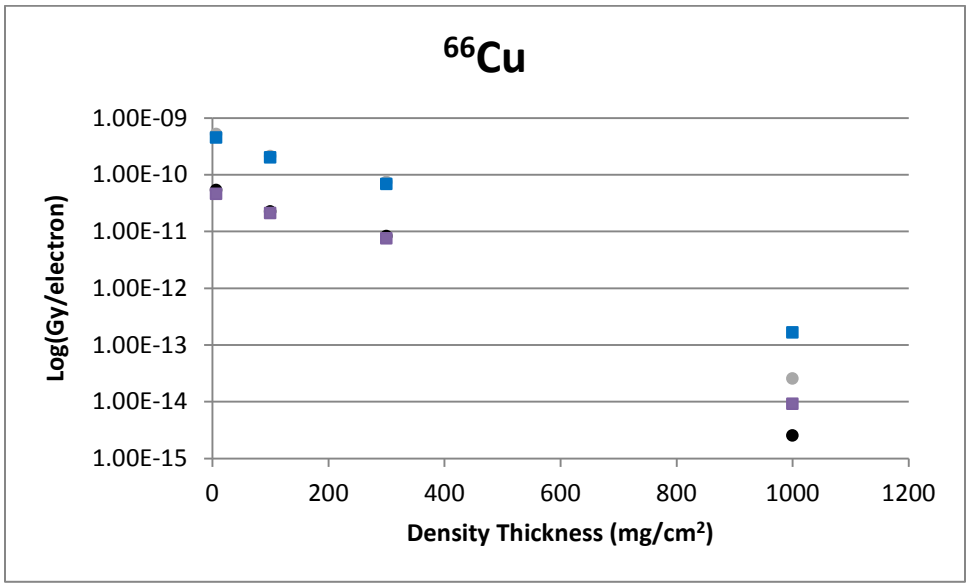

Figure A.3.7. A 1 mm diameter disk geometry comparison of VARSKIN 5 (boxes) and VARSKIN 4 (circles) predicted dose per initial beta from ^{66}Cu as a function of density thickness in tissue and a tissue volume cylinder of area 1 cm^2 (upper) and 10 cm^2 (lower), with a thickness of 20 µm

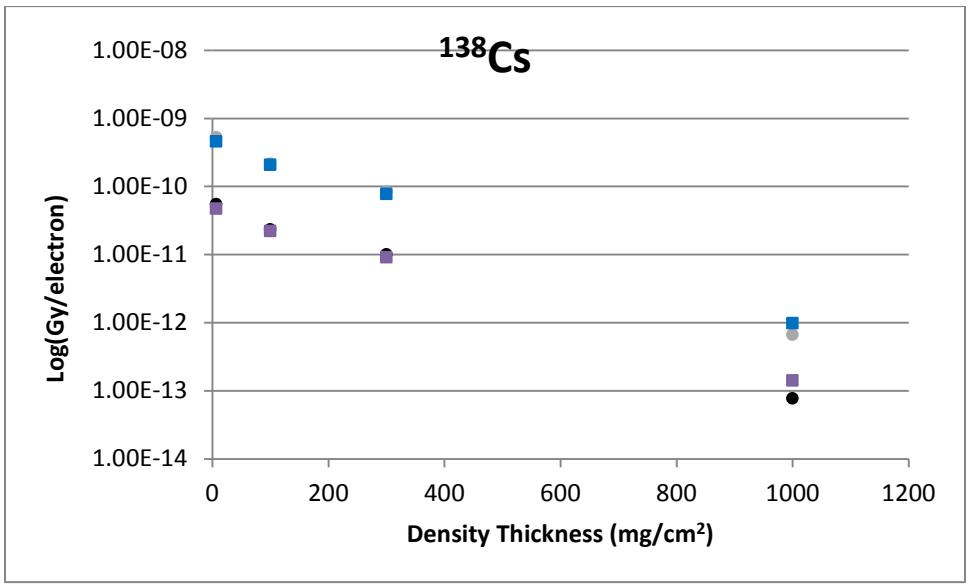

Figure A.3.8. A 1 mm diameter disk geometry comparison of VARSKIN 5 (boxes) and VARSKIN 4 (circles) predicted dose per initial beta from ^{138}Cs as a function of density thickness in tissue and a tissue volume cylinder of area 1 cm^2 (upper) and 10 cm^2 (lower), with a thickness of 20 µm

GEOMETRY 4:
DISK SOURCE (5 mm dia)

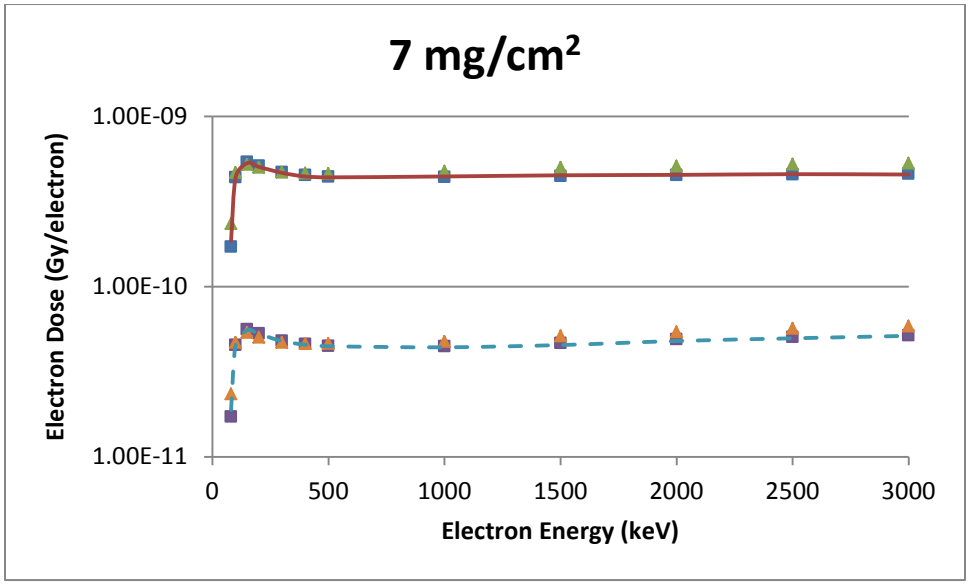

Figure A.4.1. A 5 mm diameter disk source geometry comparison of VARSKIN 5 (boxes), MCNP5 (triangles) and EGSnrc (lines) predicted dose per initial electron as a function of electron energy in tissue at a density thickness of 7 mg/cm^2 and a tissue volume cylinder of area 1 cm^2 (solid line) and 10 cm^2 (dashed line), with a thickness of 20 µm

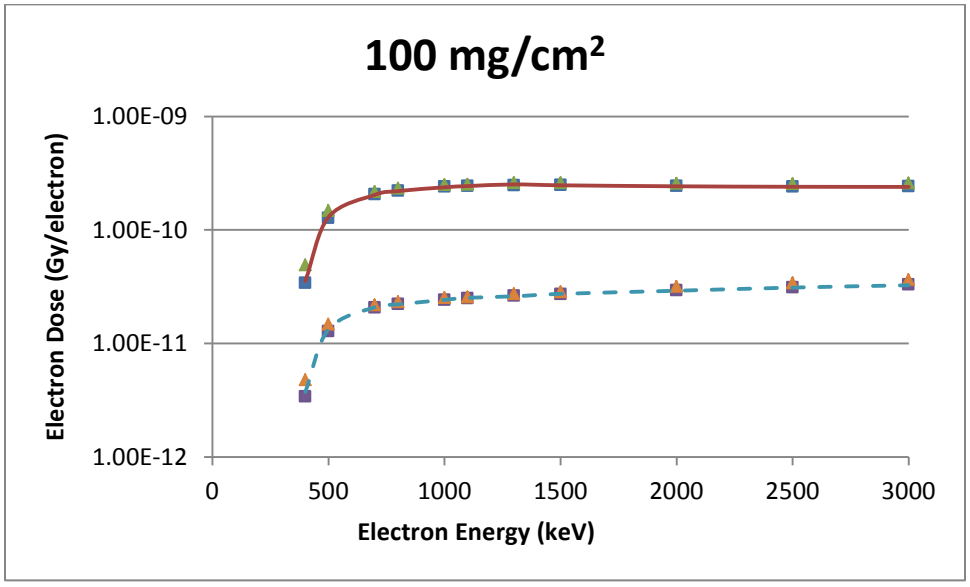

Figure A.4.2. A 5 mm diameter disk source geometry comparison of VARSKIN 5 (boxes), MCNP5 (triangles) and EGSnrc (lines) predicted dose per initial electron as a function of electron energy in tissue at a density thickness of 100 mg/cm^2 and a tissue volume cylinder of area 1 cm^2 (solid line) and 10 cm^2 (dashed line), with a thickness of 20 µm

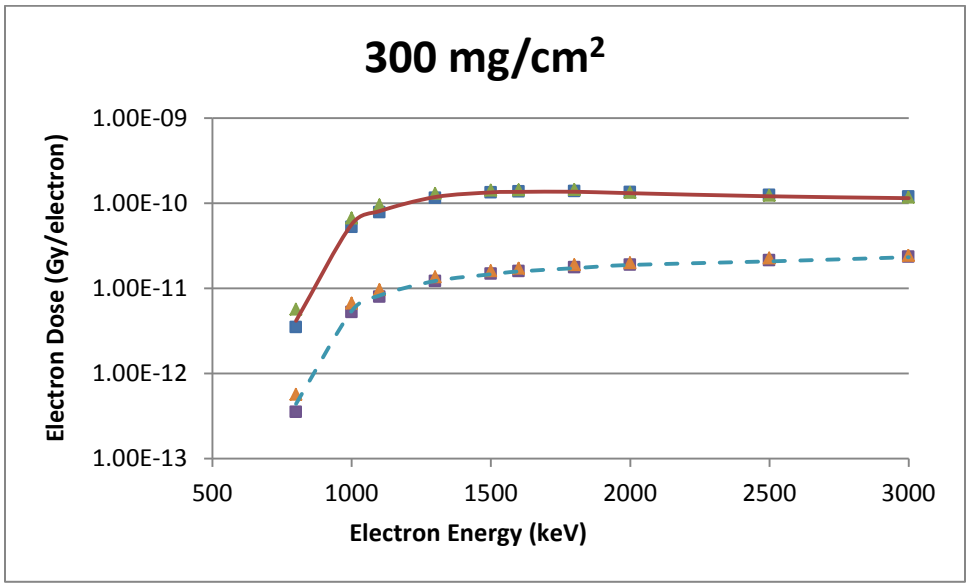

Figure A.4.3. A 5 mm diameter disk source geometry comparison of VARSKIN 5 (boxes), MCNP5 (triangles) and EGSnrc (lines) predicted dose per initial electron as a function of electron energy in tissue at a density thickness of 300 mg/cm^2 and a tissue volume cylinder of area 1 cm^2 (solid line) and 10 cm^2 (dashed line), with a thickness of 20 μm

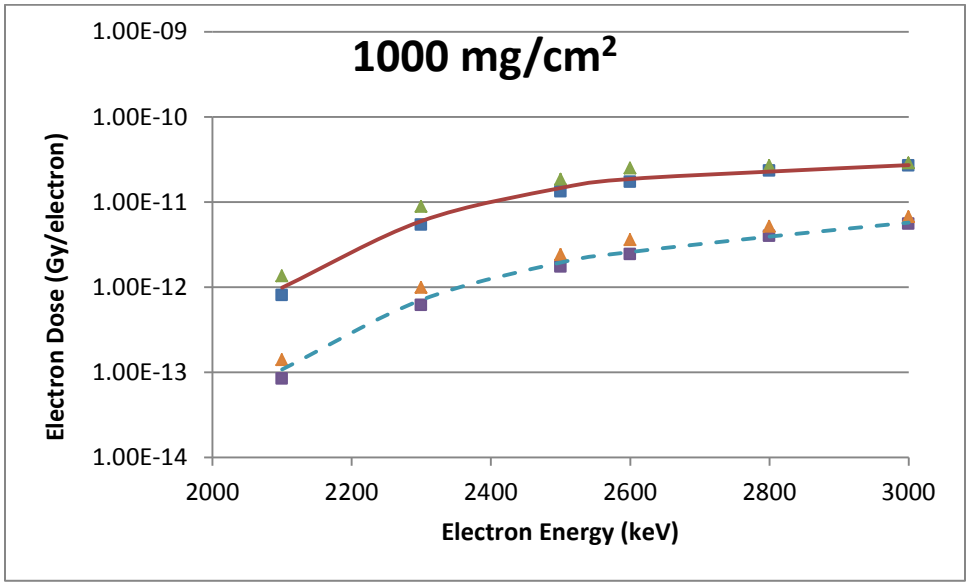

Figure A.4.4. A 5 mm diameter disk source geometry comparison of VARSKIN 5 (boxes), MCNP5 (triangles) and EGSnrc (lines) predicted dose per initial electron as a function of electron energy in tissue at a density thickness of 1000 mg/cm^2 and a tissue volume cylinder of area 1 cm^2 (solid line) and 10 cm^2 (dashed line), with a thickness of 20 μm

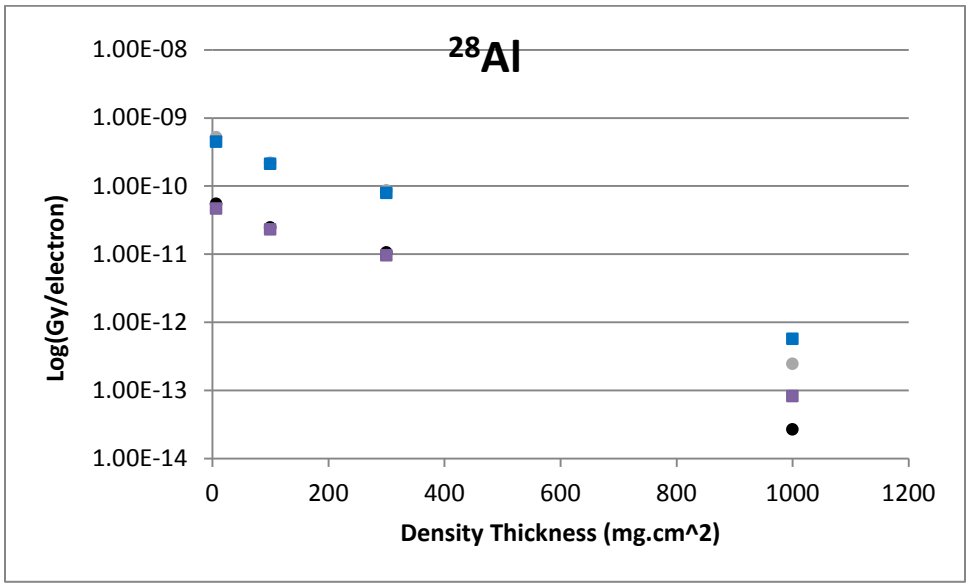

Figure A.4.5. A 5 mm diameter disk geometry comparison of VARSKIN 5 (boxes) and VARSKIN 4 (circles) predicted dose per initial beta from ^{28}Al as a function of density thickness in tissue and a tissue volume cylinder of area 1 cm^2 (upper) and 10 cm^2 (lower), with a thickness of 20 µm

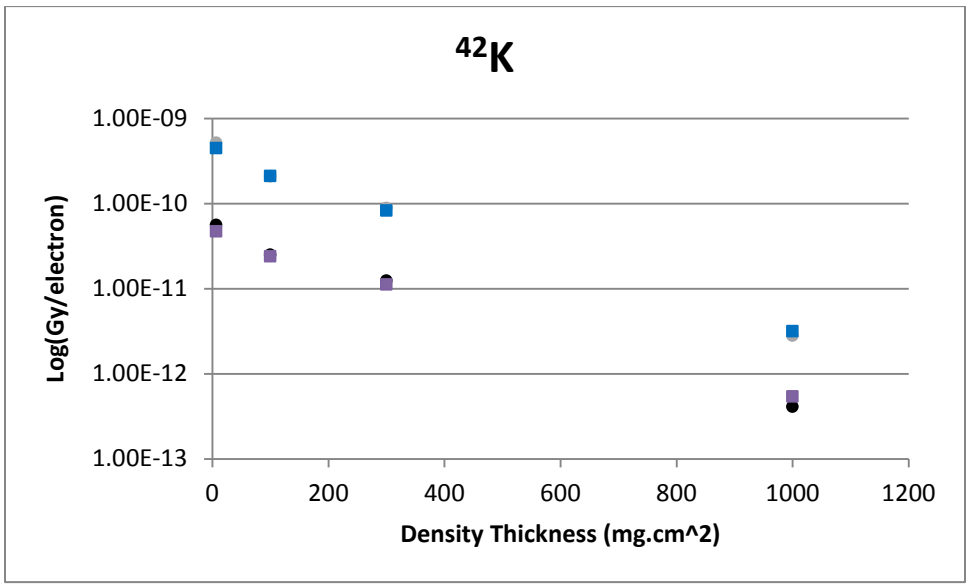

Figure A.4.6. A 5 mm diameter disk geometry comparison of VARSKIN 5 (boxes) and VARSKIN 4 (circles) predicted dose per initial beta from ^{42}K as a function of density thickness in tissue and a tissue volume cylinder of area 1 cm^2 (upper) and 10 cm^2 (lower), with a thickness of 20 µm

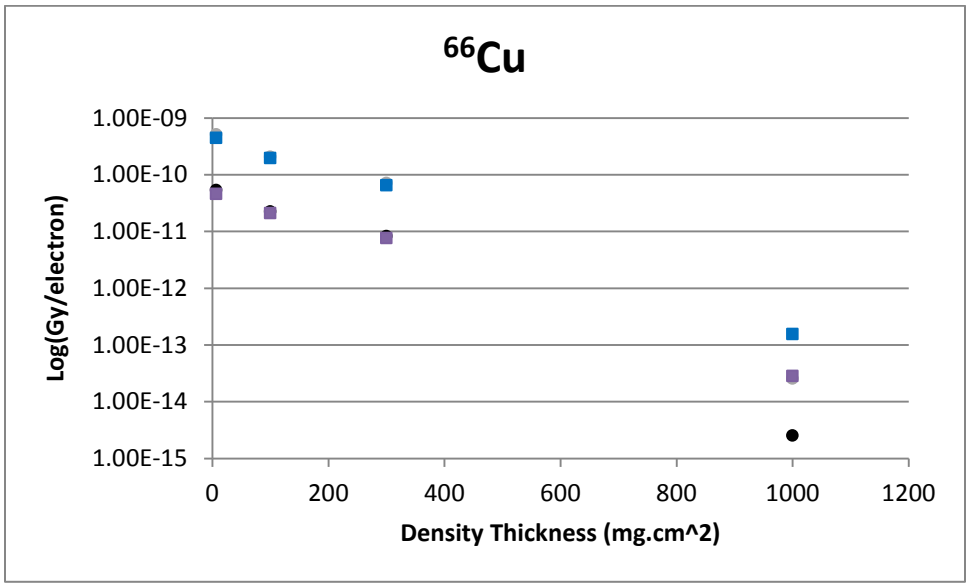

Figure A.4.7. A 5 mm diameter disk geometry comparison of VARSKIN 5 (boxes) and VARSKIN 4 (circles) predicted dose per initial beta from ^{66}Cu as a function of density thickness in tissue and a tissue volume cylinder of area 1 cm^2 (upper) and 10 cm^2 (lower), with a thickness of 20 µm

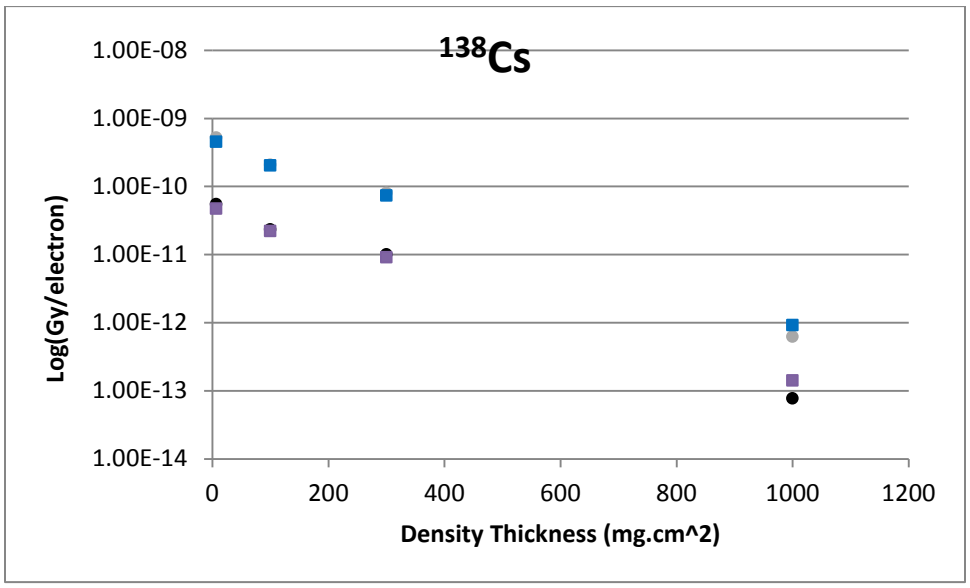

Figure A.4.8. A 5 mm diameter disk geometry comparison of VARSKIN 5 (boxes) and VARSKIN 4 (circles) predicted dose per initial beta from ^{138}Cs as a function of density thickness in tissue and a tissue volume cylinder of area 1 cm^2 (upper) and 10 cm^2 (lower), with a thickness of 20 µm

GEOMETRY 5:
CYLINDRICAL SOURCE

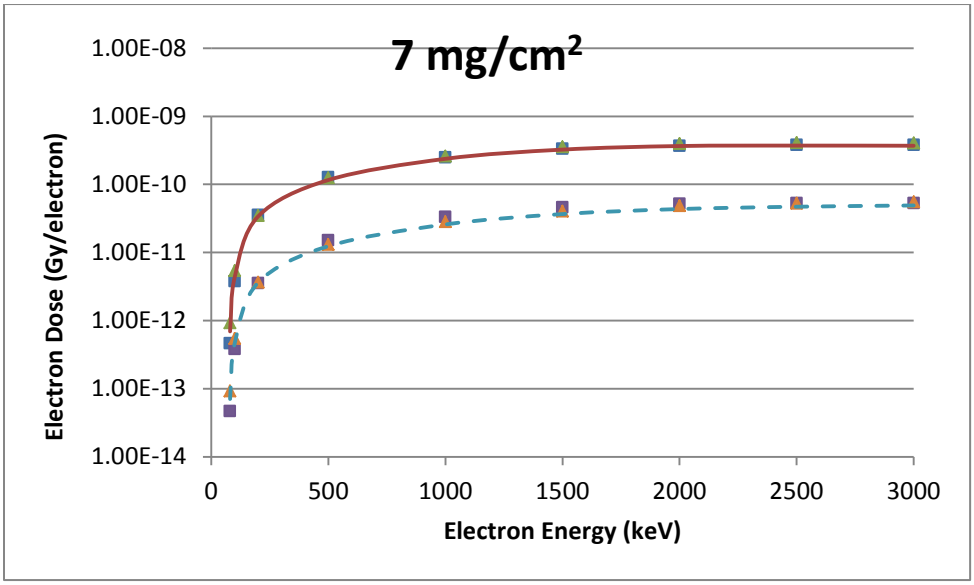

Figure A.5.1. A cylindrical source geometry comparison of VARSKIN 5 (boxes), MCNP5 (triangles) and EGSnrc (lines) predicted dose per initial electron as a function of electron energy in tissue at a density thickness of 7 mg/cm^2 and a tissue volume cylinder of area 1 cm^2 (solid line) and 10 cm^2 (dashed line), with a thickness of 20 µm

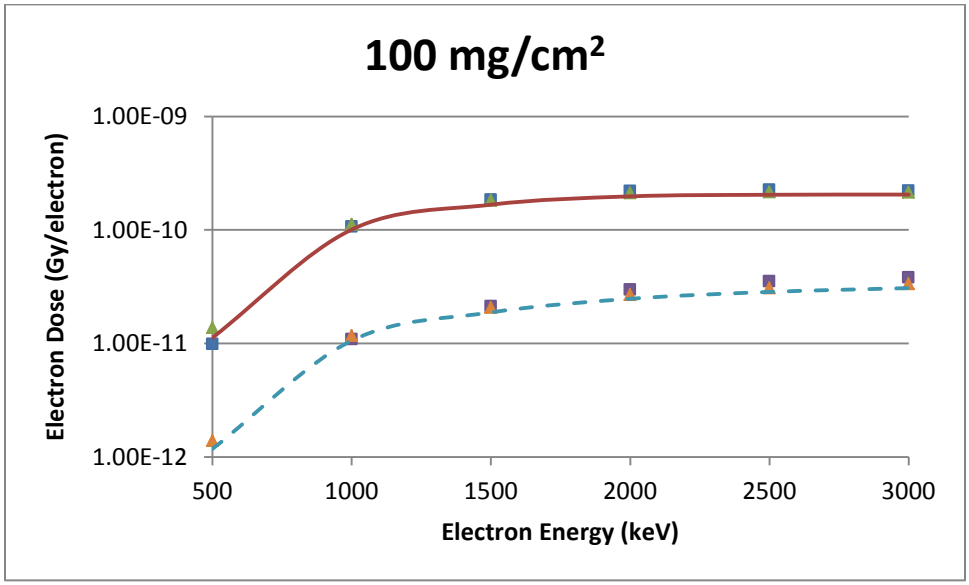

Figure A.5.2. A cylindrical source geometry comparison of VARSKIN 5 (boxes), MCNP5 (triangles) and EGSnrc (lines) predicted dose per initial electron as a function of electron energy in tissue at a density thickness of 100 mg/cm^2 and a tissue volume cylinder of area 1 cm^2 (solid line) and 10 cm^2 (dashed line), with a thickness of 20 µm

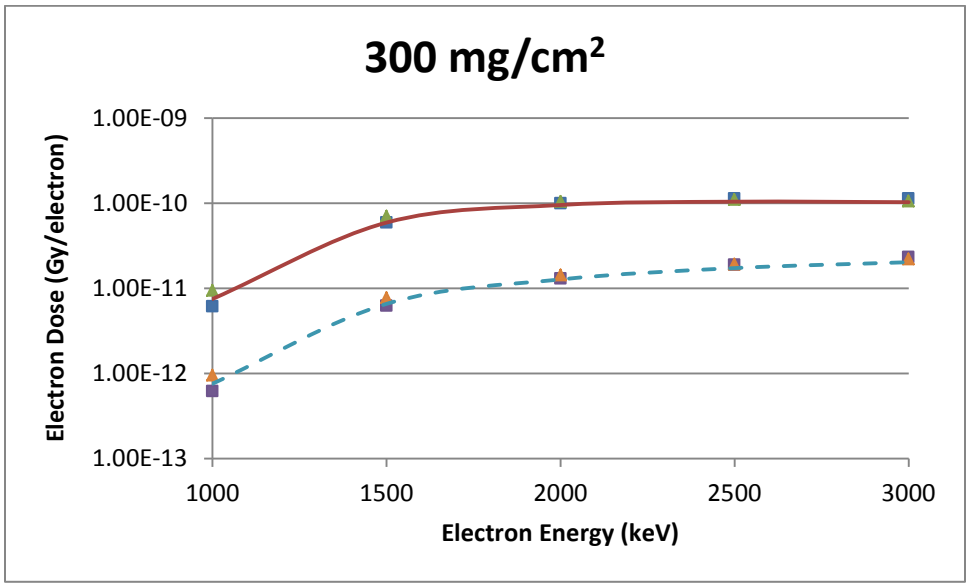

Figure A.5.3. A cylindrical source geometry comparison of VARSKIN 5 (boxes), MCNP5 (triangles) and EGSnrc (lines) predicted dose per initial electron as a function of electron energy in tissue at a density thickness of 300 mg/cm^2 and a tissue volume cylinder of area 1 cm^2 (solid line) and 10 cm^2 (dashed line), with a thickness of 20 µm

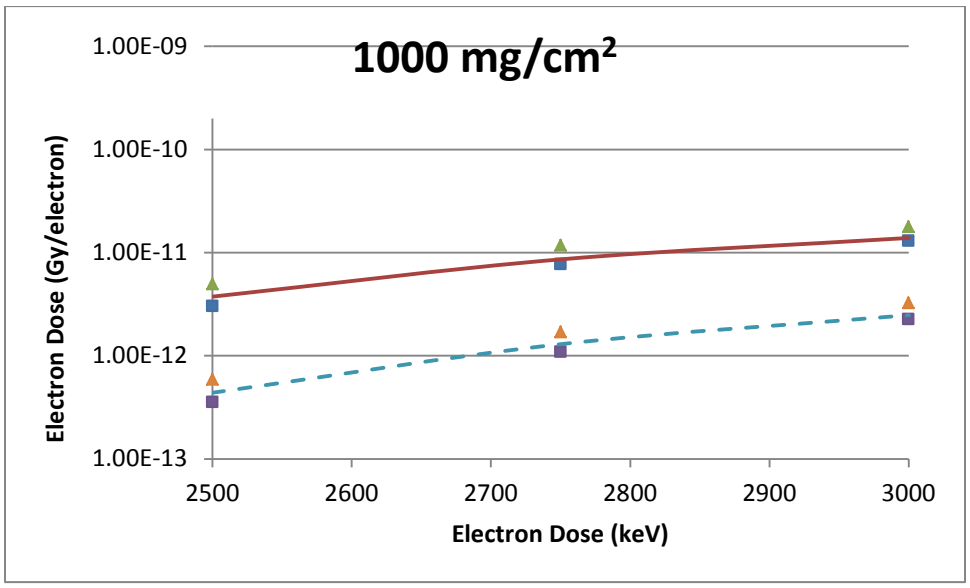

Figure A.5.4. A cylindrical source geometry comparison of VARSKIN 5 (boxes), MCNP5 (triangles) and EGSnrc (lines) predicted dose per initial electron as a function of electron energy in tissue at a density thickness of 1000 mg/cm^2 and a tissue volume cylinder of area 1 cm^2 (solid line) and 10 cm^2 (dashed line), with a thickness of 20 µm

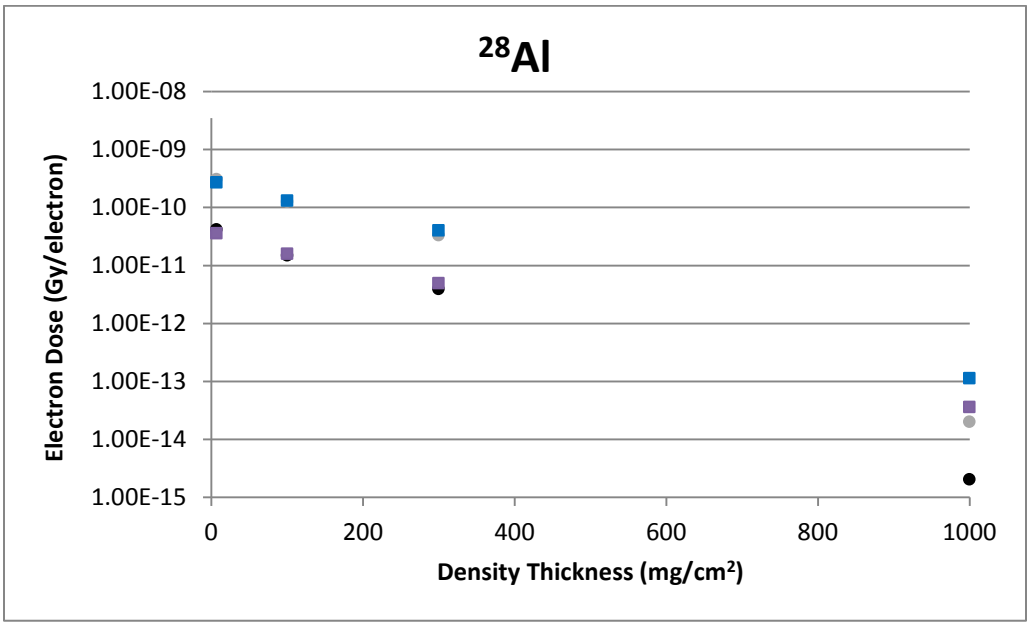

Figure A.5.5. A cylindrical source geometry comparison of VARSKIN 5 (boxes) and VARSKIN 4 (circles) predicted dose per initial beta from ^{28}Al as a function of density thickness in tissue and a tissue volume cylinder of area 1 cm^2 (upper) and 10 cm^2 (lower), with a thickness of 20 μm

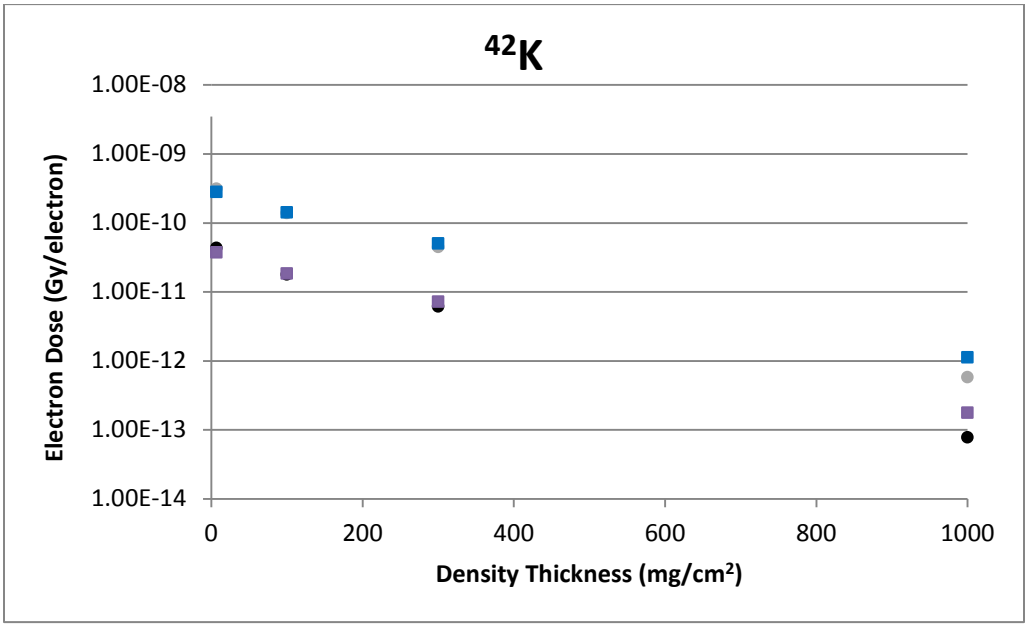

Figure A.5.6. A cylindrical source geometry comparison of VARSKIN 5 (boxes) and VARSKIN 4 (circles) predicted dose per initial beta from ^{42}K as a function of density thickness in tissue and a tissue volume cylinder of area 1 cm^2 (upper) and 10 cm^2 (lower), with a thickness of 20 μm

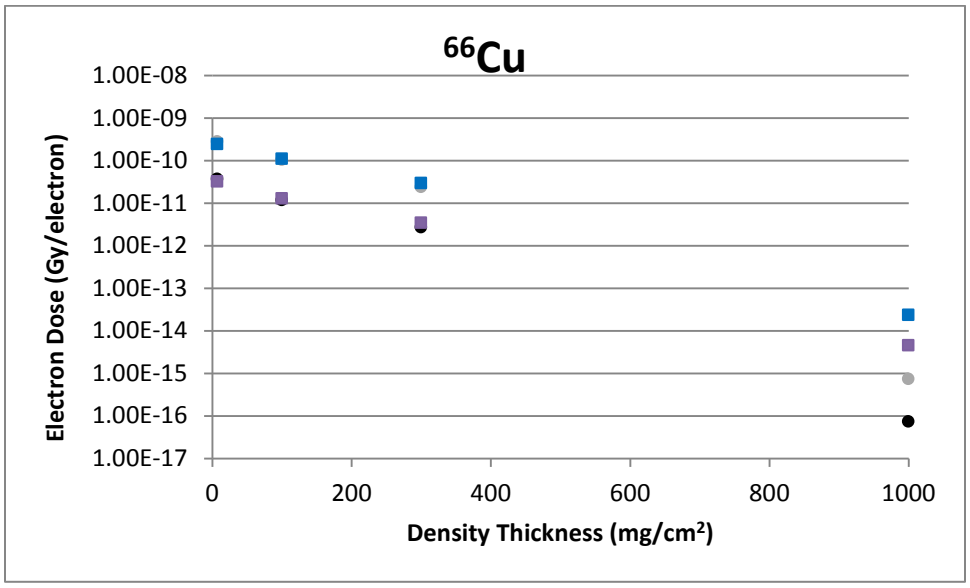

Figure A.5.7. A cylindrical source geometry comparison of VARSKIN 5 (boxes) and VARSKIN 4 (circles) predicted dose per initial beta from ^{66}Cu as a function of density thickness in tissue and a tissue volume cylinder of area 1 cm^2 (upper) and 10 cm^2 (lower), with a thickness of 20 µm

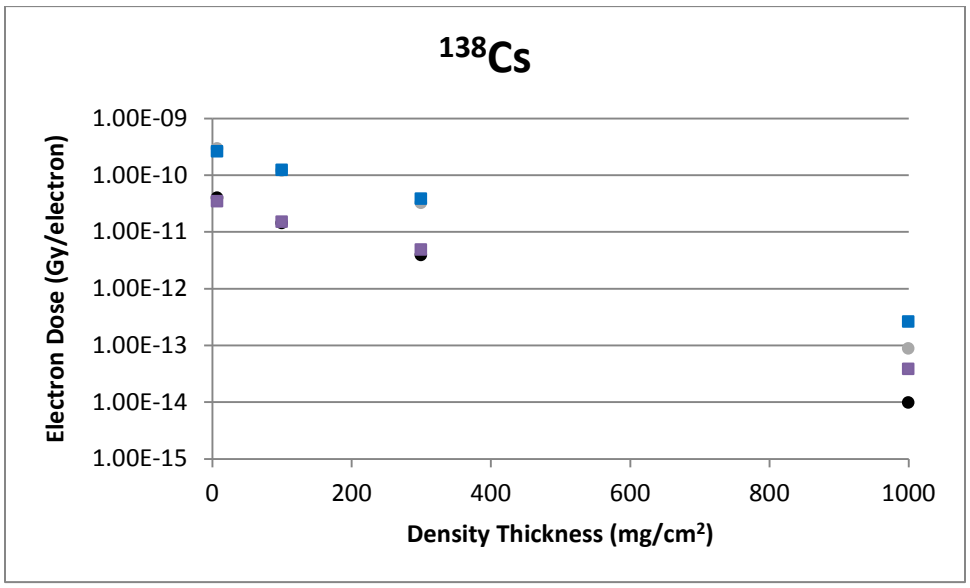

Figure A.5.8. A cylindrical source geometry comparison of VARSKIN 5 (boxes) and VARSKIN 4 (circles) predicted dose per initial beta from ^{138}Cs as a function of density thickness in tissue and a tissue volume cylinder of area 1 cm^2 (upper) and 10 cm^2 (lower), with a thickness of 20 µm

GEOMETRY 6:
SPHERICAL SOURCE

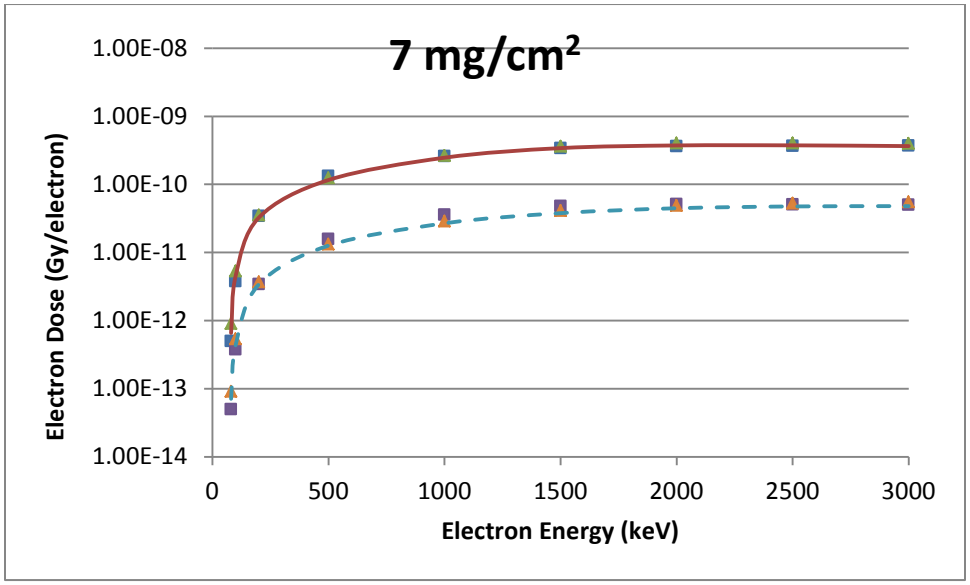

Figure A.6.1. A spherical source geometry comparison of VARSKIN 5 (boxes), MCNP5 (triangles) and EGSnrc (lines) predicted dose per initial electron as a function of electron energy in tissue at a density thickness of 7 mg/cm^2 and a tissue volume cylinder of area 1 cm^2 (solid line) and 10 cm^2 (dashed line), with a thickness of 20 µm

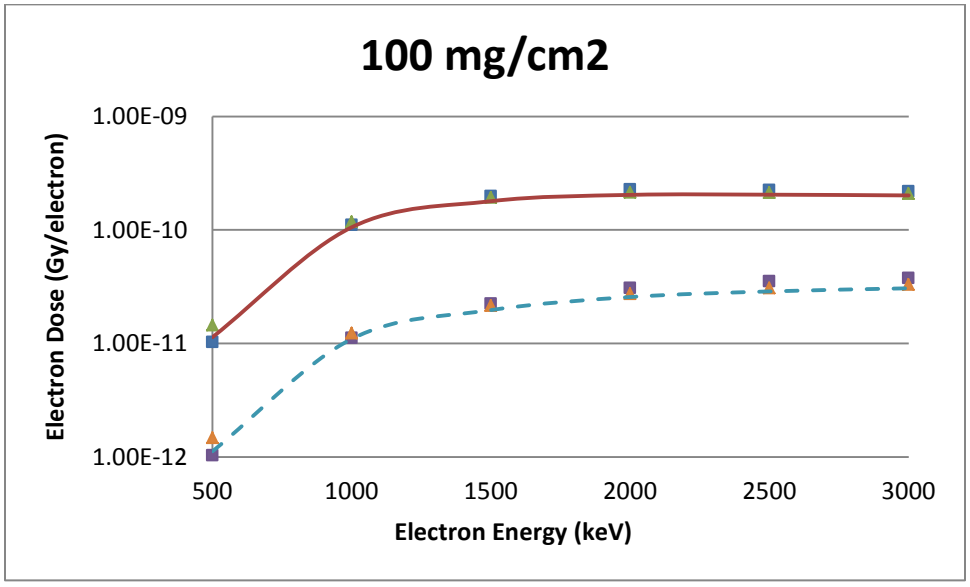

Figure A.6.2. A spherical source geometry comparison of VARSKIN 5 (boxes), MCNP5 (triangles) and EGSnrc (lines) predicted dose per initial electron as a function of electron energy in tissue at a density thickness of 100 mg/cm^2 and a tissue volume cylinder of area 1 cm^2 (solid line) and 10 cm^2 (dashed line), with a thickness of 20 µm

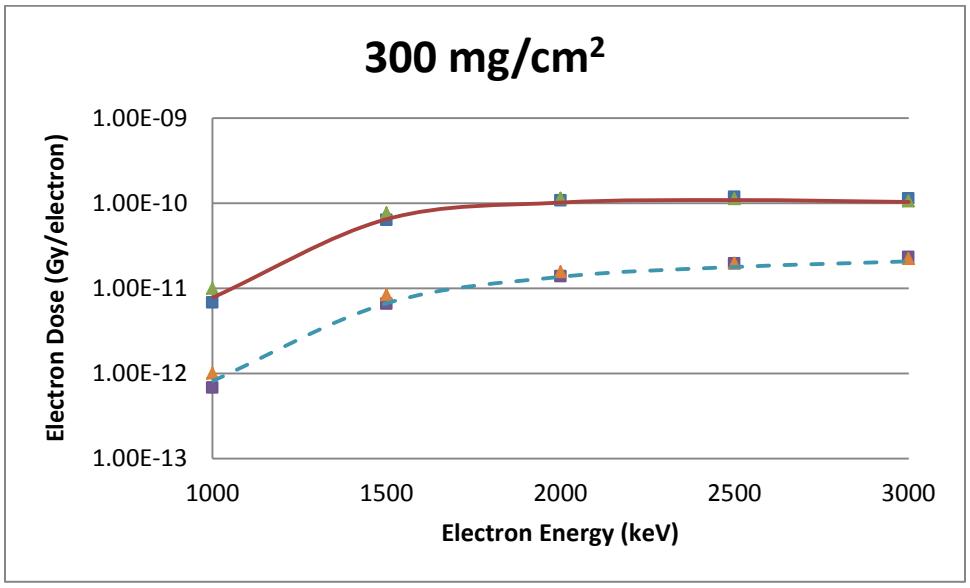

Figure A.6.3. A spherical source geometry comparison of VARSKIN 5 (boxes), MCNP5 (triangles) and EGSnrc (lines) predicted dose per initial electron as a function of electron energy in tissue at a density thickness of 300 mg/cm^2 and a tissue volume cylinder of area 1 cm^2 (solid line) and 10 cm^2 (dashed line), with a thickness of 20 µm

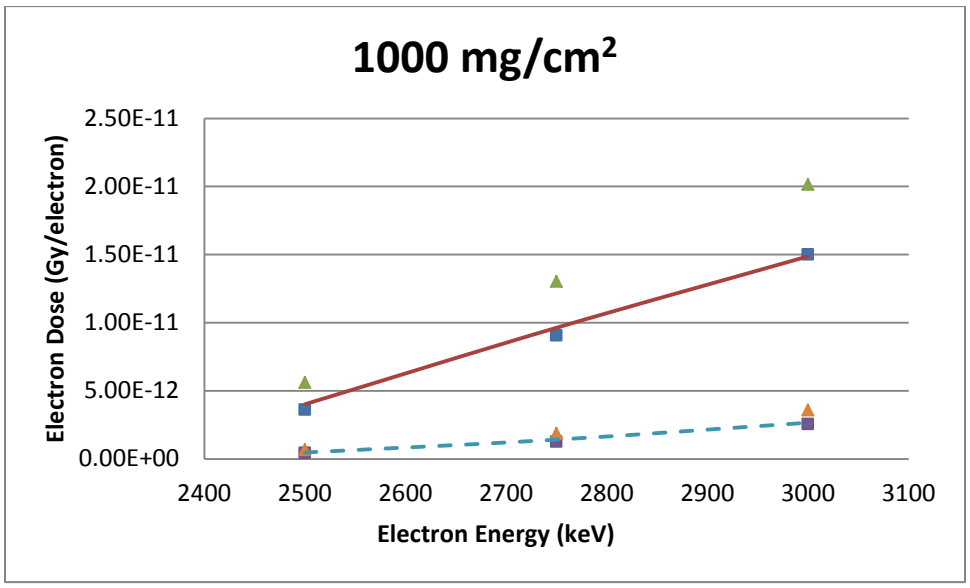

Figure A.6.4. A spherical source geometry comparison of VARSKIN 5 (boxes), MCNP5 (triangles) and EGSnrc (lines) predicted dose per initial electron as a function of electron energy in tissue at a density thickness of 1000 mg/cm^2 and a tissue volume cylinder of area 1 cm^2 (solid line) and 10 cm^2 (dashed line), with a thickness of 20 µm

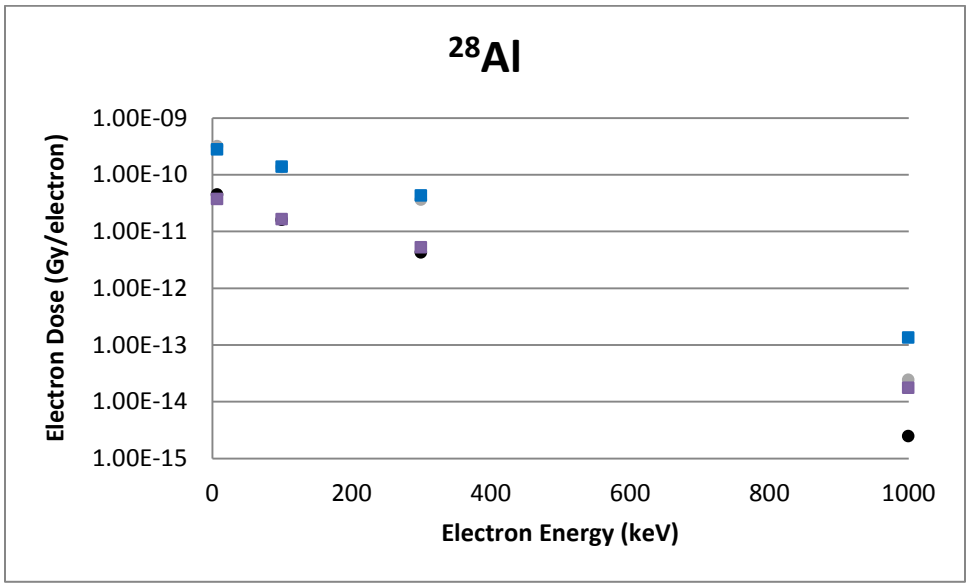

Figure A.6.5. A spherical source geometry comparison of VARSKIN 5 (boxes) and VARSKIN 4 (circles) predicted dose per initial beta from ^{28}Al as a function of density thickness in tissue and a tissue volume cylinder of area 1 cm^2 (upper) and 10 cm^2 (lower), with a thickness of 20 µm

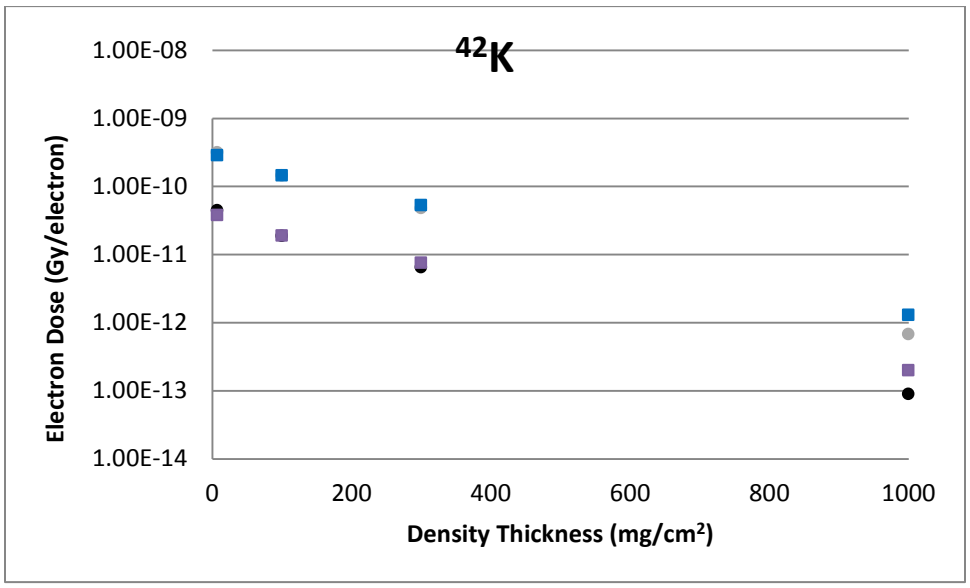

Figure A.6.6. A spherical source geometry comparison of VARSKIN 5 (boxes) and VARSKIN 4 (circles) predicted dose per initial beta from ^{42}K as a function of density thickness in tissue and a tissue volume cylinder of area 1 cm^2 (upper) and 10 cm^2 (lower), with a thickness of 20 µm

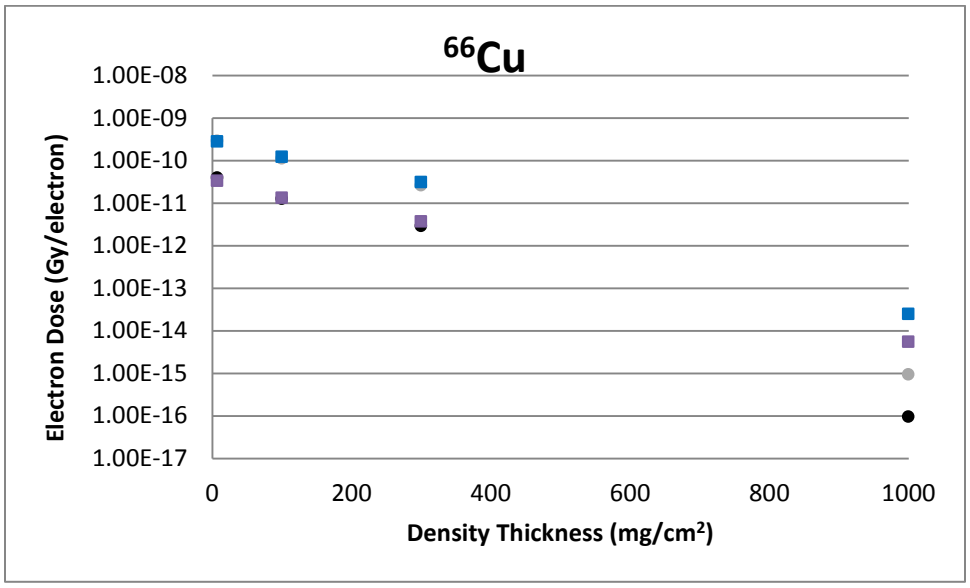

Figure A.6.7. A spherical source geometry comparison of VARSKIN 5 (boxes) and VARSKIN 4 (circles) predicted dose per initial beta from ^{66}Cu as a function of density thickness in tissue and a tissue volume cylinder of area 1 cm^2 (upper) and 10 cm^2 (lower), with a thickness of 20 µm

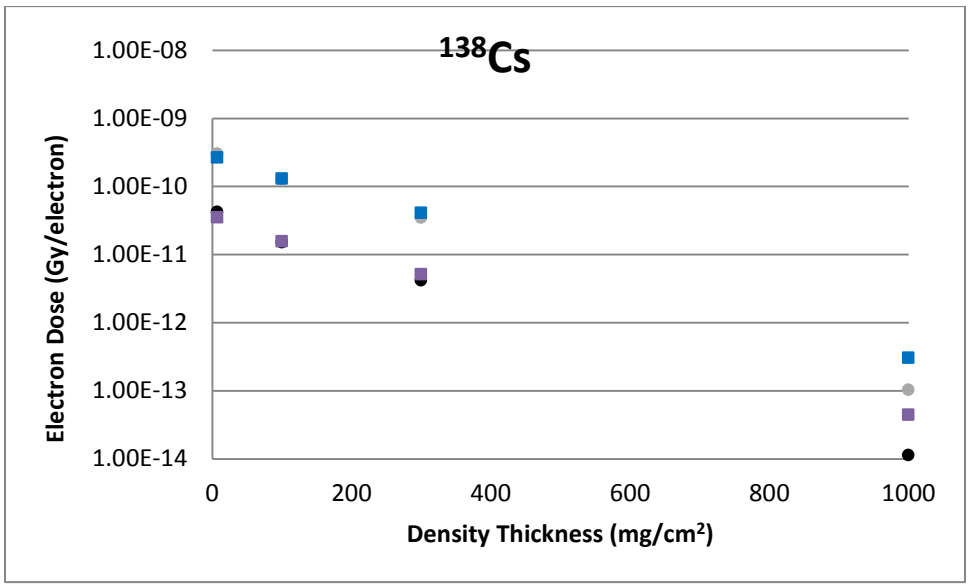

Figure A.6.8. A spherical source geometry comparison of VARSKIN 5 (boxes) and VARSKIN 4 (circles) predicted dose per initial beta from ^{138}Cs as a function of density thickness in tissue and a tissue volume cylinder of area 1 cm^2 (upper) and 10 cm^2 (lower), with a thickness of 20 µm

GEOMETRY 7:
SLAB SOURCE

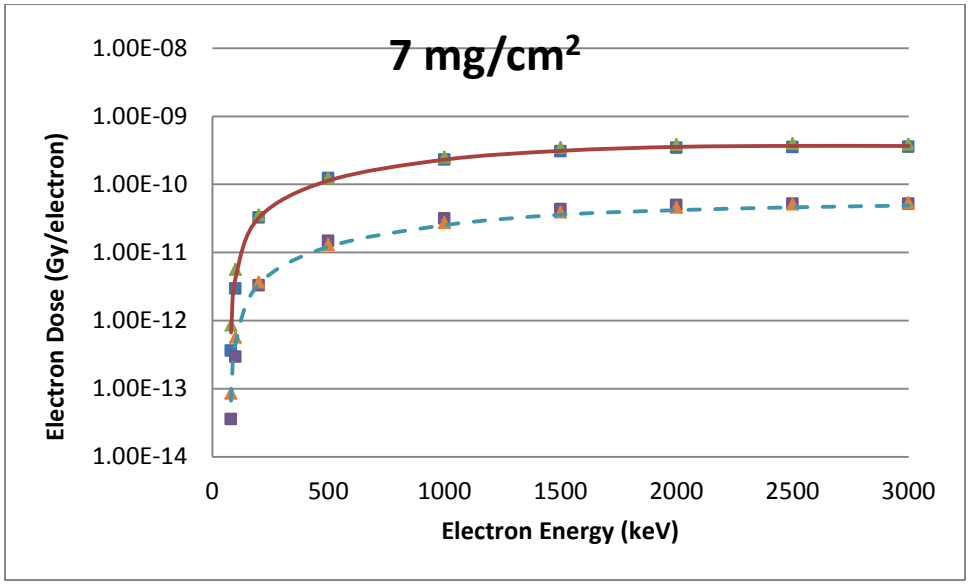

Figure A.7.1. A slab source geometry comparison of VARSKIN 5 (boxes), MCNP5 (triangles) and EGSnrc (lines) predicted dose per initial electron as a function of electron energy in tissue at a density thickness of 7 mg/cm^2 and a tissue volume cylinder of area 1 cm^2 (solid line) and 10 cm^2 (dashed line), with a thickness of 20 µm

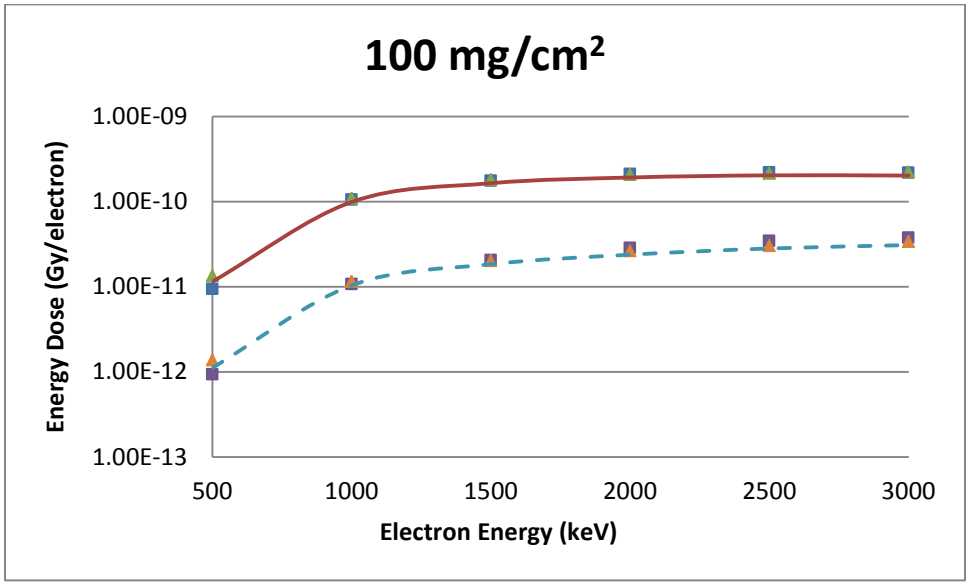

Figure A.7.2. A slab source geometry comparison of VARSKIN 5 (boxes), MCNP5 (triangles) and EGSnrc (lines) predicted dose per initial electron as a function of electron energy in tissue at a density thickness of 100 mg/cm^2 and a tissue volume cylinder of area 1 cm^2 (solid line) and 10 cm^2 (dashed line), with a thickness of 20 µm

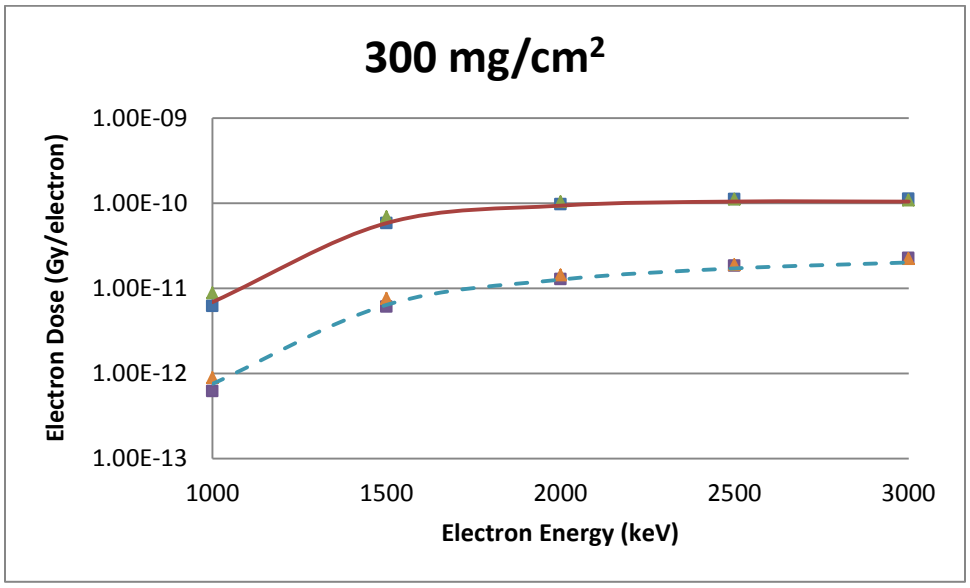

Figure A.7.3. A slab source geometry comparison of VARSKIN 5 (boxes), MCNP5 (triangles) and EGSnrc (lines) predicted dose per initial electron as a function of electron energy in tissue at a density thickness of 300 mg/cm^2 and a tissue volume cylinder of area 1 cm^2 (solid line) and 10 cm^2 (dashed line), with a thickness of 20 µm

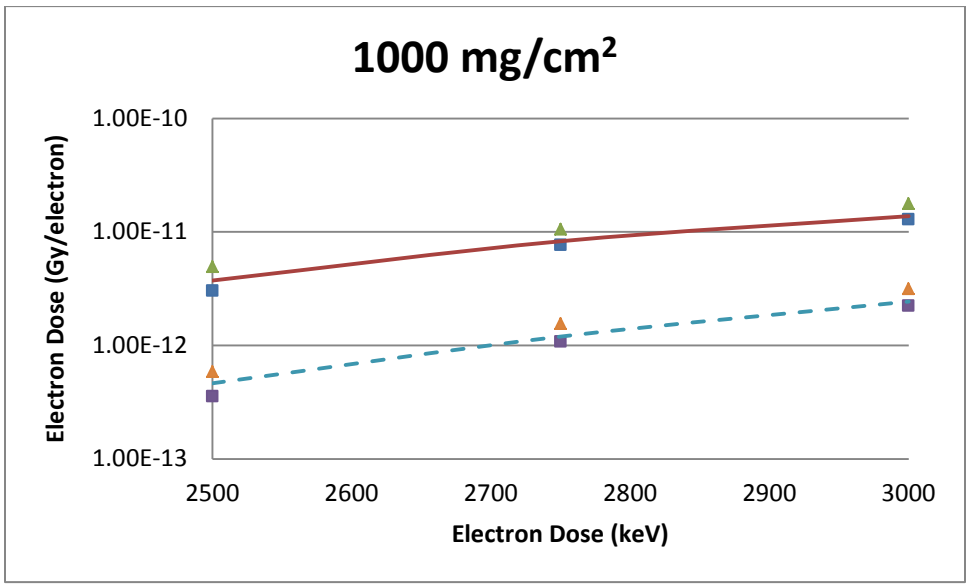

Figure A.7.4. A slab source geometry comparison of VARSKIN 5 (boxes), MCNP5 (triangles) and EGSnrc (lines) predicted dose per initial electron as a function of electron energy in tissue at a density thickness of 1000 mg/cm^2 and a tissue volume cylinder of area 1 cm^2 (solid line) and 10 cm^2 (dashed line), with a thickness of 20 µm

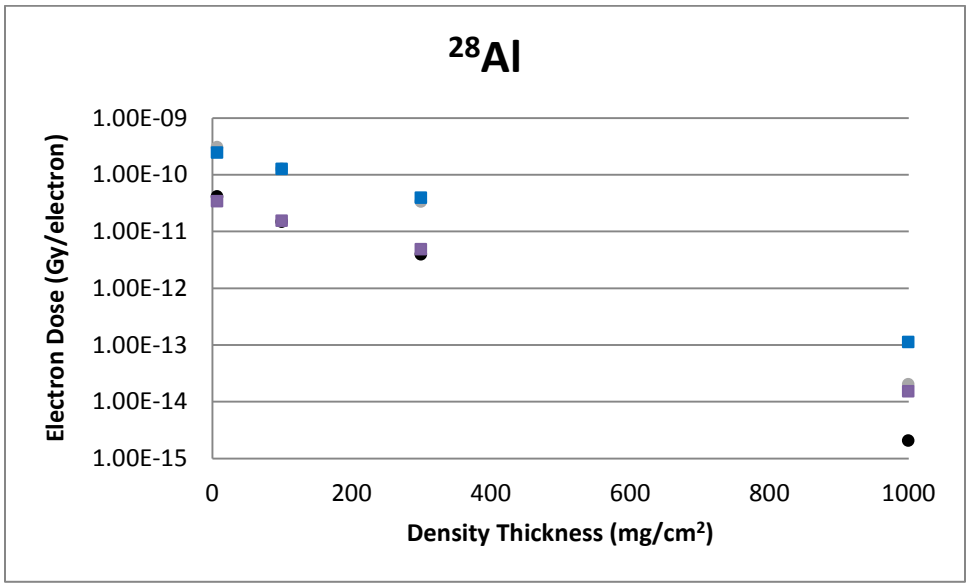

Figure A.7.5. A slab source geometry comparison of VARSKIN 5 (boxes) and VARSKIN 4 (circles) predicted dose per initial beta from ^{28}Al as a function of density thickness in tissue and a tissue volume cylinder of area 1 cm^2 (upper) and 10 cm^2 (lower), with a thickness of 20 µm

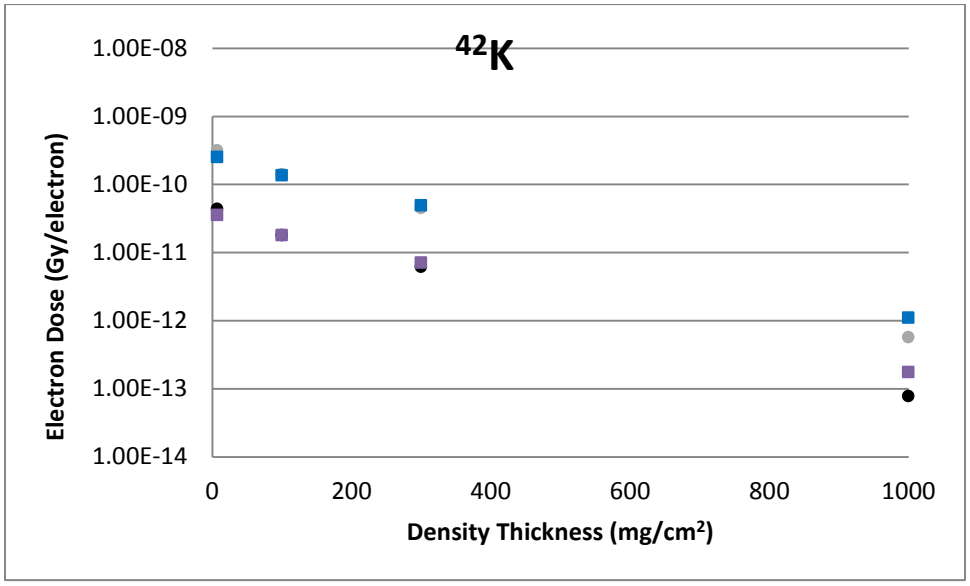

Figure A.7.6. A slab source geometry comparison of VARSKIN 5 (boxes) and VARSKIN 4 (circles) predicted dose per initial beta from ^{42}K as a function of density thickness in tissue and a tissue volume cylinder of area 1 cm^2 (upper) and 10 cm^2 (lower), with a thickness of 20 µm

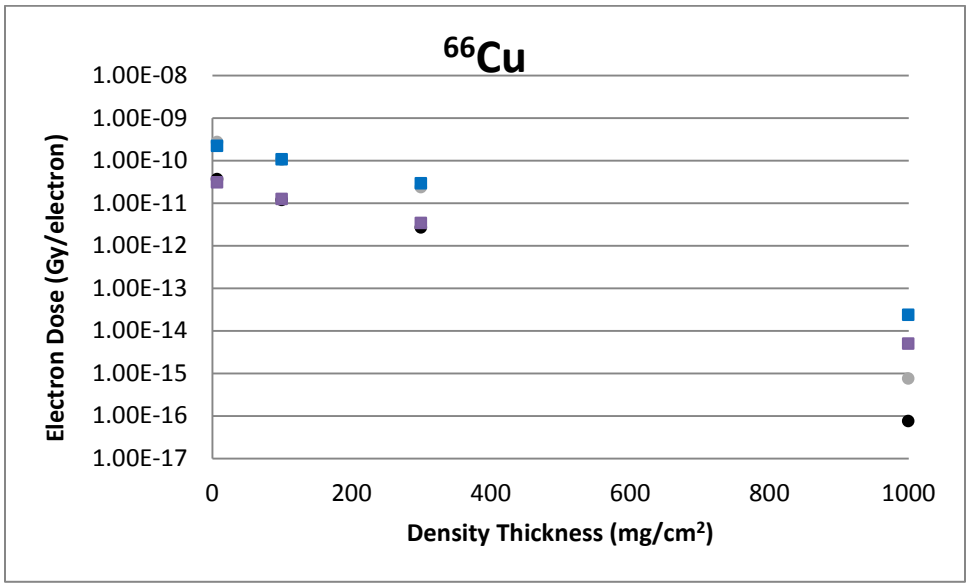

Figure A.7.7. A slab source geometry comparison of VARSKIN 5 (boxes) and VARSKIN 4 (circles) predicted dose per initial beta from ^{66}Cu as a function of density thickness in tissue and a tissue volume cylinder of area 1 cm^2 (upper) and 10 cm^2 (lower), with a thickness of 20 µm

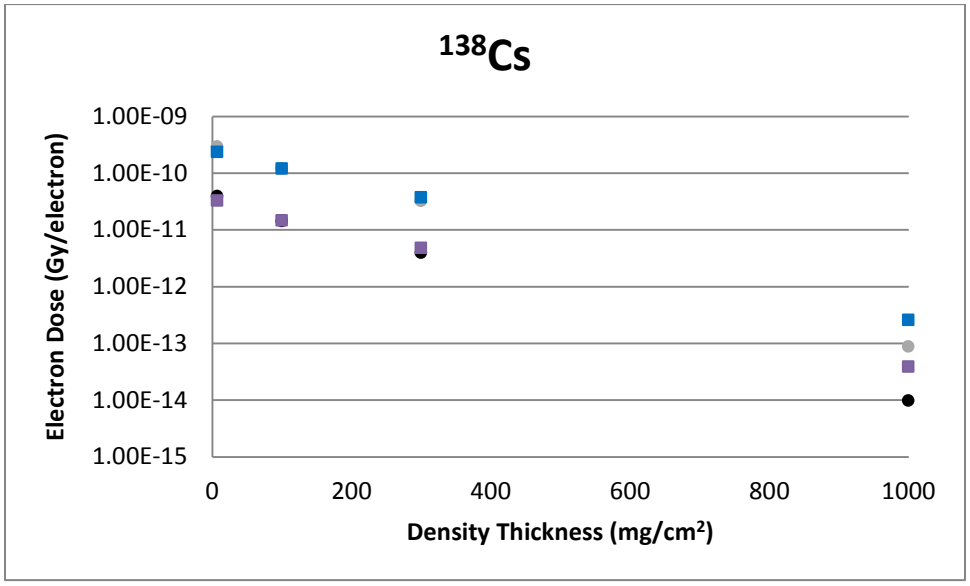

Figure A.7.8. A slab source geometry comparison of VARSKIN 5 (boxes) and VARSKIN 4 (circles) predicted dose per initial beta from ^{138}Cs as a function of density thickness in tissue and a tissue volume cylinder of area 1 cm^2 (upper) and 10 cm^2 (lower), with a thickness of 20 µm

APPENDIX B

Figures for the Supporting Photon Dosimetry V&V

GEOMETRY 1: POINT SOURCE

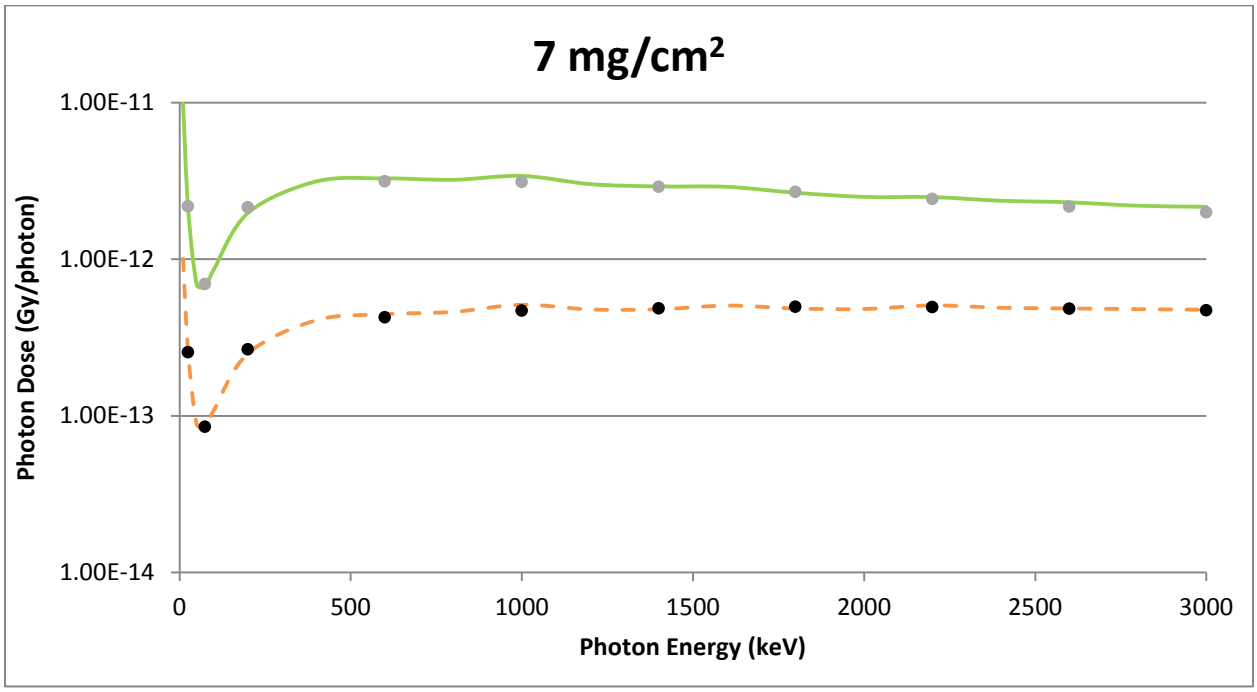

Figure B.1.1. A point source geometry comparison of VARSKIN 5 (circles) and MCNP5 (lines) predicted dose per initial photon as a function of photon energy in tissue at a density thickness of 7 mg/cm^2 and a tissue volume cylinder of area 1 cm^2 (solid line) and 10 cm^2 (dashed line), with a thickness of 20 µm

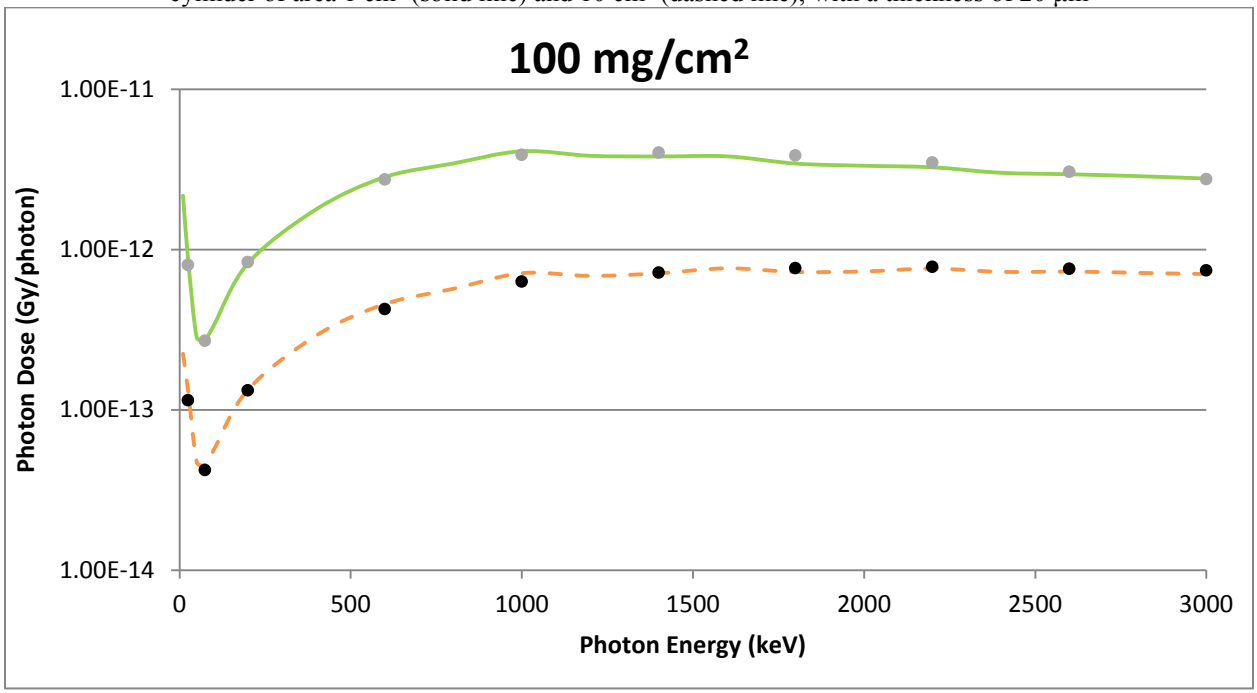

Figure B.1.2. A point source geometry comparison of VARSKIN 5 (circles) and MCNP5 (lines) predicted dose per

initial photon as a function of photon energy in tissue at a density thickness of 100 mg/cm^2 and a tissue volume cylinder of area 1 cm^2 (solid line) and 10 cm^2 (dashed line), with a thickness of 20 µm

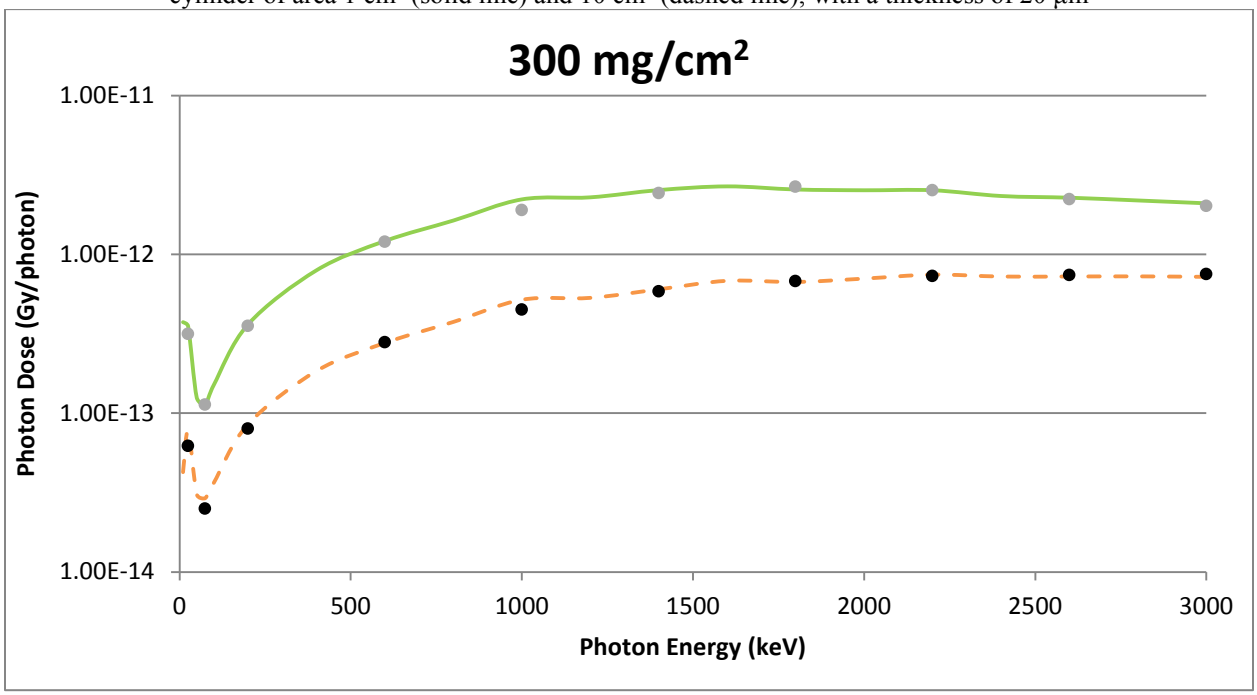

Figure B.1.3. A point source geometry comparison of VARSKIN 5 (circles) and MCNP5 (lines) predicted dose per initial photon as a function of photon energy in tissue at a density thickness of 300 mg/cm^2 and a tissue volume cylinder of area 1 cm^2 (solid line) and 10 cm^2 (dashed line), with a thickness of 20 µm

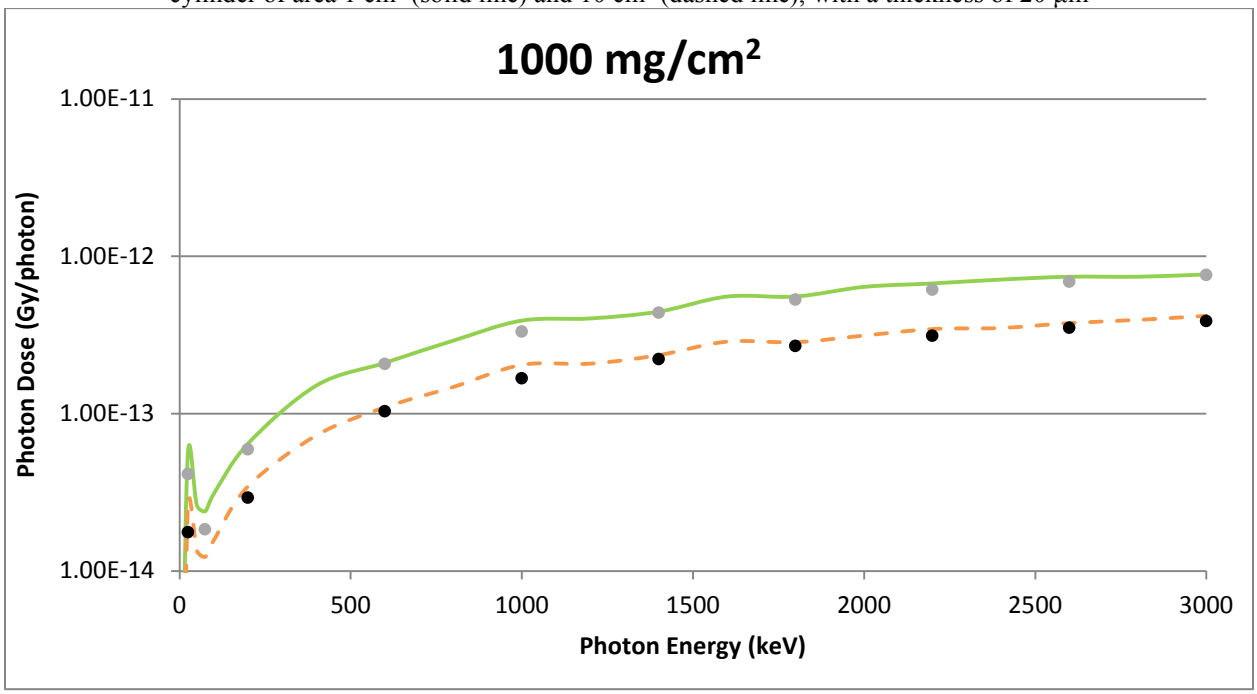

Figure B.1.4. A point source geometry comparison of VARSKIN 5 (circles) and MCNP5 (lines) predicted dose per initial photon as a function of photon energy in tissue at a density thickness of 1000 mg/cm^2 and a tissue volume cylinder of area 1 cm^2 (solid line) and 10 cm^2 (dashed line), with a thickness of 20 µm

GEOMETRY 2: DISK SOURCE

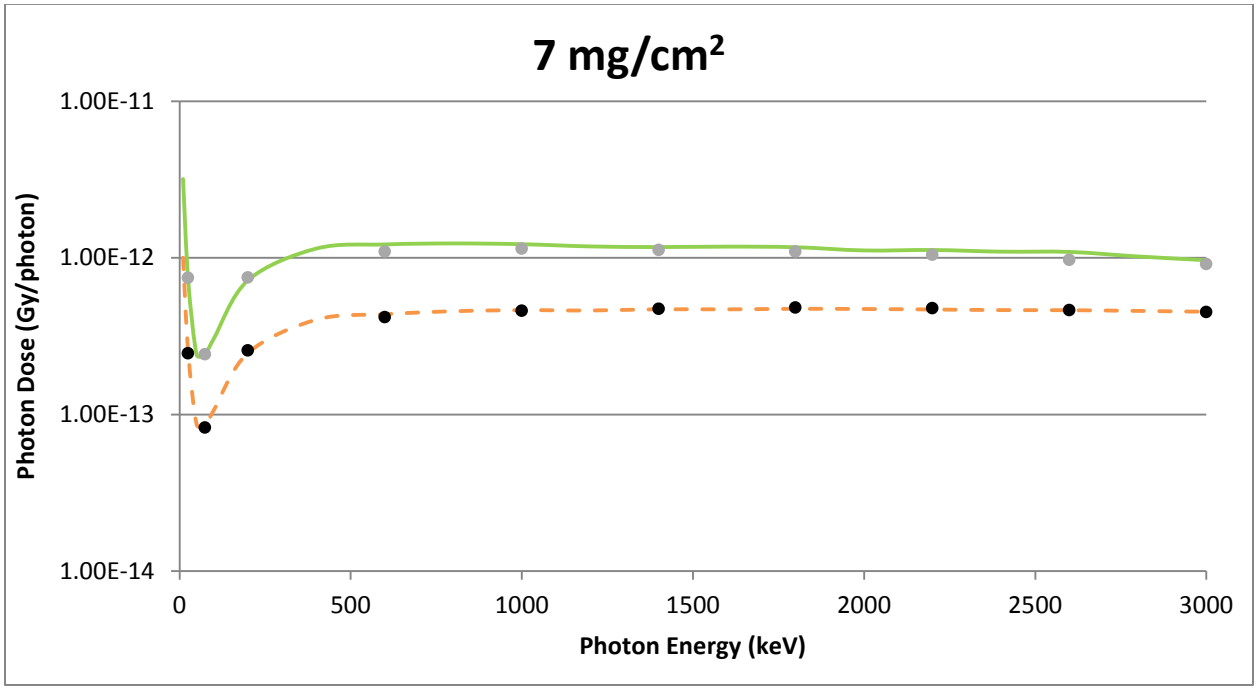

Figure B.2.1. A disk source geometry comparison of VARSKIN 5 (circles) and MCNP5 (lines) predicted dose per initial photon as a function of photon energy in tissue at a density thickness of 7 mg/cm^2 and a tissue volume cylinder of area 1 cm^2 (solid line) and 10 cm^2 (dashed line), with a thickness of 20 µm

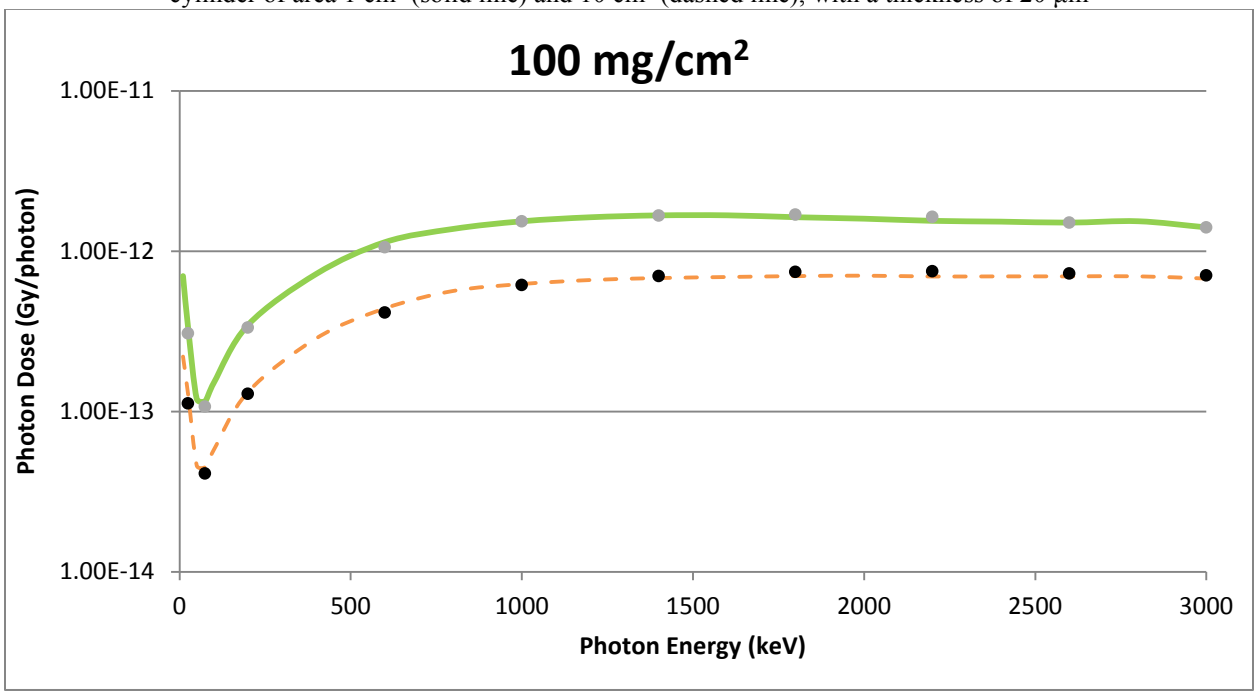

Figure B.2.2. A disk source geometry comparison of VARSKIN 5 (circles) and MCNP5 (lines) predicted dose per

initial photon as a function of photon energy in tissue at a density thickness of 100 mg/cm^2 and a tissue volume cylinder of area 1 cm^2 (solid line) and 10 cm^2 (dashed line), with a thickness of 20 µm

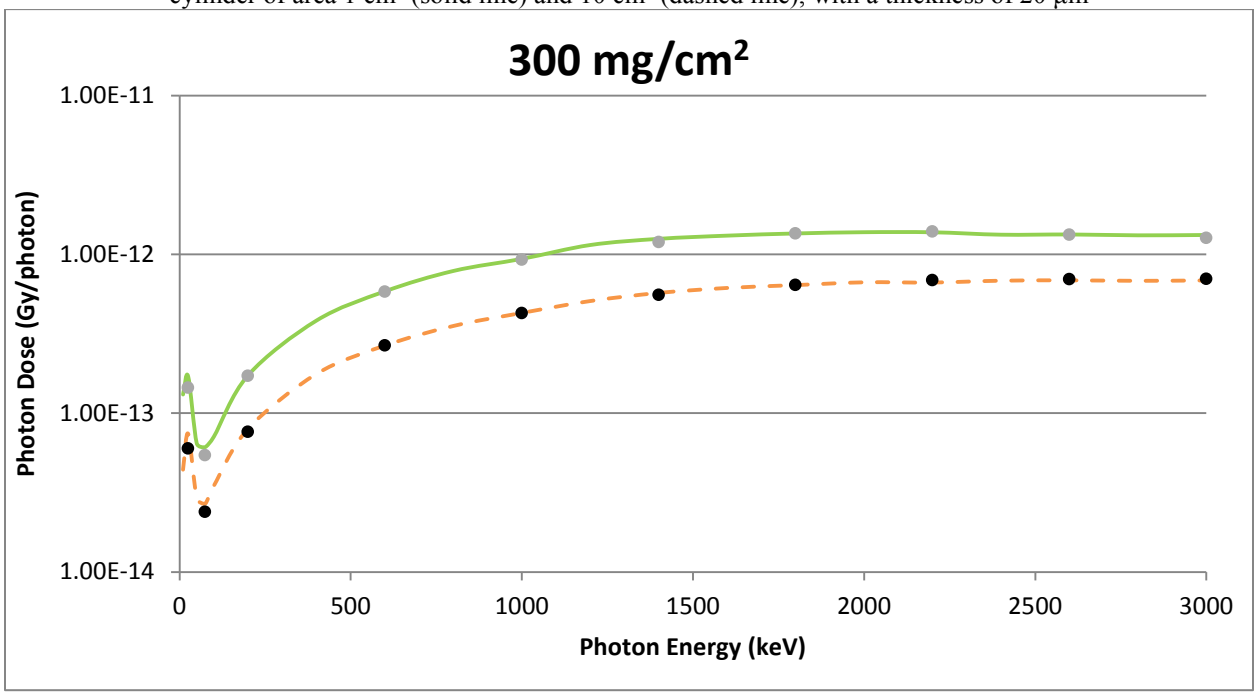

Figure B.2.3. A disk source geometry comparison of VARSKIN 5 (circles) and MCNP5 (lines) predicted dose per initial photon as a function of photon energy in tissue at a density thickness of 300 mg/cm^2 and a tissue volume cylinder of area 1 cm^2 (solid line) and 10 cm^2 (dashed line), with a thickness of 20 µm

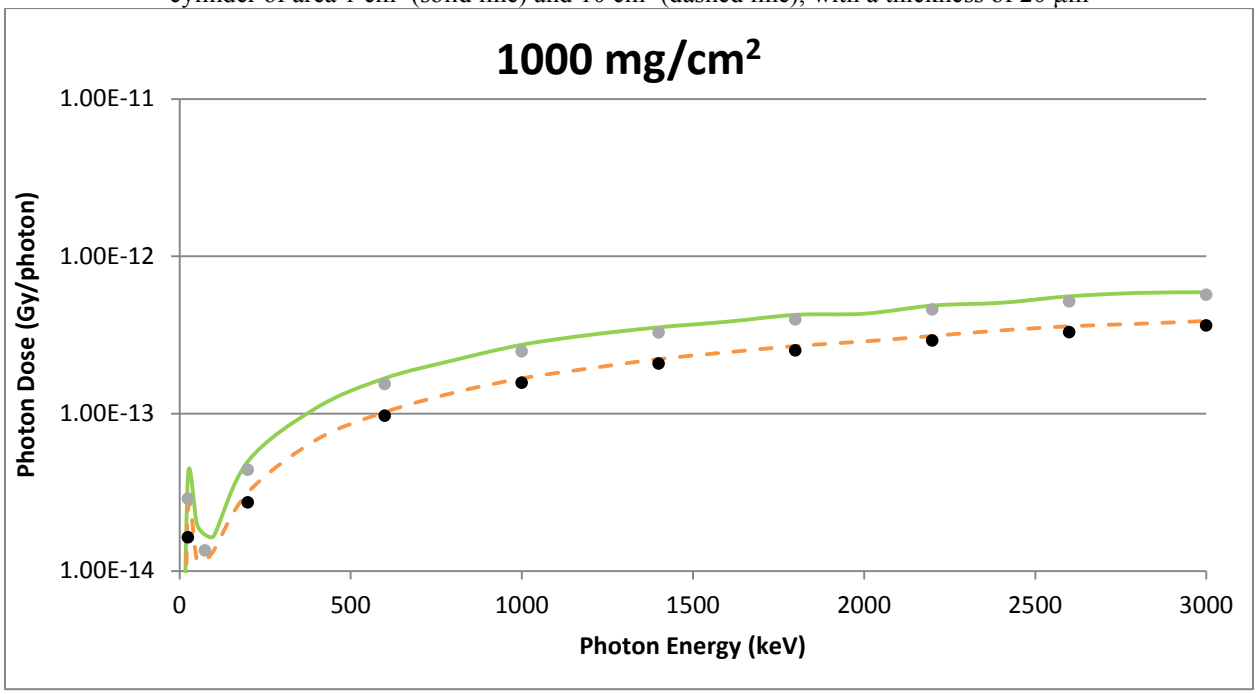

Figure B.2.4. A disk source geometry comparison of VARSKIN 5 (circles) and MCNP5 (lines) predicted dose per initial photon as a function of photon energy in tissue at a density thickness of 1000 mg/cm^2 and a tissue volume cylinder of area 1 cm^2 (solid line) and 10 cm^2 (dashed line), with a thickness of 20 µm

GEOMETRY 3: CYLINDRICAL SOURCE

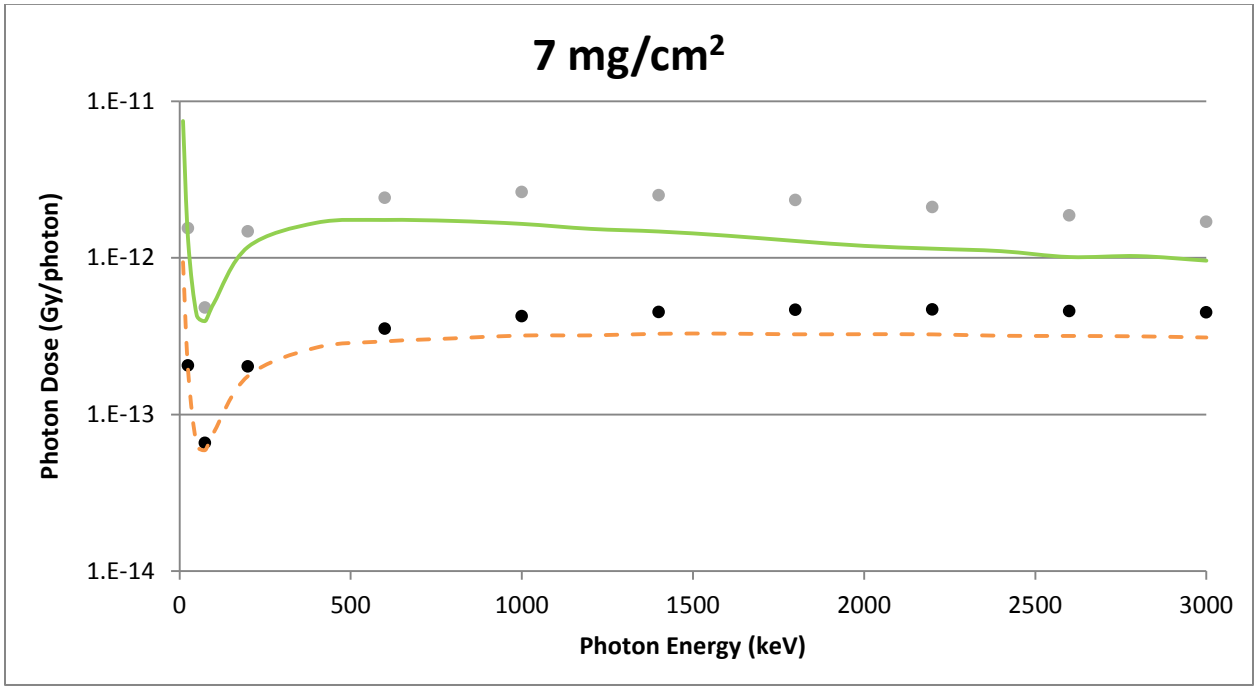

Figure B.3.1. A cylindrical source geometry comparison of VARSKIN 5 (circles) and MCNP5 (lines) predicted dose per initial photon as a function of photon energy in tissue at a density thickness of 7 mg/cm^2 and a tissue volume cylinder of area 1 cm^2 (solid line) and 10 cm^2 (dashed line), with a thickness of 20 µm

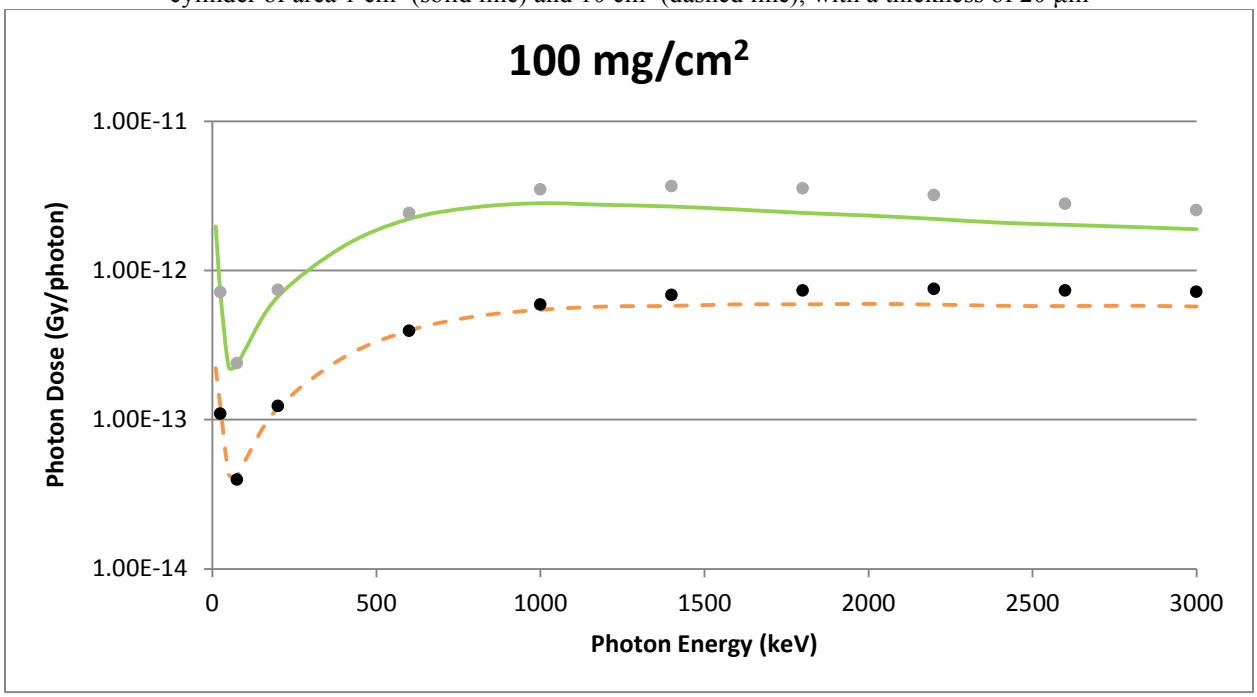

Figure B.3.2. A cylindrical source geometry comparison of VARSKIN 5 (circles) and MCNP5 (lines) predicted dose

per initial photon as a function of photon energy in tissue at a density thickness of 100 mg/cm^2 and a tissue volume cylinder of area 1 cm^2 (solid line) and 10 cm^2 (dashed line), with a thickness of 20 µm

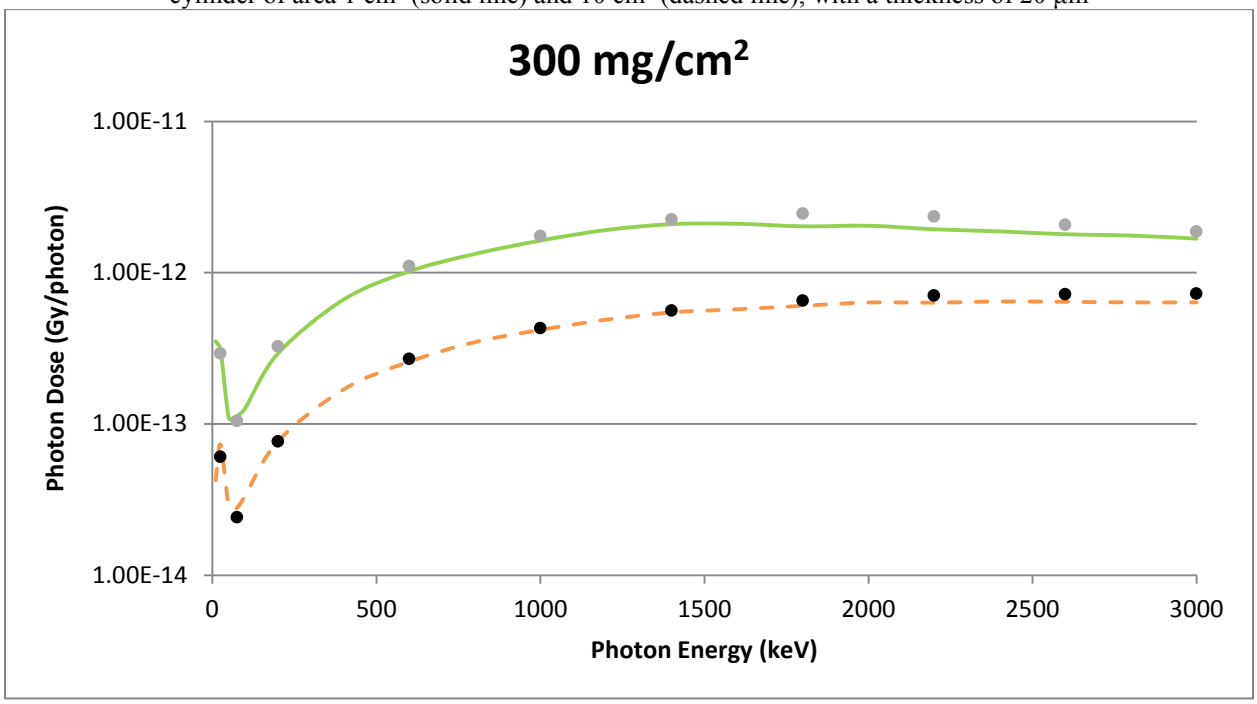

Figure B.3.3. A cylindrical source geometry comparison of VARSKIN 5 (circles) and MCNP5 (lines) predicted dose per initial photon as a function of photon energy in tissue at a density thickness of 300 mg/cm^2 and a tissue volume cylinder of area 1 cm^2 (solid line) and 10 cm^2 (dashed line), with a thickness of 20 µm

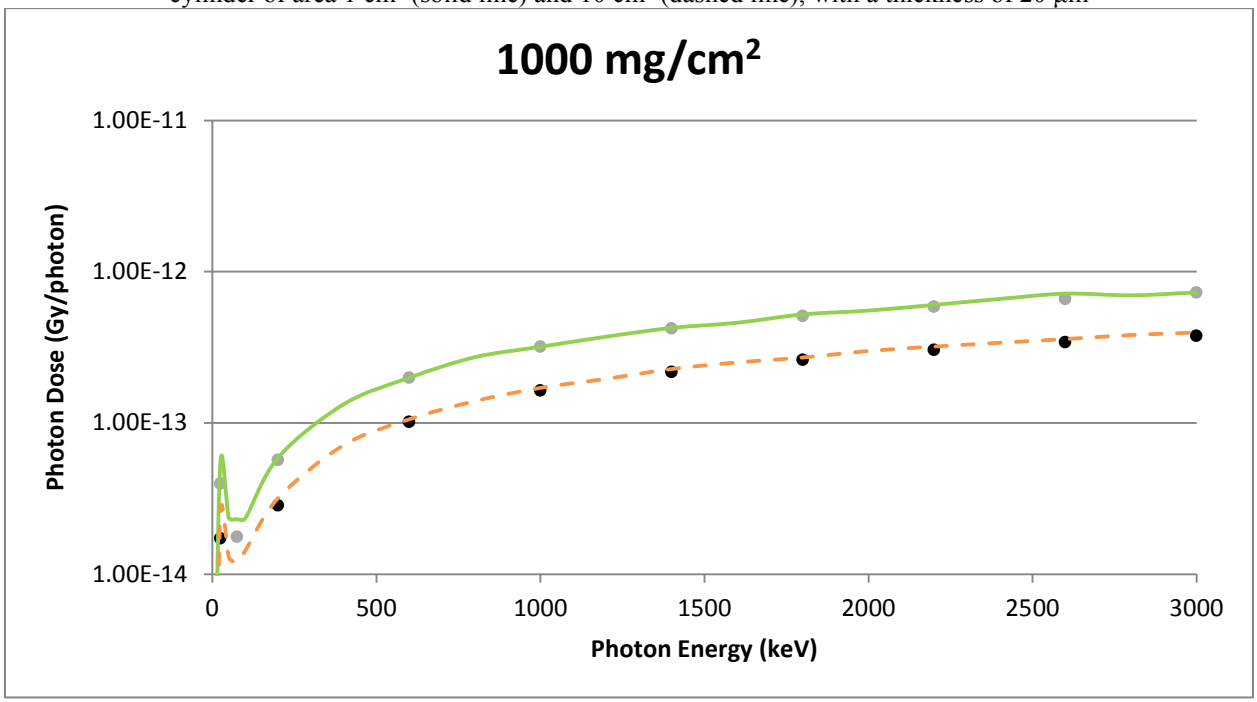

Figure B.3.4. A cylindrical source geometry comparison of VARSKIN 5 (circles) and MCNP5 (lines) predicted dose

per initial photon as a function of photon energy in tissue at a density thickness of 1000 mg/cm^2 and a tissue volume cylinder of area 1 cm^2 (solid line) and 10 cm^2 (dashed line), with a thickness of 20 µm

GEOMETRY 4: SLAB SOURCE

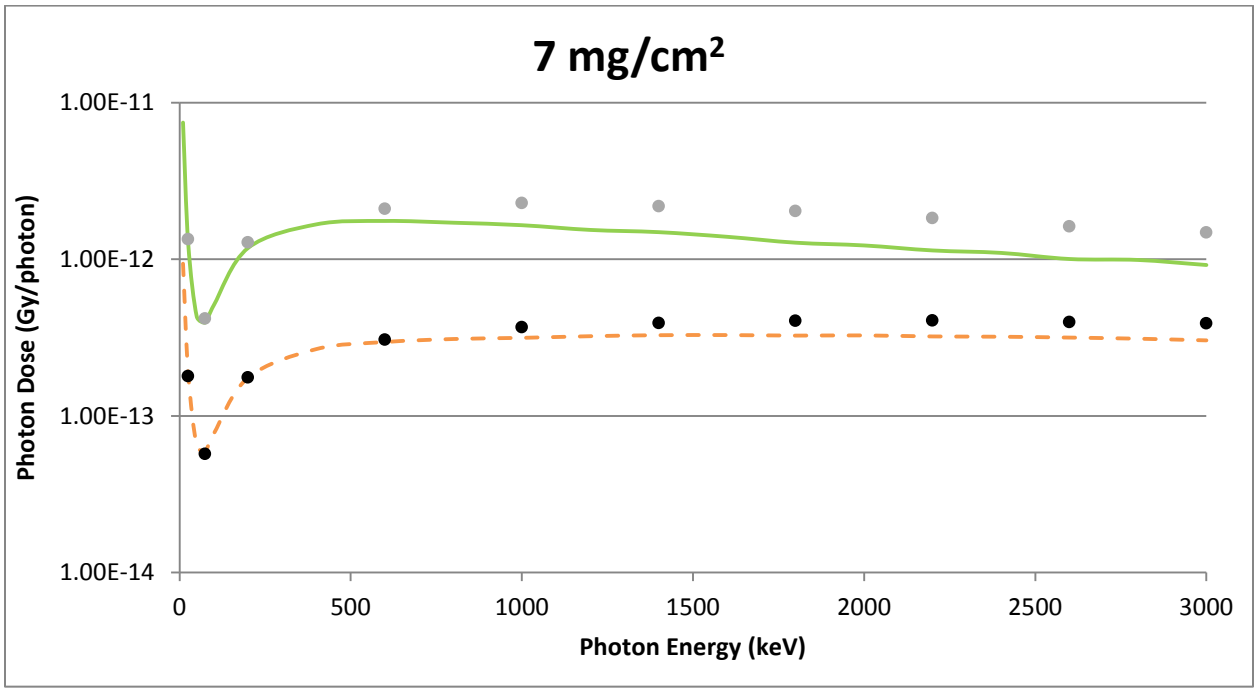

Figure B.4.1. A slab source geometry comparison of VARSKIN 5 (circles) and MCNP5 (lines) predicted dose per initial photon as a function of photon energy in tissue at a density thickness of 7 mg/cm^2 and a tissue volume cylinder of area 1 cm^2 (solid line) and 10 cm^2 (dashed line), with a thickness of 20 µm

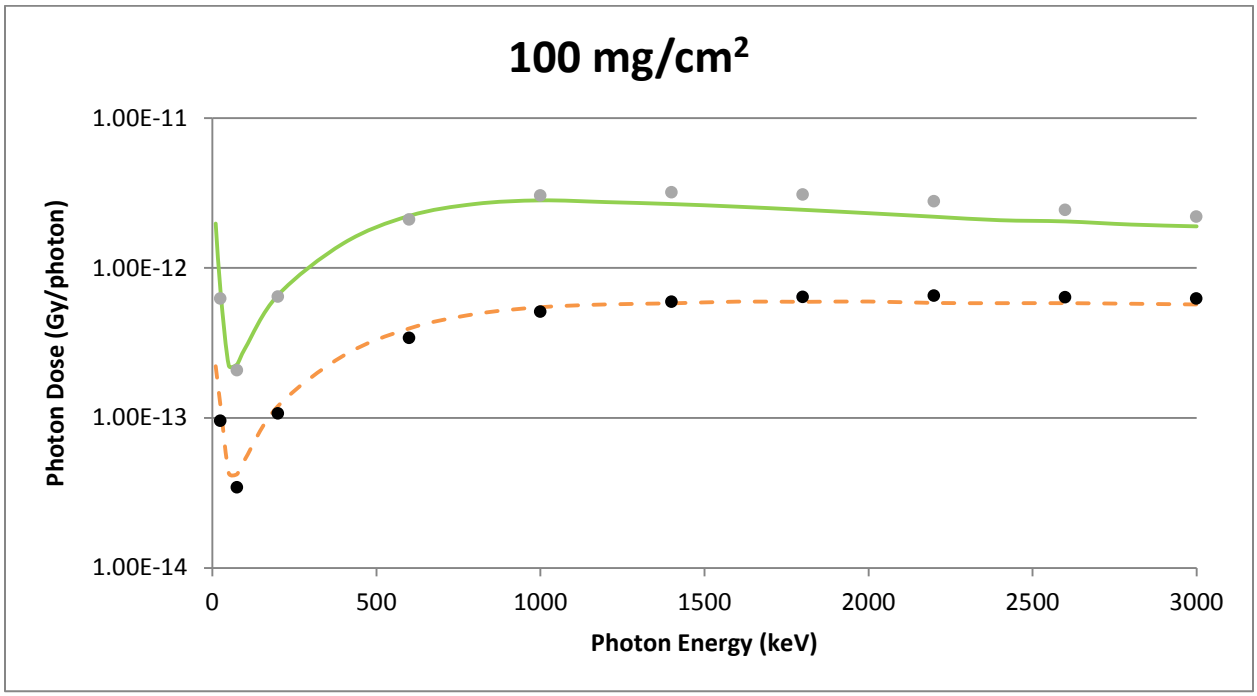

Figure B.4.2. A slab source geometry comparison of VARSKIN 5 (circles) and MCNP5 (lines) predicted dose per initial photon as a function of photon energy in tissue at a density thickness of 100 mg/cm^2 and a tissue volume cylinder of area 1 cm^2 (solid line) and 10 cm^2 (dashed line), with a thickness of 20 µm

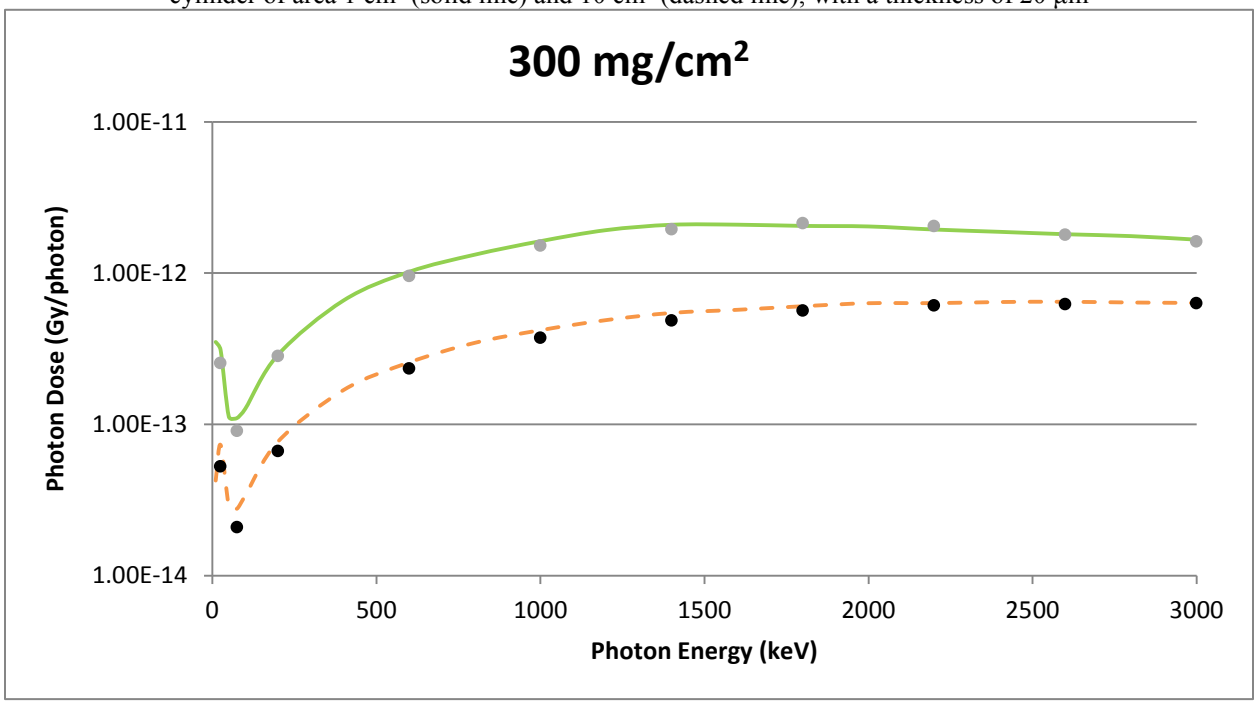

Figure B.4.3. A slab source geometry comparison of VARSKIN 5 (circles) and MCNP5 (lines) predicted dose per initial photon as a function of photon energy in tissue at a density thickness of 300 mg/cm^2 and a tissue volume cylinder of area 1 cm^2 (solid line) and 10 cm^2 (dashed line), with a thickness of 20 µm

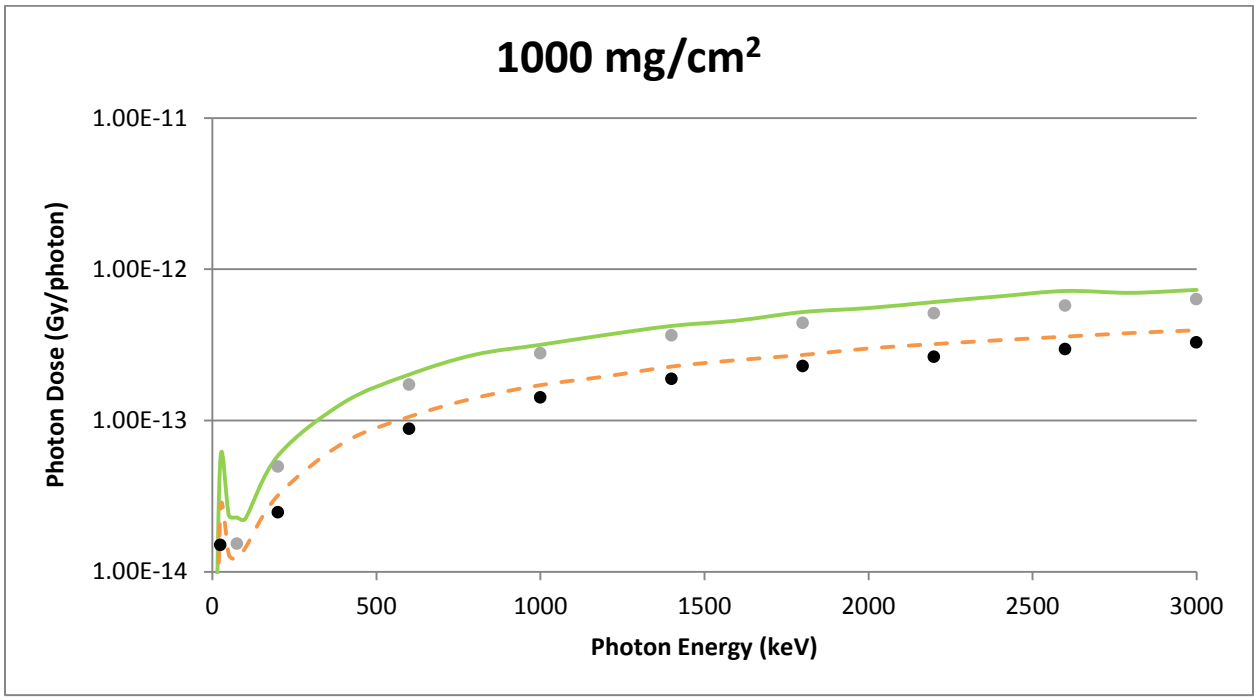

Figure B.4.4. A slab source geometry comparison of VARSKIN 5 (circles) and MCNP5 (lines) predicted dose per initial photon as a function of photon energy in tissue at a density thickness of 1000 mg/cm^2 and a tissue volume cylinder of area 1 cm^2 (solid line) and 10 cm^2 (dashed line), with a thickness of 20 µm

GEOMETRY 5: SPHERICAL SOURCE

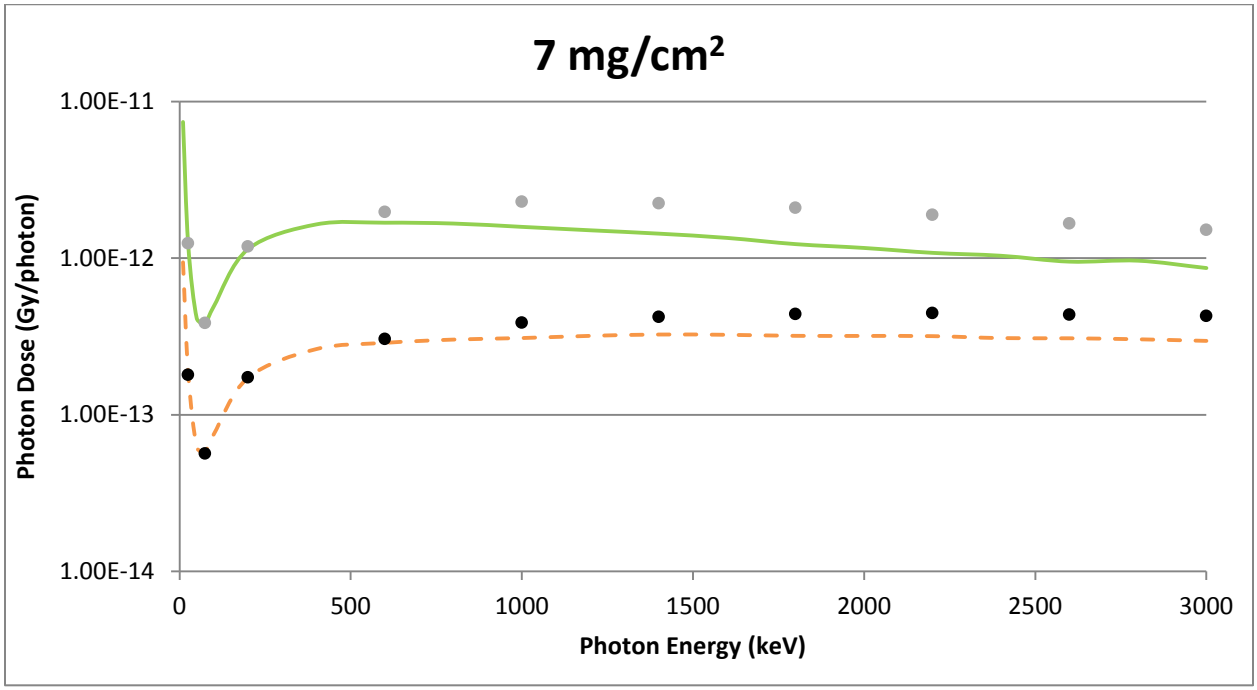

Figure B.5.1. A spherical source geometry comparison of VARSKIN 5 (circles) and MCNP5 (lines) predicted dose

per initial photon as a function of photon energy in tissue at a density thickness of 7 mg/cm^2 and a tissue volume cylinder of area 1 cm^2 (solid line) and 10 cm^2 (dashed line), with a thickness of 20 µm

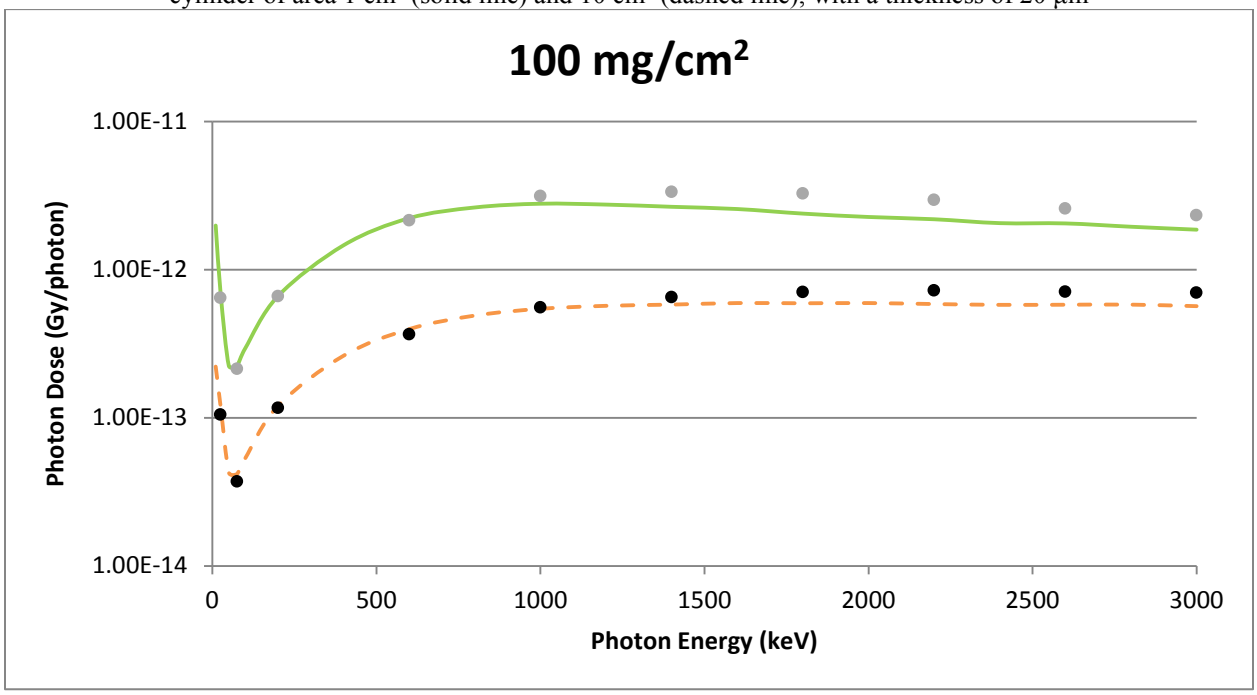

Figure B.5.2. A spherical source geometry comparison of VARSKIN 5 (circles) and MCNP5 (lines) predicted dose per initial photon as a function of photon energy in tissue at a density thickness of 100 mg/cm^2 and a tissue volume cylinder of area 1 cm^2 (solid line) and 10 cm^2 (dashed line), with a thickness of 20 µm

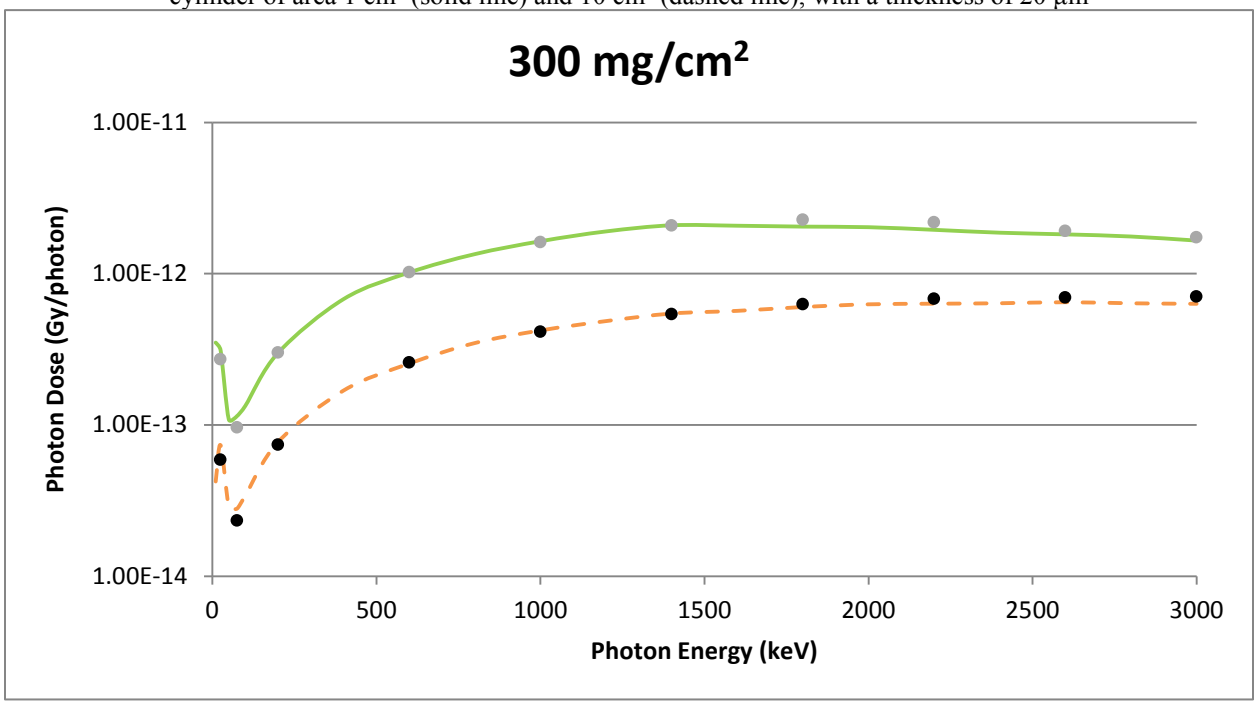

Figure B.5.3. A spherical source geometry comparison of VARSKIN 5 (circles) and MCNP5 (lines) predicted dose

per initial photon as a function of photon energy in tissue at a density thickness of 300 mg/cm^2 and a tissue volume cylinder of area 1 cm^2 (solid line) and 10 cm^2 (dashed line), with a thickness of 20 µm

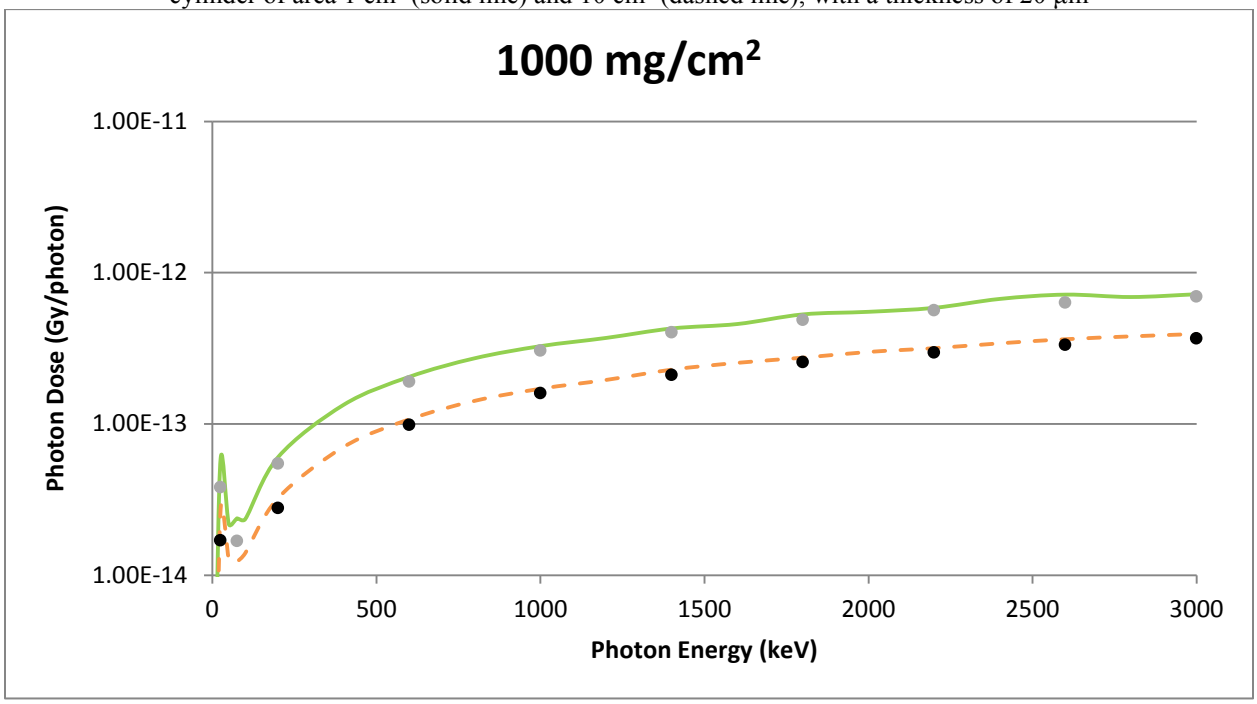

Figure B.5.4. A spherical source geometry comparison of VARSKIN 5 (circles) and MCNP5 (lines) predicted dose per initial photon as a function of photon energy in tissue at a density thickness of 1000 mg/cm^2 and a tissue volume cylinder of area 1 cm^2 (solid line) and 10 cm^2 (dashed line), with a thickness of 20 µm

GEOMETRY 6: POINT SOURCE (with Air Gap And Cotton Cover)

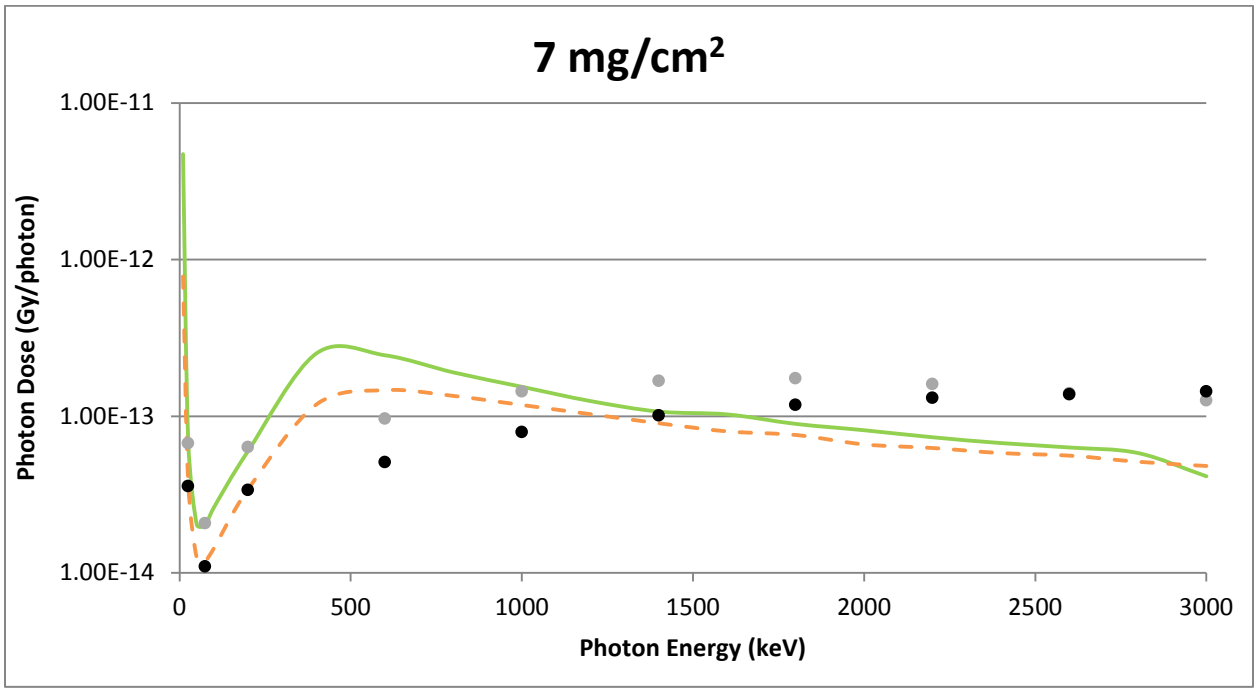

Figure B.6.1. A point source geometry with a cotton cover and a 1 cm air gap comparison of VARSKIN 5 (circles) and MCNP5 (lines) predicted dose per initial photon as a function of photon energy in tissue at a density thickness of 7 mg/cm^2 and a tissue volume cylinder of area 1 cm^2 (solid line) and 10 cm^2 (dashed line); thickness of 20 µm

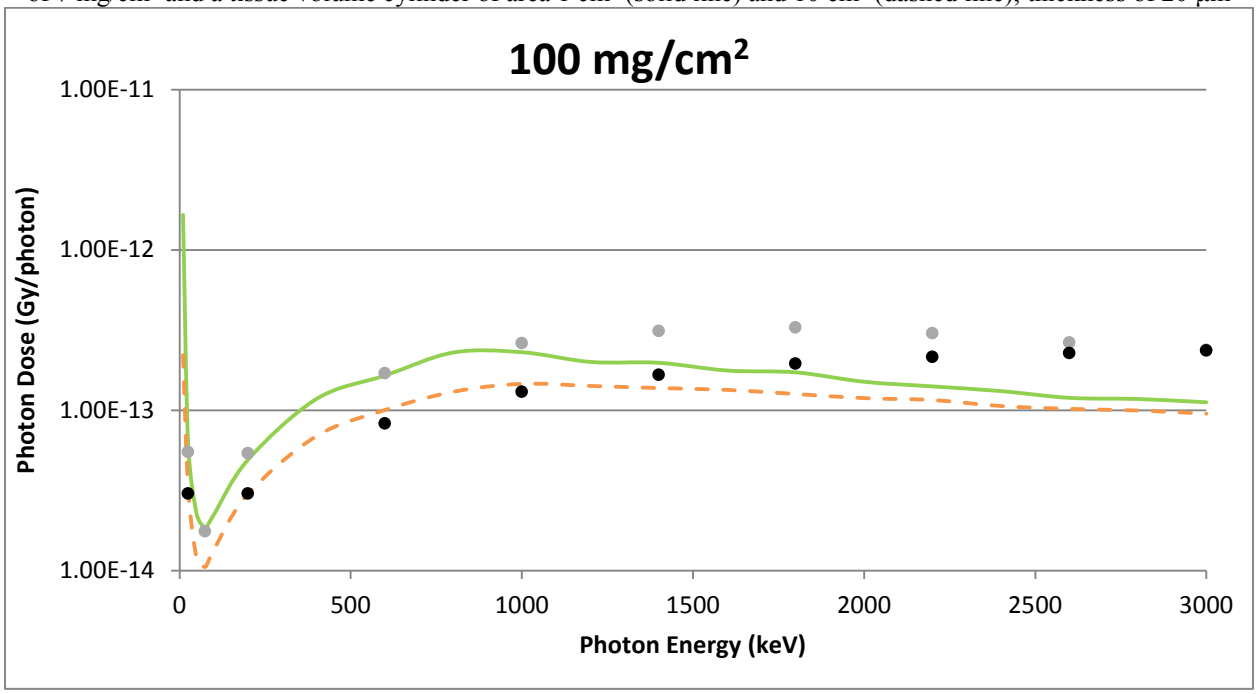

Figure B.6.2. A point source geometry with a cotton cover and a 1 cm air gap comparison of VARSKIN 5 (circles) and MCNP5 (lines) predicted dose per initial photon as a function of photon energy in tissue at a density thickness of 100 mg/cm^2 and a tissue volume cylinder of area 1 cm^2 (solid line) and 10 cm^2 (dashed line); thickness of 20 µm

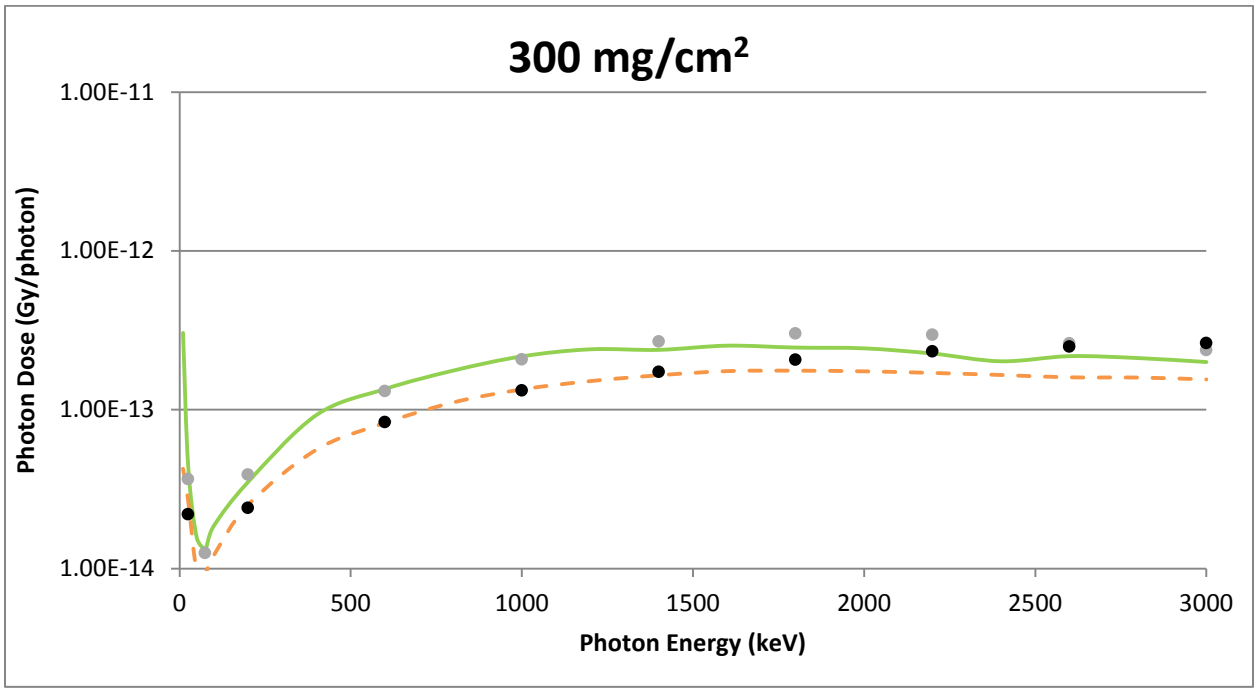

Figure B.6.3. A point source geometry with a cotton cover and a 1 cm air gap comparison of VARSKIN 5 (circles) and MCNP5 (lines) predicted dose per initial photon as a function of photon energy in tissue at a density thickness of 300 mg/cm^2 and a tissue volume cylinder of area 1 cm^2 (solid line) and 10 cm^2 (dashed line); thickness of 20 μm

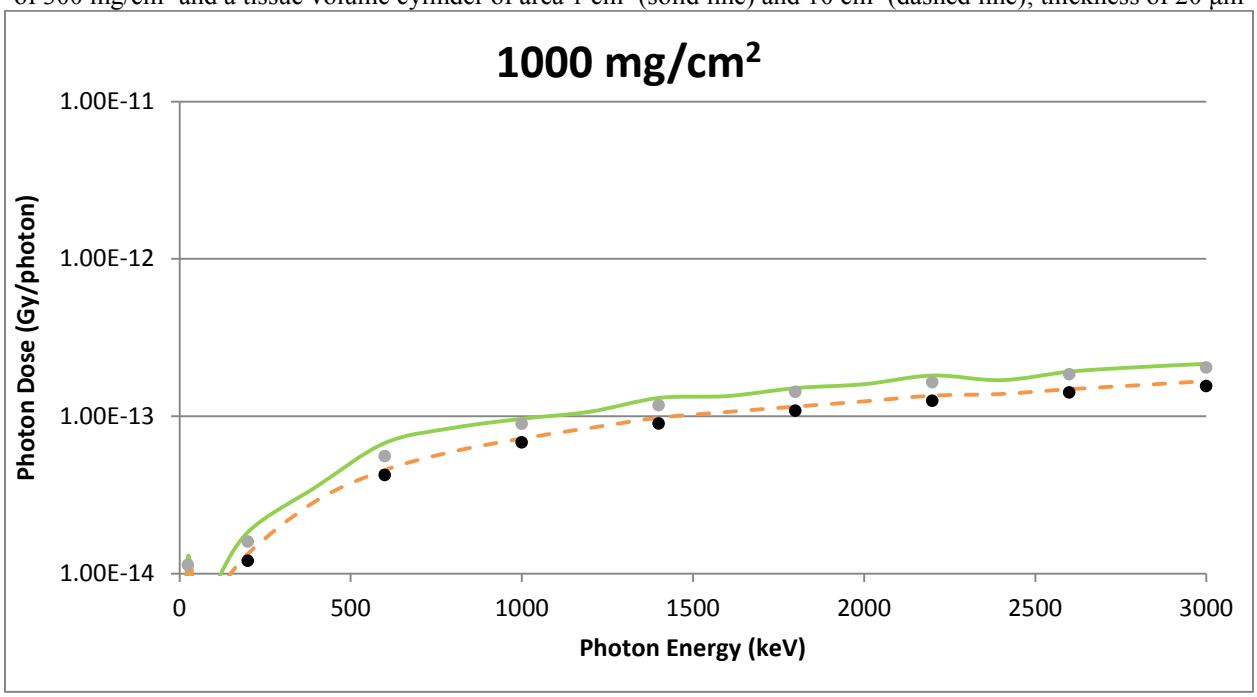

Figure B.6.4. A point source geometry with a cotton cover and a 1 cm air gap comparison of VARSKIN 5 (circles) and MCNP5 (lines) predicted dose per initial photon as a function of photon energy in tissue at a density thickness of 1000 mg/cm^2 and a tissue volume cylinder of area 1 cm^2 (solid line) and 10 cm^2 (dashed line); thickness of 20 μm

GEOMETRY 7: POINT SOURCE (1 cm off axis)

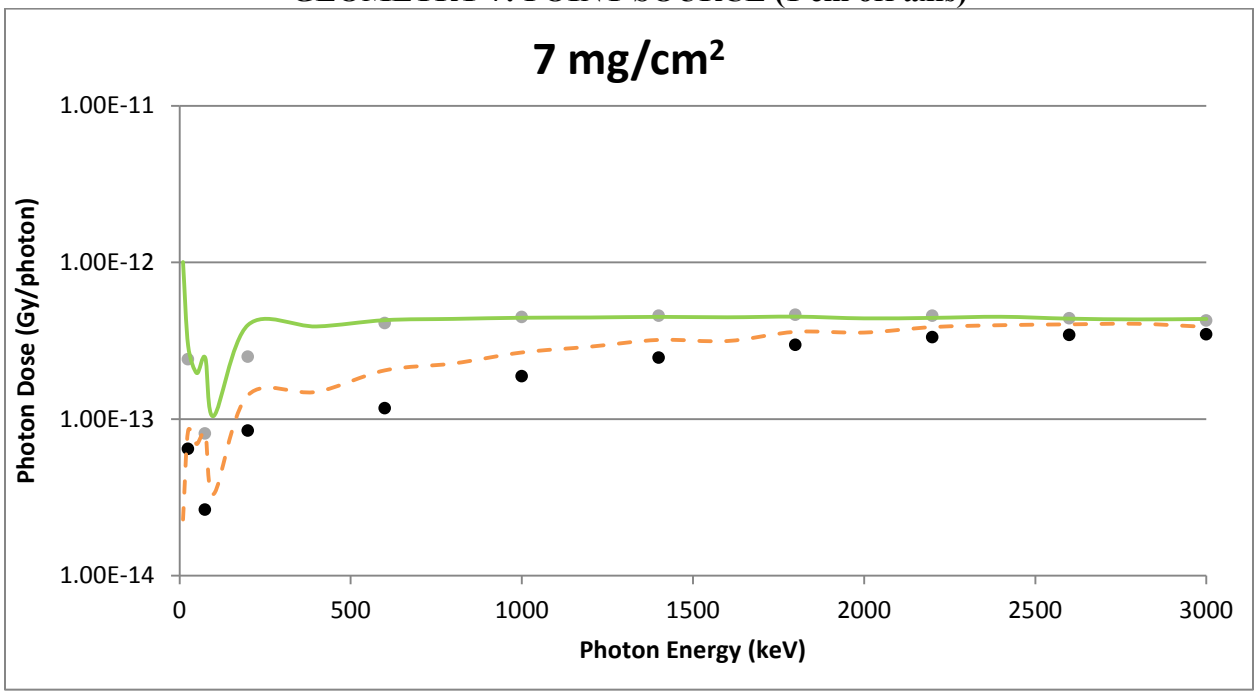

Figure B.7.1. A point source geometry 1 cm off-axis comparison of VARSKIN 5 (circles) and MCNP5 (lines) predicted dose per initial photon as a function of photon energy in tissue at a density thickness of 7 mg/cm^2 and a tissue volume cylinder of area 1 cm^2 (solid line) and 10 cm^2 (dashed line), with a thickness of 20 μm

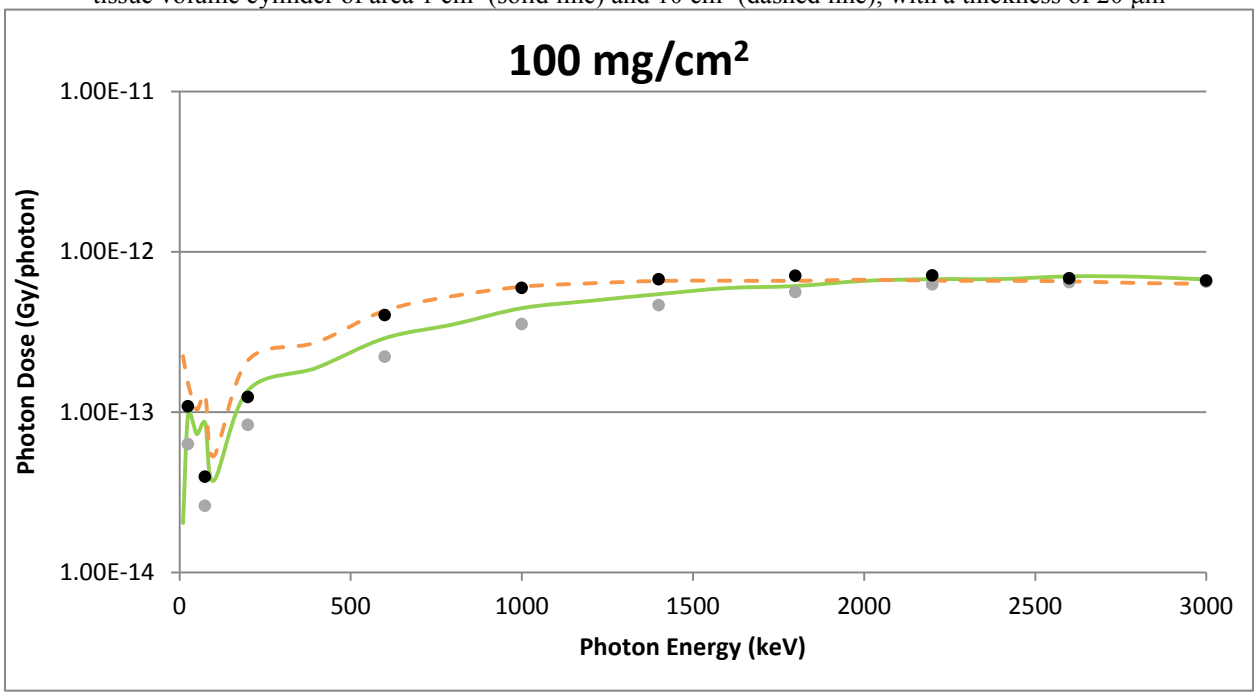

Figure B.7.2. A point source geometry 1 cm off-axis comparison of VARSKIN 5 (circles) and MCNP5 (lines) predicted dose per initial photon as a function of photon energy in tissue at a density thickness of 100 mg/cm^2 and a tissue volume cylinder of area 1 cm^2 (solid line) and 10 cm^2 (dashed line), with a thickness of 20 μm

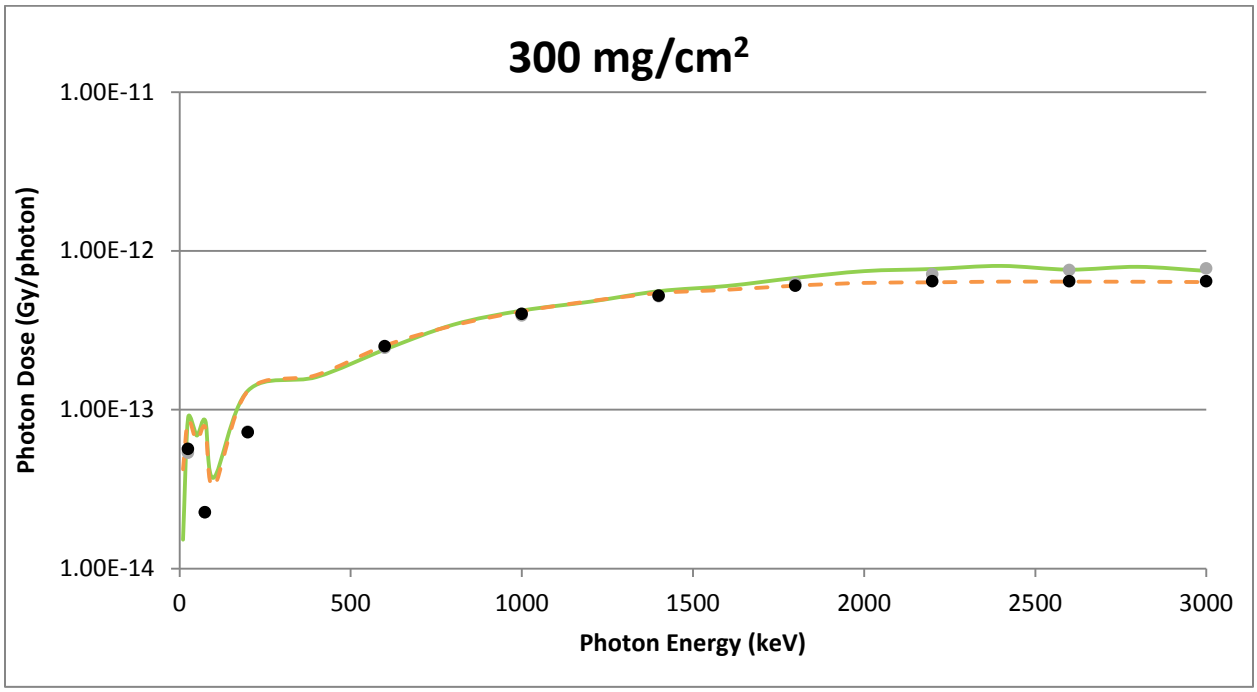

Figure B.7.3. A point source geometry 1 cm off-axis comparison of VARSKIN 5 (circles) and MCNP5 (lines) predicted dose per initial photon as a function of photon energy in tissue at a density thickness of 300 mg/cm^2 and a tissue volume cylinder of area 1 cm^2 (solid line) and 10 cm^2 (dashed line), with a thickness of 20 μm

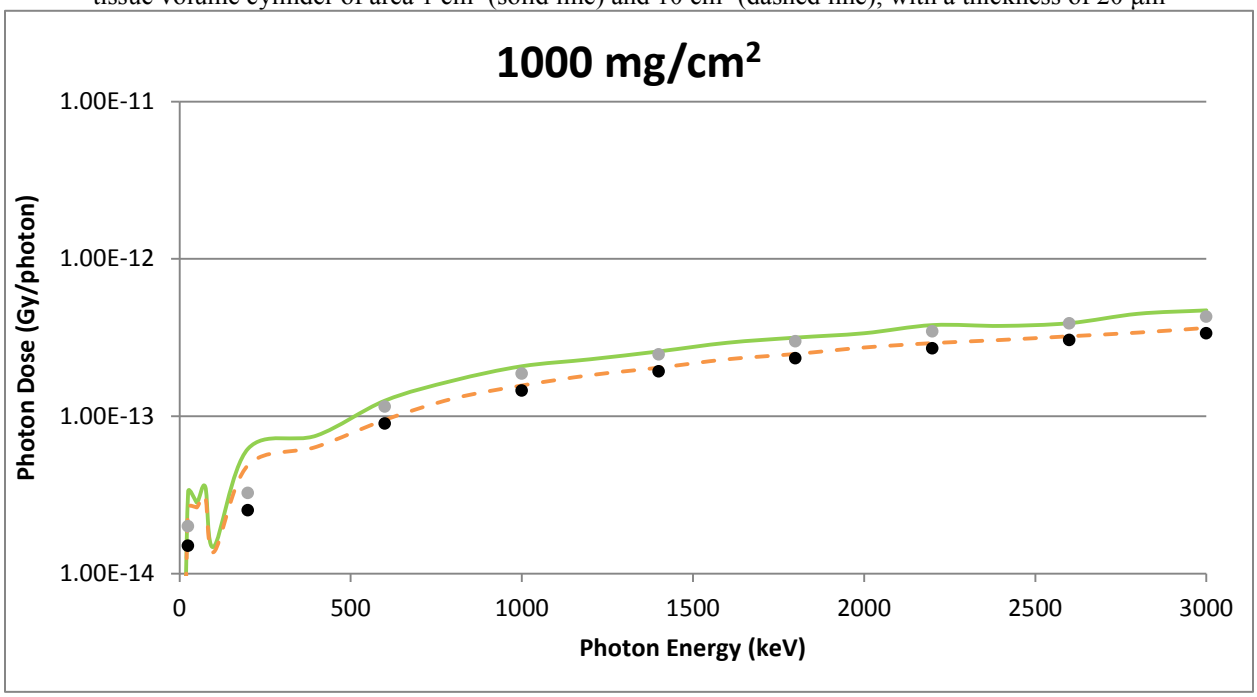

Figure B.7.4. A point source geometry 1 cm off-axis comparison of VARSKIN 5 (circles) and MCNP5 (lines) predicted dose per initial photon as a function of photon energy in tissue at a density thickness of 1000 mg/cm^2 and a tissue volume cylinder of area 1 cm^2 (solid line) and 10 cm^2 (dashed line), with a thickness of 20 μm

APPENDIX C

Examples and Solutions Using VARSKIN 5

EXAMPLES AND SOLUTIONS USING VARSKIN 5

This appendix describes three different practical applications of VARSKIN 5 using an example/solution format. Each example describes a situation followed by a solution that involves the use of VARSKIN to estimate skin dose and deep-dose equivalent. The purpose of these examples is to lead a new user of VARSKIN through several calculations that highlight many of its features. Because VARSKIN is a flexible tool, there are always several ways to calculate the dose for a given example. The solutions presented here reflect the recommendations that are provided throughout the user's manual. With some experience, most VARSKIN users will not need to perform all of the steps described in the solution in an actual situation. It is suggested that the user complete all three examples in the order in which they are presented to develop familiarity with VARSKIN.

Example 1: Radiopharmaceutical Technician in Nuclear Medicine

At a research hospital, a doctor prescribes a 5-milliliter (mL) administration from a stock solution containing 10 microcuries per milliliter (μCi/mL) of rhenium-186 (^{186}Re) for a clinical research study at 1 p.m. that day. Around 12:30 p.m., a lab technician loads the dose under the hood. Subsequently, a fellow employee bumps into her, and the needle slips out of its container. The entire 5 mL of the solution is spilled on the arm of her cloth lab coat in a circular shape with an area of approximately 50 square centimeters (cm^2). She is unaware of the accident and continues with her work until the end of the day. Around 5 p.m., a routine survey for contamination is performed, and the contamination is discovered.

Solution 1: Radiopharmaceutical Technician in Nuclear Medicine

The point source geometry is suggested as a starting point to estimate the magnitude of the dose and to collect some other useful information. Run VARSKIN 5 and check the user "Radionuclide Library." If ^{186}Re does not appear in the "Radionuclide Library" window, add ^{186}Re by selecting the "Add" button and double-clicking ^{186}Re in the Add Radionuclide to Library window (with an effective Z of equivalent-water, Z = 7.42). Enter the Exposure Time as 4.5 and change the time unit to hours using the drop-down menu or the down-arrow key. Because the point source geometry is being used, it is necessary to calculate the source strength by multiplying the concentration of the stock solution (10 μCi/mL) by the size of the administration (5 mL) to get a total source strength of 50 μCi. Be sure that the source strength units are set to μCi, then double-click the ^{186}Re library entry. When VARSKIN asks for the source strength, enter 50. The other defaults will establish a dose calculation at 7 mg/cm^2 and a dose-averaging disk of 10 cm^2. All other entries should retain their default values. Click "Calculate Doses." After the calculation is performed, the VARSKIN Non-Volume Averaged Results window will appear.

The results window shows two groups of nine dose or dose-rate values (the group to the left is for nuclide-specific doses and the group to the right is total (over all nuclides) dose). Since only one nuclide has been selected, the two groups will display the same dose values. For each of beta, photon, and total, the initial dose rate, the dose with no decay, and the decay-corrected dose are displayed. The dose with no decay is provided so that the user can assume that either the source has a very long half-life or that the radionuclide is in secular equilibrium with its

parent. Note that ^{186}Re has a relatively short half-life; therefore, the decay-corrected dose is the appropriate dose for the current calculation. Looking at either the VARSKIN results window or the results printout (by clicking the "Print Results" button) will show that the decay-corrected total dose is **1.31 Gray (Gy)** (**1.31 Gy** from beta and **0.673 milliGy (mGy)** from photons), a value that exceeds regulatory limits. To calculate the deep dose, return to the main VARSKIN window (i.e., close the results window), change the value of the Skin Thickness or Skin Density Thickness to 1,000 milligrams per square centimeter (mg/cm^2), and click "Calculate Doses." The VARSKIN results screen now displays a decay-corrected beta dose of **0** (zero) and a photon dose of **0.0712 mGy**.

The total shallow dose calculated using the point geometry was above regulatory limits. However, the situation described in this example will obviously be more accurately modeled using the disk or cylinder geometries. A more realistic, yet conservative approach would be to use the disk geometry and calculate the dose as if all of the contamination were directly on the skin. Return to the main VARSKIN window and choose "Disk" in the Source Geometry frame. Confirm the Exposure Time of 4.5 hours. Next, enter the Source Area as 50 cm^2 (don't forget to change the units from the default setting). Note that the Source Diameter is automatically calculated to be 7.98 cm (this value will be needed for the next model). Change the Skin Thickness or Skin Density Thickness back to the shallow depth of 7 mg/cm^2 and click "Calculate Doses." The results screen shows a decay-corrected beta dose of **0.262 Gy** and a photon dose of **0.149 mGy**. While the dose is still quite high, it is now below regulatory limits.

Even more realism can be introduced by using the cylinder model to simulate contamination that is uniformly distributed throughout the thickness of the lab coat. In this case, the lab coat is assumed to soak up the contamination instead of acting as a protective cover material. The data in Table 2-2 for a cloth lab coat give a thickness of 0.4 millimeters (mm) and a density of 0.9 g/cm^3. After returning to the main VARSKIN window, choose "Cylinder" in the Source Geometry frame. Confirm the exposure time of 4.5 hours. Paying close attention to each unit's entry, confirm the Source Diameter as 7.98 cm (from the disk calculation), and establish a Source Thickness of 0.4 mm (the thickness of the lab coat) and a Source Density of 0.9 g/cm^3 (the density of the lab coat). Click "Calculate Doses"; after a longer calculational period (due to the geometric complexity), the VARSKIN results screen then will display **0.169 Gy** and **0.149 mGy** as the decay-corrected beta and photon doses, respectively.

It is interesting to see what the beta dose would be if the lab coat was impervious to the liquid contamination, and the contamination resided as an infinitely thin layer of contamination on the plastic. In this case, the plastic lab coat acts as a cover material instead of defining the size and density of the source. To perform this calculation, return to the main VARSKIN window and change the Source Geometry to a "Disk" source. Confirm the Exposure Time of 4.5 hours and the source area of 50 cm^2. Enter a Cover Thickness of 0.2 mm with a density of 0.36 g/cm^3. After the user clicks "Calculate Doses," the VARSKIN results screen will display decay-corrected doses of **0.186 Gy** for beta and **0.124 mGy** for photons. It can be concluded that, based on the above calculations, a thicker, absorbent lab coat will give more protection than a thin, impervious material.

Example 2: Radiation Worker in Reactor Containment

A worker damages his outer glove while working inside containment during an outage at a nuclear reactor. His outer glove is removed, leaving only a surgeon's glove. The worker proceeds to the step-off pad, which takes about 15 minutes. During the exit survey, contamination is detected on the surgeon's glove, and the glove is removed and taken to the laboratory for analysis. The laboratory report concludes that the contamination is a stellite hot particle with the following characteristics:

- Radioactive contaminant: ^{60}Co
- Source strength: 2.5 mCi
- Particle thickness and density: 50 μm; 8.3 g/cm^3
- Particle size: 80 μm x 70 μm
- Glove thickness: 0.3 mm
- Glove density: 0.6 g/cm^3

Solution 2: Radiation Worker in Reactor Containment

First, we will use the point source geometry to estimate the magnitude of the dose and to collect some other useful information. Start or "Reset" (from the File drop-down menu) VARSKIN 5. If Co-60 does not appear in the Radionuclide Library frame, add Co-60 by selecting the "Add" key and double-clicking "Co-60" in the Add Radionuclide to Library window (with an effective Z of 7.42). Enter an Exposure Time of 15 minutes. Double-click "Co-60" in the Radionuclide Library, and enter 2.5 millicuries (mCi). Enter a Cover Thickness of 0.3 mm and a Cover Density of 0.6 g/cm^3. After you click "Calculate Doses," the VARSKIN results window will display a beta dose of **0.325 Gy**, a photon dose of **0.105 Gy,** and a total dose of **0.431 Gy**, a value approaching the regulatory limit. Thus, a more realistic calculation is desirable. In addition, there is a gamma component to the dose, so a deep-dose calculation is needed.

Using the cylinder model will result in a more realistic calculation because the effects of self-shielding of the beta particles will be considered. As described in Section 2.2, the cylinder model should be used for a particle that is known to be rectangular. Return to the main VARSKIN window, and choose the "Cylinder" source geometry. Confirm 15 minutes as the Exposure Time, 0.3 mm as the Cover Thickness, and 0.6 g/cm^3 as the Cover Density. Enter 50 μm as the Source Thickness. The diameter of a disk source, with the same area as the rectangular source, is found by:

$$d = 2\sqrt{X \cdot Y/\pi} = 2\sqrt{80\ \mu m \cdot 70\ \mu m/\pi} = 84\ \mu m.$$

Enter 84 μm for the Source Diameter and 8.3 g/cm^3 for the Source Density, and then click "Calculate Doses." After a short time, the VARSKIN results screen will display a beta dose of **0.130 Gy**, a photon dose of **0.105 Gy**, and a total dose of **0.235 Gy**. Including the effects of self-shielding greatly reduced the beta dose and resulted in a dose that is now below regulatory limits. To calculate deep dose, simply return to the main window, change the Skin Thickness or Skin Density Thickness to 1,000 mg/cm^2, and click "Calculate Doses." The VARSKIN results screen will display a deep dose of **0.0325 Gy**, all from photons.

Example 3: Contaminated Metal in a University Laboratory Hood

During a radiation survey of a fume hood, a new Radiation Safety Officer (RSO) at a university discovers a contaminated aluminum plate inside the hood. Upon further investigation, it is found that the plate was used to hold beakers of solution containing carbon-14 (^{14}C) for use in radiobiology experiments. The RSO decides that the plate should be disposed of as low-level radioactive waste and that the activity of ^{14}C on the plate must be determined. The plate is 6 inches (in.) by 6 in. and is uniformly contaminated over the entire surface. The RSO uses a calibrated circular detector with an area of 50 cm^2 and a window thickness of 3 mg/cm^2 to measure a dose rate of 1.90 mGy/hr on contact and 0.60 mGy/hr at a distance of 1 in.

Solution 3: Contaminated Metal in a University Laboratory Hood

The solution to this example demonstrates a method of using VARSKIN 5 for applications other than skin contamination events. In this situation, the Skin Averaging Area will be set to 50 cm^2 to correspond to the area of the probe, the Skin Density Thickness will be set to 3 mg/cm^2 to correspond to the thickness of the probe window, and the Source Area will be set to 36 in^2 to correspond to the area of the contaminated plate. A source strength of 1 $\mu Ci/cm^2$ will be used for the calculation, and the results of the calculation will be scaled to the measurements obtained by the RSO. Both of the measurements can be modeled because the air gap in Example 3 is smaller than 5 cm, the limit for air gaps in VARSKIN 5.

For this solution, first "Reset" VARSKIN and choose the "Disk" geometry. If the Radionuclide Library does not contain ^{14}C, add it by clicking "Add" and double-clicking "C-14" in the Add Radionuclide to Library screen (with an effective Z of 7.42). From the main VARSKIN window, click the "Use Distributed Source" checkbox. Notice that the default unit for activity has changed; set that to "$\mu Ci/cm^2$". Double-click "C-14" and set the source strength to 1 $\mu Ci/cm^2$. Set the Skin Averaging Area to 50 cm^2, the Skin Thickness or Skin Density Thickness to 3 mg/cm^2, and the Source Area to 36 $in.^2$. For this example, the dose rate is of interest so the irradiation time can remain at the default value of 60 minutes. Click "Calculate Doses"; the VARSKIN results window will appear, displaying an initial beta dose rate of **0.0447 Gy/hr**, with no photon dose. The activity concentration on the plate then can be found using,

$$\frac{[A_{act}]}{[A_{cal}]} = \frac{\dot{D}_{meas}}{\dot{D}_{cal}}.$$

Therefore, the activity concentration on the plate is given by:

$$\frac{\left(1\ {}^{\mu Ci}/_{cm^2}\right)\left(1.90\ {}^{mGy}/_{hr}\right)}{44.70\ {}^{mGy}/_{hr}} = 0.0425\ {}^{\mu Ci}/_{cm^2}$$

Multiplying the activity concentration by the area of the plate (6 in. x 6 in. = 232 cm^2) results in a total activity of 9.86 μCi.

The measurement at a distance of 1 inch can be used to verify this result. Close the results window and return to the main window; enter an Air Gap Thickness of 1 inch and change the activity to 9.86 μCi. After you click "Calculating Doses," the VARSKIN results window will display an initial beta dose rate of **0.604 mGy/hr**, compared to the measurement of 0.60 mGy/hr with the calibrated detector.

NRC FORM 335
(12-2010)
NRCMD 3.7

U.S. NUCLEAR REGULATORY COMMISSION

BIBLIOGRAPHIC DATA SHEET

(See instructions on the reverse)

1. REPORT NUMBER
(Assigned by NRC, Add Vol., Supp., Rev., and Addendum Numbers, if any.)

NUREG/CR-6918, Rev. 2

2. TITLE AND SUBTITLE

VARSKIN 5:A COMPUTER CODE FOR SKIN CONTAMINATION DOSIMETRY

3. DATE REPORT PUBLISHED

MONTH	YEAR
July	2014

4. FIN OR GRANT NUMBER

RES-13-331

5. AUTHOR(S)

David M. Hamby, C.D. Mangini, J.A. Caffrey, M. Tang

6. TYPE OF REPORT

Final

7. PERIOD COVERED (Inclusive Dates)

3//09/2011-3/15/2013

8. PERFORMING ORGANIZATION - NAME AND ADDRESS (If NRC, provide Division, Office or Region, U. S. Nuclear Regulatory Commission, and mailing address; if contractor, provide name and mailing address.)

Department of Nuclear Engineering and Radiation Health Physics
Oregon State University
Corvallis, OR 97331-5902

9. SPONSORING ORGANIZATION - NAME AND ADDRESS (If NRC, type "Same as above", if contractor, provide NRC Division, Office or Region, U. S. Nuclear Regulatory Commission, and mailing address.)

Division of System Analysis
Office of Nuclear Regulatory Research
U.S. Nuclear Regulatory Research

10. SUPPLEMENTARY NOTES

This report supersedes NUREG/CR-6918, Rev. 1

11. ABSTRACT (200 words or less)

This report is a user manual for the VARSKIN 5 which is used by the NRC staff to verify the licensees' skin dose calculations, as required by 10 CFR 20.1201(c). The new VARSKIN 5 version has been updated to better predict beta dosimetry in shallow skin targets. A variety of unit options are provided (including both British and international system (SI) units). The output page and the user's ability to add radionuclides to the library are greatly simplified. A library file contains data on gamma rays, x-rays, beta particles, internal conversion electrons, and Auger electrons. VARSKIN 5 allows the user to eliminate radionuclides that are not of interest and thus build a customized library. Finally, an extensive, context-sensitive help file is made available for VARSKIN 5 to provide guidance in the use of the skin dosimetry software.

The beta dosimetry model has been upgraded in VARSKIN 5 to better account for beta energy loss and particle scatter. Dose point kernels are now Monte Carlo based and the code agrees very well with the EGSnrc Monte Carlo code. The document provides basic operating instructions, dosimety models, and methods for avoiding misuse of the code.

12. KEY WORDS/DESCRIPTORS (List words or phrases that will assist researchers in locating the report.)

NUREG/CR-6918, Rev. 2
skin dose
skin dosimetry
VARSKIN 5
photon dose
beta dose
skin contaminatio

13. AVAILABILITY STATEMENT

unlimited

14. SECURITY CLASSIFICATION

(This Page)
unclassified

(This Report)
unclassified

15. NUMBER OF PAGES

16. PRICE

Federal Recycling Program

UNITED STATES
NUCLEAR REGULATORY COMMISSION
WASHINGTON, DC 20555-0001

OFFICIAL BUSINESS